Analysis of a putative cyclooxygenase from *Trypanosoma brucei* and its eligibility as a possible drug target

Analyse einer putativen Cyclooxygenase aus *Trypanosoma brucei* und ihrer Eignung als mögliches Medikamenten-Ziel

Dissertation

der Mathematisch-Naturwissenschaftlichen Fakultät

der Eberhard Karls Universität Tübingen

zur Erlangung des Grades eines

Doktors der Naturwissenschaften

(Dr. rer. nat.)

vorgelegt von

Célestin Nzanzu Mudogo

aus

Kinshasa, DR Kongo

Tübingen

2017

Tag der mündlichen Qualifikation: 28.07.2017

Dekan: Prof. Dr. Wolfgang Rosenstiel

1. Berichterstatter: Prof. Dr. Michael Duszenko

2. Berichterstatter: PD. Dr. Benjamin Mordmüller

I Dedicate this thesis

to my beloved parents Mudogo Virima and Vumilia Nsigayehe and

to Wolf and Batzner families in Würzburg & Mudogo´s family members in DRCongo

Contents

Abbreviations

AA	Arachidonic acid
AP	Alkaline phosphatase
APS	Ammonium persulfate
BBB	Blood-brain barrier
BCB	Blood-CSF-barrier
BCIP	5-Bromo-4-chloro-3-indolyl phosphate
BCS	Bathocuproine disulfonic acid
BF	Bloodstream form
BME	2-ß-Mercarptoethanol
Bp	Base pairs
BSA	Bovine serum albumin
CATT	Card agglutination test for trypanosomiasis
CD	Circular dichroism
CGA	Citrate glucose anticoagulant
CNS	Central nervous system
COX	Cyclooxygenase
CSF	Cerebrospinal fluid
CVOs	Circumventricular organs
DAPI	4´, 6-Diamidino-2-phenylindole
DDSA	Dodecenylsuccinic Anhydride
DEAE	Diethylaminoethyl
DFMO	Difluoromethylornithine
dH$_2$O	Distilled water
DLS	Dynamic light scattering
DMSO	Dimethyl sulfoxide

DNA	Deoxyribonucleic acid
DNDi	Drugs for Neglected Diseases Initiative
dsRNA	double-stranded RNA
EDTA	Ethylenediaminetetraacetic acid
eGFP	Enhanced green fluorescent protein
EGTA	Ethyleneglycol-bis (ß-aminoethyl ether)-N,N,N´,N´-tetraacetic acid
ER	Endoplasmic reticulum
FAZ	Flagellum attachment zone
FBS	Fetal bovine serum
FCS	Fetal calf serum
FIND	Foundation for Innovative New Diagnosis
FPLC	Fast protein liquid chromatography
gDNA	Genomic DNA
GPI	Glycosylphosphatidylinositol
GSG	L-Glutathione reduced
GSSG	L-Glutathione oxidized
GuHCl	Guanidine hydrochloride
HAT	Human african trypanosomiasis
HEPES	N-2-hydroxyethylpiperazine-N´-2-ethanesulfonic acid
HMI-9	Hirumi's Modified Iscove's medium
IBs	Inclusions bodies
IFN-γ	Interferon gamma
IMDM	Iscove's Modified Dulbecco's Medium
IPTG	Isopropyl ß-D-1-thiogalactopyranoside
KD	Knockdown
KDa	Kilodalton

LAMP	Loop-mediated isothermal amplification
MicroED	micro-electronmicroscopy diffraction
MITat	Molteno institute trypanozoon antigenic type
MOI	Multiplicity of infection
mRNA	Messenger RNA
MSP-B	Major surface protease B
NADPH	Nicotinamide adenine dinucleotide phosphate
NBT	Nitro Blue tetrazolium
NECT	Nifurtimox-Eflornithine combination therapy
NTD	neglected tropical disease
ODC	Ornithine decarboxylase
PBS	Phosphate buffered saline
PCR	Polymerase chain reaction
PDB	Protein data bank
PEG	Polyethylenglycol
PFR	Paraflagellar rod
pfu/ml	Plaque forming unit/ml
PG	Prostaglandins
PGD_2	Prostaglandin D2
PGE_2	Prostaglandin E2
$PGF_{2\alpha}$	Prostaglandin F2 alpha
pTbCOX	putative Trypanosoma brucei Cyclooxygenase
pTbCOX-KD	putative Trypanosoma brucei Cyclooxygenase knockdown
PTRE	Post-treatment reactive encephalopathy
qRT-PCR	quantitative real time polymerase chain reaction
RDT	rapid diagnostic test

RISC	RNA-induced silencing (complex)
RNA	Ribonucleic acid
RNAi	RNA-Interference
rpm	Revolutions per minute
RT	Room temperature
SDS	Sodium dodecylsulfate
SDS-PAGE	Sodium dodecylsulfate polyacrylamide gel electrophoresis
SEM	Scanning electron microscopy
Sf9	Spodoptera frugiperda insect cell
SFX	Serial femtosecond crystallography
SIF	Stumpy induction factor
siRNA	Small interfering RNA
SMB	Single marker bloodstream form
SOREM	sleep-onset rapid eye movement
SSX	Serial synchrotron crystallography
T.	Trypanosoma
T. b.	Trypanosoma brucei
TAE	Tris acetate EDTA
Tb	Trypanosoma brucei
TbMSP-B	Trypanosoma brucei Major surface protease B
TbPGFS	Trypanosoma brucei Prostaglandin 2 alpha synthase
TBS	Tris buffered saline
$TCID_{50}$	50% tissue-culture infection dose
TDB	Trypanosoma dilution buffer
TEM	Transmission electron microscopy
TEMED	Tetramethylethylenediamine

TNF-α	Tumor necrosis factor alpha
Tris	Tris (hydroxymethyl) aminomethane
TrypanoFAN	Trypanosoma brucei Functional Genomic Project
VSG	Variant surface glycoprotein
WHO	World Health Organization
XFEL	X-free electron laser

List of Figures

1 Introduction

1.1 Human African Trypanosomiasis

1.1.1 Epidemiology

Human African trypanosomiasis (HAT), also known as sleeping sickness, is one of the "neglected tropical diseases" (Hotez and Kamath, 2009). The concept of neglected tropical diseases (NTDs) was first proposed in the 1970s by Ken Warren (Keating, 2014; Croft, 2016). He brought attention to a significant proportion of the human population that was poor, suffered from chronic, disabling but rarely fatal diseases, and who were often stigmatized and unemployed (Croft, 2016). Also, these diseases are neglected by the pharmaceutical companies, as affected low developed countries do not receive too many priorities for research funding and field investigations.

HAT is a vector-borne parasitic disease which primarily affects poor rural populations in some of the least developed countries of East and Central Africa (Berriman et al., 2005). Moreover, HAT is the world's third most important parasitic disease affecting human health after malaria and schistosomiasis as defined by the global burden of parasitic disease, calculated as the disability-adjusted life years lost (Kennedy, 2008).

HAT is caused by two subspecies of *Trypanosoma brucei*, namely *Trypanosoma brucei gambiense* and *Trypanosoma brucei rhodesiense*, which are transmitted to the human host by tsetse flies. Other parasites like *T. congolense* or the subspecies (*T. brucei brucei*) are not human infective, but cause animal trypanosomiasis in wild and domestic animals (http://www.who.int/mediacentre/factsheets/fs259/en/).

T. b. gambiense causes disease in Central and Western Africa that is called Gambian HAT (Figure 1.1). It is a chronic illness that can take years or decades before fatality (Checchi et al., 2008). It is an anthroponotic disease with a minor role for animal reservoirs. It is responsible for 98% of HAT cases reported in the last decade (Franco et al., 2014). *T. b. rhodesiense* causes disease in Eastern and Southern Africa that is called Rhodesian HAT (Figure 1.1). It is an acute disease causing death within weeks or months upon infection (Odiit et al., 1997). It is a zoonotic disease, affecting mainly animals (livestock and wildlife) (Franco et al., 2014).

The prevalence of HAT is between 14° North and 29° South in many countries of sub-Saharan Africa. Therefore, about 60 million people are estimated to be at the risk of getting infected (Kennedy, 2013). Countries mostly affected are the Democratic Republic of Congo, Angola, and South Sudan, where it mainly affects impoverished rural communities. Several human epidemics of HAT have been recorded in Africa over the last century. The major one occurred between 1896 and 1906 and affected mostly Uganda and the Congo

basin. This outbreak was followed by one in 1920 which struck several African countries. The disease did resurge in the 1970s and led to alarming epidemics in the 1990s. In the Central African Republic, Chad, Democratic Republic of Congo, Cote d'Ivoire, Guinea, Malawi, Uganda and the United Republic of Tanzania the threat of HAT remains a significant public health problem, with 50-1000 new cases reported every year (www.who.int). Countries such as Burkina Faso, Cameroon, Equatorial Guinea, Gabon, Kenya, Mozambique, Nigeria, Rwanda, Zambia, and Zimbabwe are reporting fewer than 50 new cases per year (Figure 1.1). In countries such as Benin, Botswana, Burundi, Ethiopia, Gambia, Ghana, Guinea-Bissau, Liberia, Mali, Namibia, Niger, Senegal, Sierra Leone, Swaziland and Togo transmission seems to have stopped and no new cases have been reported for several decades (www.who.int).

The steady decrease of HAT cases reported during the last 10 years in Africa has led the World Health Organization (WHO) to speculate about the elimination of HAT as a public health problem (defined as less than 1 annual case/10.000 inhabitants in HAT endemic foci) being achieved by 2020. However, it is estimated that a significant number of new cases are still unreported or undiagnosed (Brun et al., 2010; Fevre et al., 2008; Kennedy, 2013). The non-diagnosed population has been recently explained by the discovery of healthy carriers, i.e. infected but asymptomatic patients (Capewell et al., 2016; Casas-Sánchez and Acosta-Serrano, 2016; Sudarshi et al., 2014). This is supported by the recent description of skin or fat dwelling trypanosomes (Capewell et al., 2016; Trindade et al., 2016) and the meningeal stage from which trypanosomes could invade the brain via the Virchow-Robin space thereby bypassing the blood-brain barrier (Mogk et al., 2016). These results provide strong arguments to raise up attention on potentially overlooked human and animal reservoirs.
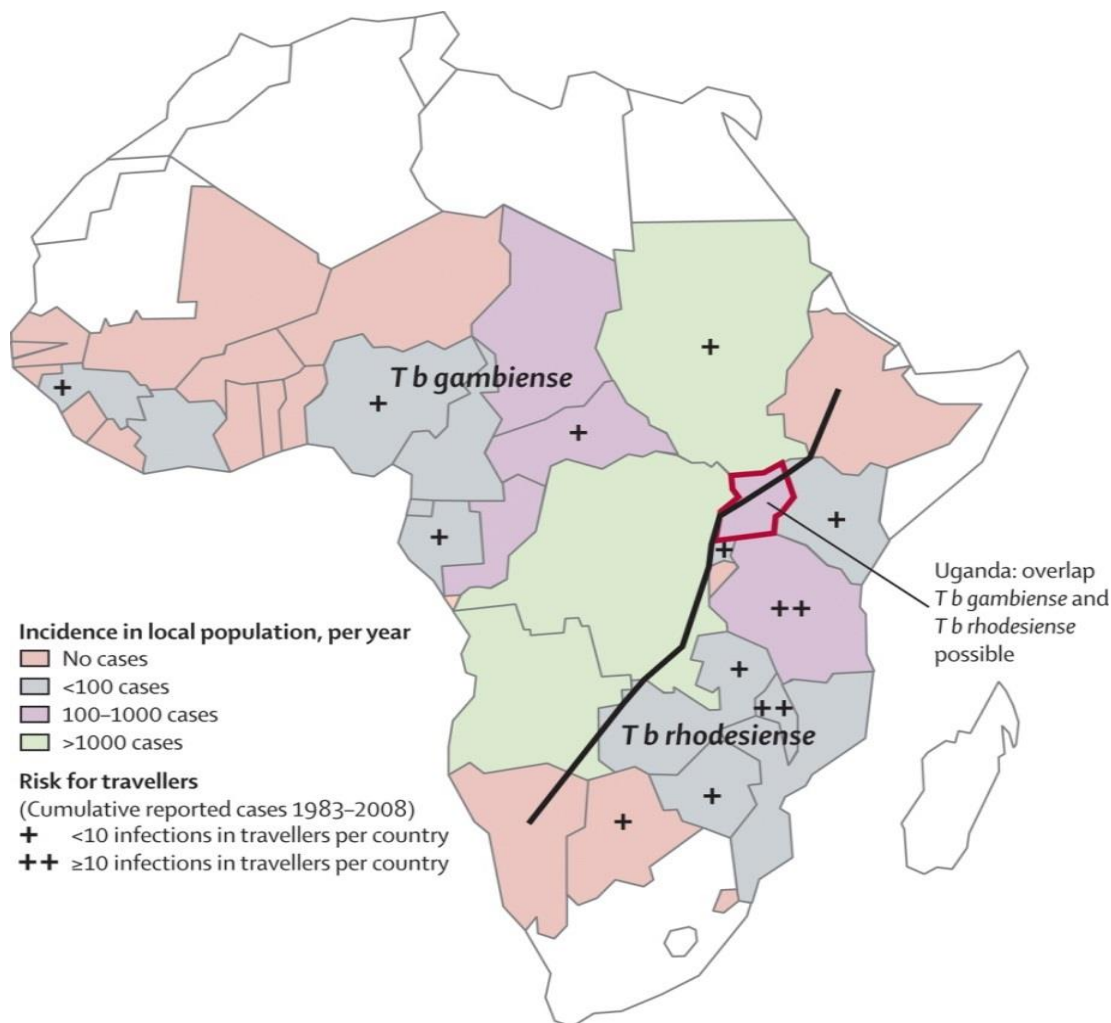
Figure 1.1: Distribution of human African trypanosomiasis with incidences and risk for travelers. The black line divides the areas in which *Trypanosoma brucei gambiense* prevails and those in which *Trypanosoma brucei rhodesiense* predominates (Brun et al., 2010).

1.1.2 Clinical Features

The clinical presentation of HAT depends on the parasite species, the stage of the disease and the host. The signs and symptoms that characterize sleeping sickness are mainly the same for both forms of the disease but differ in their frequency, severity, and kinetics of appearance. Rhodesiense HAT is an acute illness, which progresses to second-stage within a few weeks and usually to death within 6 months. Gambiense HAT is a more chronic disease; the second stage is usually reached within weeks to months. Usually, both stages of the illness are considered fatal if untreated. The human population living in HAT endemic countries could be divided into different groups: susceptible (uninfected); infected asymptomatic and infected symptomatic. The healthy carriers or infected asymptomatic HAT patients are defined as people living symptomless with the

disease with up to several decades (Sudarshi et al., 2014). This indicates that many more people might be carrying the transmissible parasites and remained out of control in endemics countries.

So far it has been described that both forms of HAT progress in two stages, the first called haemolymphatic stage and the second called meningo-encephalitic stage. The first stage starts when the parasite enters the human blood and lymph vessels, they spread into the lymph node and systemic organs like spleen, liver, eyes and endocrine organs. The second stage is when the parasite invades the CNS via crossing the blood-brain barrier (BBB) or blood-CSF barrier (BCB).

During the first or haemolymphatic stage of the disease, Gambiense HAT patients can present intermittent nonspecific symptoms such as fever, fatigue, headaches, arthralgies, and pruritus. Afterward, the cervical lymph nodes in the neck may swell, an often observed symptom called "the Winterbottom sign". This observation was recognized as an alert sign for HAT long ago by Sir Thomas Masterman Winterbottom, who noted that slave traders in the last 18th century used neck swelling as an indicator of sleepiness or abnormal behavior that made particular slaves undesirable (Chappuis et al., 2005).

During the second stage, the sleep disorder is the main major symptom. It leads to sleep-wake cycle disruption and sleep structure alterations (Buguet et al., 2005). The structure of sleep is altered and characterized by episodes of sleep-onset rapid eye movement (SOREM) (Buguet et al., 2001, 2005). The hallmark of sleeping sickness, i.e. changes of the sleep/wake cycles, leads to a profound polyphasic sleep-wake pattern, characterized by SOREM episodes, which may appear earlier than the sleep-wake alterations (Kristensson et al., 2010).

The sleep structure alterations, including SOREM episodes, have been shown to recede or disappear after treatment of infection and improvements may take several months after treatment to unfold (Buguet, 1999). It has been indicated that sleep-wake changes in HAT are not directly related to the presence of the parasite in the brain, and points to slowly reversible functional alteration and/or to compensatory mechanisms over time, rather than to severe structural damage of sleep-wake regulating regions during the disease (Kristensson et al., 2010).

Based on our experimental findings that trypanosomes cannot survive in CSF, the cyclic appearance of the parasite in CSF, location of the parasite in the pia mater (meningeal stage) and the variability of the time interval from the initial infection (skin or blood stage) before brain invasion (encephalitic stage) are proof of the exitence of trypanosome populations in other tisues playing important to sustain the cycle infection versus transmission. Those findings reveal that the trypanosome must adapt itself for surviving at different selection pressure area during the HAT infection progression. Afterward, the selected survived parasite will spread from those various stages to susceptible tissues close to the ventricular system that does not have the blood-brain barrier like the circumventricular organs (CVOs) and pia matter or basal meninges. The localization of basal

meninge or CVOs trypanosomes may impair the CVOs physiological functions and correspond to commonly observed HAT symptoms. This lead us to recently propose a correlation between the symptoms and infected organs in a three-stage model (Mogk et al., 2016) (Figure 1.2).
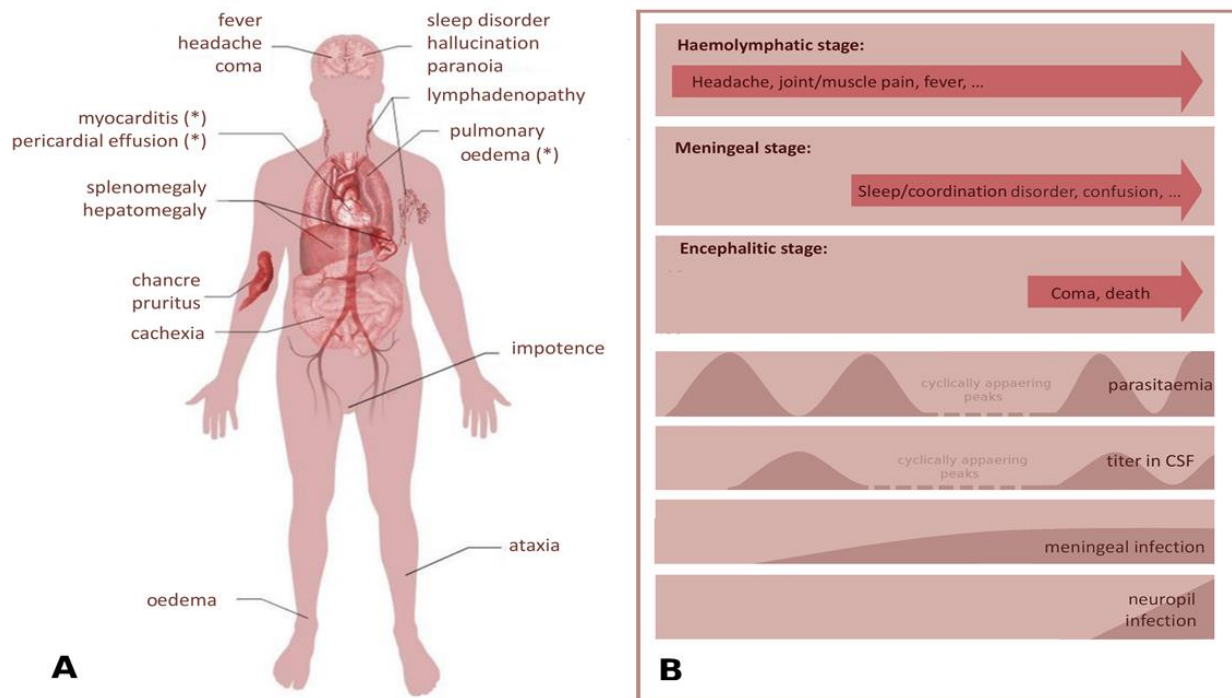
Figure 1.2: **(A)** Symptoms of HAT (Enanga et al., 2002). (*) symptoms only observed in East African trypanosomiasis, which is caused by *T. brucei rhodesiense*. Body scheme derived from Mikael Häggström (University of Uppsala). **(B)** Suggested correlation between symptoms and infected organs in a three-stage model of HAT infection (haemolymphatic, meningeal and encephalitic). (A) and (B) figures derived from Mogk et al., 2016.

It was reported that molecules produced by trypanosomes, especially the prostaglandins D_2 (Duszenko et al., 2006; Figarella et al., 2005, 2006), may also be involved in the dysfunction of sleep-wake cycles (Urade and Hayaishi, 2011).

Moreover, cytokines such us TNF-α and IFN-γ released by the host immune response may also trigger the sleep-wake deregulation during the HAT infection (Kristensson et al., 2010).

Neurological and psychological symptoms have been observed during second-stage HAT such as personality changes, hallucination, and coma.

1.1.3 Diagnosis

In general, clinical signs and symptoms such as fever, swollen lymph nodes or neurological signs are not unique to make HAT diagnosis specific. They just provide a hint for diagnosis but are not sufficient to start treatment. The correct diagnosis of HAT is therefore field- and laboratory-based and consists of three steps (Chappuis et al., 2005): screening, diagnosis confirmation, and staging of the disease.

For screening of the Gambiense HAT infection, a card agglutination test for trypanosomiasis (CATT) was developed in the late 1970s that can be performed on blood and serum. CATT is a rapid, simple assay for the detection of specific antibodies in blood of Gambiense HAT patients (Lejon et al., 1998). The CATT antigen present on the card was raised against the complete bloodstream form of *T. b. gambiense* variable antigen type LiTat 1.3, i.e. containing also the invariant cross-reacting determinant. The sensitivity of CATT is about 87-98% and the specificity about 93-95% (Brun et al., 2010; Chappuis et al., 2005). CATT is the best adapted and most efficient screening method and is widely used in endemics areas (Brun et al., 2010). However, the CATT is not available in a single format, requires a cold chain for storage, and uses equipment that requires electricity (Bisser et al., 2016).This challenge is ongoing to be solved by recent progress and development of acurate and sensitive rapid diagnostic test (RDT) for HAT (Bisser et al., 2016; Sternberg et al., 2014).

For diagnostic confirmation, the demonstration of the parasite in body fluids provides explicit evidence of trypanosome infection. This diagnosis is made by microscopic examination using a lymph node aspirate or a blood sample. The delay between sampling and examination should be kept as short as possible to avoid lysis of trypanosomes. The sensitivity of lymph node palpation and aspiration varies from 40% to 80% dependent on parasite strains, stage of the disease (this test is more sensitive during the first stage) (Brun et al., 2010), and prevalence of other diseases that cause lymphadenopathy.

Because examination of thin or thick blood films has very low sensitivity, concentration methods such as the microhaematocrit centrifugation technique (Woo and others, 1970), the quantitative buffy coat test (Ancelle et al., 1997; Truc et al., 1998), or the miniature anion-exchange centrifugation technique have been developed and are widely used (Lutumba et al., 2006, 2007). Molecular tests such as polymerase chain reaction (PCR) and loop-mediated isothermal amplification (LAMP) based on detection of the parasite's nucleic acids (DNA or RNA) are attractive alternatives for parasite detection (Deborggraeve and Büscher, 2010, 2012; Hayashida et al., 2015).

For staging of the disease, the presence of parasites, more than five white blood cells per µl, or an increased protein content (>370 mg/L) within CSF defines the second stage according to WHO recommendations (Brun et al., 2010). This recommendation is now subjected to controversy that may have some impact on the staging decision.

Diagnosis of Rhodesiense HAT differs from that for Gambiense HAT in several ways. First, there is no serological screening test for Rhodesiense infections, and second, the parasitological confirmation is easier because the density of parasites in blood is usually higher than in Gambiense infections (Brun et al., 2010). Research and development of methods for diagnosis and staging of HAT are still under investigation through an initiative by WHO and the Foundation for Innovative New Diagnosis (FIND) (Brun et al., 2010).

1.1.4 Treatment

The chemotherapy of HAT has historical roots that date back to the pioneering work by Paul Ehrlich on dyes and arsenicals (Fairlamb, 2003). The drugs currently used depend on the stage of the disease. Unfortunately, they all have many adverse side effects.

For early stage HAT, pentamidine and suramin are used for treatment. Pentamidine was developed in the 1930s by the English chemist Arthur James Ewins, an employee of the May and Baker pharmaceutical company (Steverding, 2008). It is administered by intramuscular or intravenous injection once daily for 7 days. The drug is effective but associated with pain at the injection site, hypo- or hyperglycemia, hypotension, leukopenia, a prolonged QT interval on electrocardiograms, nephrotoxicity and gastrointestinal symptoms (Nagle et al., 2014; Stein et al., 2014).

It binds to tissue proteins, thus contributing to a large application volume, and has a long terminal half-life (Nagle et al., 2014). It does not cross the blood-brain barrier. It is concentrated in trypanosomes via uptake by aminopurin (P2) and other surface transporters (Nagle et al., 2014). The mechanism by which pentamidine kills the parasite is not well understood and nonspecific. It may act by binding to DNA or by disrupting mitochondrial functions.

Suramin, introduced in 1922, is till today the first line drug to treat Rhodesiense HAT given by slow intravenous infusion every 3-7 days for a 4 week period (Brun et al., 2011). It is highly protein bound and has a very long terminal half-life of 41-78 days; it does not cross the blood-brain barrier (Nagle et al., 2014). Suramine adverse effects include neuropathy, rash, fatigue, anemia, hyperglycemia, hypocalcemia, coagulopathies, neutropenia, and nephrotoxicity (Stein et al., 2014).

For late stage HAT, the arsenical melarsoprol or a nifurtimox-eflornithine combination therapy (NECT) are currently used for treatment. Arsenicals were the first drug group introduced in 1906 to treat HAT starting with a drug called atoxyl. It was often fatally or caused blindness due to optic nerve atrophy (Stein et al., 2014). Melarsoprol drug was effective for treatment of late stage HAT due to *T. b. rhodesiense* and *T. b. gambiense*. It is extremely toxic with up to 10% of all patients developing a post-treatment reactive encephalopathy (PTRE) that lead to death in about 50% of these cases (Blum et al., 2001). It is also associated

with pyrexia, headache, pruritus, thrombocytopenia and heart failure (Stein et al., 2014). It is concentrated in trypanosomes via uptake by the aminopurin (P2) transporter and disrupts the redox environment within the cell by interacting with the protein trypanothione (Fairlamb et al., 1989; Nagle et al., 2014).

Difluoromethylornithine (DFMO) (named: eflornithine) was repurposed from investigations as an anticancer agent (Stein et al., 2014). It is a specific inhibitor of ornithine decarboxylase (ODC) and the first enzyme that converts ornithine to its biogenic amine putrescine as the first step in polyamine biosynthesis. It acts on the mammalian enzyme as well as on the trypanosomal ODC but owing to the rapid turnover to the mammalian ODC; the drug exerts much less toxicity on host cells as compared to bloodstream trypanosomes (Stein et al., 2014). DFMO is more efficient as melarsoprol and has a superior safety profile (Chappuis et al., 2005). It was called "resurrection drug" due to its spectacular effect on comatose sleeping sickness patients (Stein et al., 2014). The problems with eflornithine are the dose regimen (administration is intravenous: 100 mg/Kg every 6 h for 14 days) and the high cost of the production process (Stein et al., 2014). It is also associated with side effects such as fever, headache, hypertension, macular rash, peripherical neuropathy, tremor and gastrointestinal problems (Fairlamb, 2003; Stein et al., 2014).

A significant advancement in HAT chemotherapy was the introduction of eflornithine combined with nifurtimox (NECT) to solve the problem of large dose intravenous infusion administration at 200 mg/Kg every 12 h for 7 days (rather than 100 mg/Kg every 6 h for 14 days as monotherapy) combined with nifurtimox orally administered at 15 mg/Kg three times a day for 10 days (Priotto et al., 2009). Nifurtimox was repurposed as a drug for treating American trypanosomiasis (Chagas disease). However, the need of intravenous infusion coupled with the high cost of distribution remained the drawback of NECT. Therefore, more research efforts must be made to develop a better suited drug that is ideally easy to administer (preferably orally) over a short time course and effective against both, early and late stage HAT.

At the moment, Fexinidazole and Oxaboroles (SCYX-7158) are drug candidates in clinical trials of HAT. Fexinidazole was initially identified through the screening of a collection of nitroheterocyclic molecules by the Drugs for Neglected Disease initiative (DNDi) (Jones and Avery, 2015). It is available in an oral formulation as nitroimidazole prodrug and has been shown to be active *in vivo* in both, acute *T. b. rhodesiense* and *T. b. brucei* CNS murine models; the compound entered clinical trials in 2014 (Kaiser et al., 2011; Torreele et al., 2010). For the phase I trials, it has been reported that Fexinidazole was well tolerated at doses up to 3600 mg with headache and vomiting (that resolved spontaneously) being the only adverse effects (Tarral et al., 2014). Phase II/III (safety and efficacy) trials, evaluating this regimen in late-stage patient infections, are still ongoing in the Democratic Republic of the Congo (DRCongo) and the Central African Republic (CAR) under the direction of DNDi in collaboration with the Swiss Tropical and Public Health Institute (Swiss TPH).

The oxaborole (SCYX-7158) compound derived from a screening of a library of boron-based compounds from Anacor Pharmaceuticals against *T. brucei* cultures (Ding et al., 2010). It entered Phase I clinical trials for the treatment of HAT. Previous studies revealed that SCYX-7158 is an effective, safe, orally active treatment in both acute and chronic murine models of HAT. Pharmacokinetic studies suggest that once a day dosing would be sufficient due to the maintenance of drug concentrations above the minimum trypanocidal concentration for 14 to 20 h (Jacobs et al., 2011; Jones and Avery, 2015). Like fexinidazole, phase II/III trials evaluating the treatment are still ongoing in DRCongo and CAR. So far, preliminary outcomes from the trials have not been reported.

1.2 *Trypanosoma brucei* as pathogen

1.2.1 Taxonomy of trypanosomes

Trypanosomes are flagellated protozoa that are classified as members of the kingdom of *Excavata*, the phylum *Euglenozoa,* and the phylogenetic order *Kinetoplastida* (Figure 1.3).

Euglenozoa are cells with one or two flagella that emerge from an apical or subapical flagellar pocket. *Kinetoplastida* are *Euglenozoa* that contain a kinetoplast, which is a large mass of fibrillar DNA in the mitochondrion and closely associated with the flagellar bases.

The taxonomy of *Kinetoplastida* is divided into two groups: *Bodoninae* and *Trypanosomatinae*, which is based on morphology and life cycles. The Bodoninae group is characterized by a large kinetoplast and two flagella. This group is formed by free-living organisms and parasites of fish and snails. The *Trypanosomatinae* have a smaller kinetoplast and a single flagellum. This group is formed by parasites of invertebrates.

The phylogenetic tree of *Trypanosomatinae* was generated using the comparison of nuclear small and large ribosomal RNA gene sequences. It revealed that *Trypanosoma* is the most ancient Trypanosomatinae, followed by *Blastocrithida* and Phytomonas lineages, some time later *Crithida* and *Leptomonas* separated while *Leishmania* and *Endotrypanum* branched off after that. The genus *Trypanosoma* is divided into two sections: *Salivaria* and *Stercoraria* according to the place where the parasite develops in the insect host. Salivaria develop in the anterior portion of the digestive tract and within the salivary gland, while the Stercoraria develop in the hindgut.

The section Stercoraria includes only the American trypanosome, *T. cruzi*, that causes Chagas disease. It is transmitted via the feces of its reduviid vector. *T. brucei* belongs to the Salivaria section consisting of the subspecies *T. b. brucei* that is not a human pathogen, as well as of *T. b. gambiense* and *T. b. rhodesiense*, which induce HAT. The Salivaria are injected into the mammalian lymph and blood system via the bite of a tsetse fly.
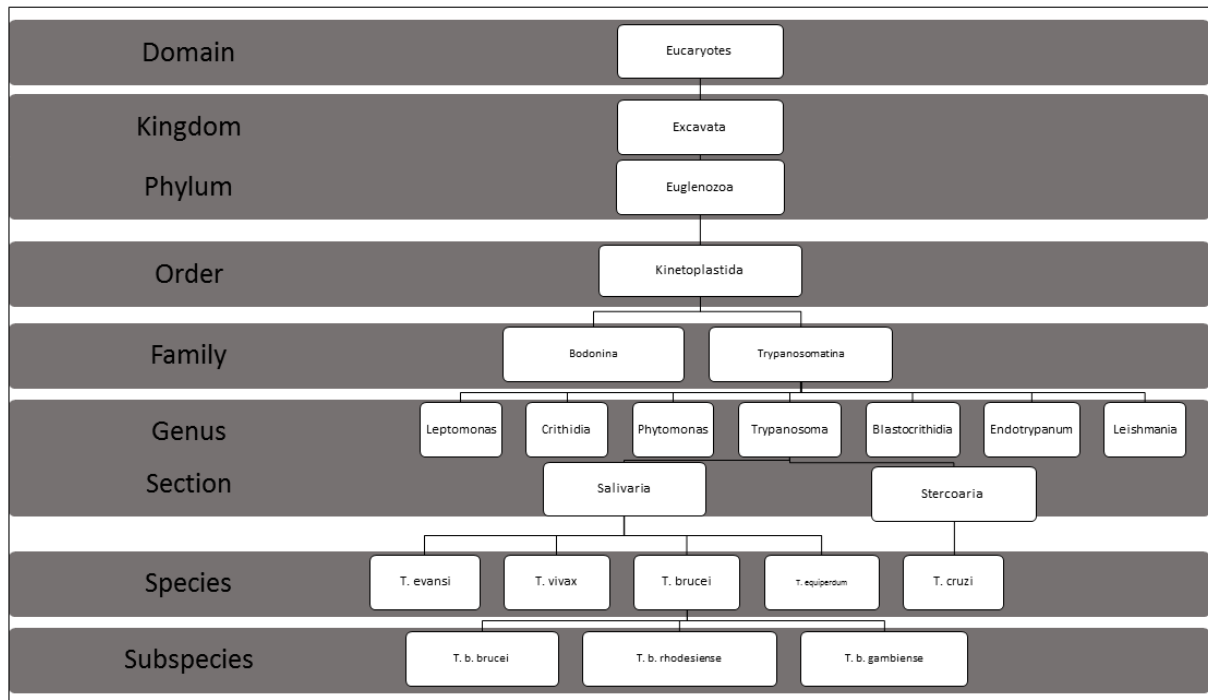
Figure 1.3: Systematic classification of *Trypanosoma brucei*.

1.2.2 Morphology and Cell structure

The African trypanosome is an elongated hemoflagellate containing a highly polarized cytoskeleton formed by microtubules (Matthews, 2005). The polarity of the cell is determined by the polarity of the microtubules comprising its cytoskeleton, with the positive pole as its posterior and its negative pole at its anterior end (Ooi and Bastin, 2013). The microtubular cytoskeleton defines the cell shape and remains intact throughout the cell cycle. During cell division, new microtubules are beeing assembled and interdigitated between existing microtubules, so that cytoskeletal inheritance is semiconservative (Sherwin and Gull, 1989).

The trypanosome cell is about 14-40 µm long (Mogk et al., 2014), 5 µm thick (Field et al., 2004) and has a single flagellum that is responsible for the parasite's motility. Trypanosomes can be easily identified microscopically using Giemsa or DAPI staining, which clearly labels the two essential nucleic acid containing organelles, the nucleus, and the kinetoplast. The single-copy organelles within trypanosomes (i.e. the flagellar pocket, flagellum, kinetoplast, mitochondrion, and nucleus) are precisely positioned within the cytoskeletal corset and are concentrated between the posterior end and the center of the cell (Figure 1.4) (Field et al., 2004).

The single flagellum possesses a conventional axonemal structure consisting of a 9+2 array of microtubules and a large lattice-like structure called paraflagellar rod (PFR) (Vaughan and Gull, 2003). It exits from the

flagellar pocket at the posterior end of the cell and attaches along exterior length of the trypanosome's body via a specialized cytoskeletal structure termed flagellum attachment zone (FAZ). The FAZ is composed of a single protein filament and specialized four microtubules that associate with the smooth endoplasmic reticulum (Kohl et al., 1999). The FAZ protein composition is still not known, but some proteins have been localized to the FAZ filament. It has been shown that RNA interference (RNAi) inhibiting FAZ protein biosynthesis causes a defective cytokinesis (Morriswood et al., 2013; Vaughan et al., 2008; Zhou et al., 2011).

In trypanosomatids, the flagellum beats from tip to the base, with anterior and posterior poles of the cell defined according to their position during motility (Robinson et al., 1995).

The flagellar pocket is the only site of endo- and exocytosis (Engstler et al., 2004). Endocytosis is of great significance in bloodstream form trypanosomes, because essential exchanges into and out of the cell and VSG recycling occurs at the flagellar pocket (Ooi and Bastin, 2013).

The nucleus is located in the central region of the cell and contains 11 diploid pairs of megabase chromosomes, 1-5 intermediate chromosomes, and roughly 100 minichromosomes of unknown ploidy (Akiyoshi and Gull, 2013). These chromosomes are linear and have typical telomeres repeats (TTAGGG) at the ends. It has been shown that all the trypanosome housekeeping genes are encoded mainly in the megabase chromosomes and are transcribed as long polycistronic units (Ersfeld, 2011). The 26-Mb megabase chromosomes genomes contain approximately 9000 genes, including 1000 non-expressed variant surface glycoproteins (VSG). The VSG is a single surface coat protein, highly immunogenic and expresses by *T. brucei* from one of approximately 15 expression sites (ESs), which are located to the telomeres of megabase or intermediate chromosomes (Akiyoshi and Gull, 2013). *T. brucei* as extracellular protozoa manage to escape the host immune system by switching the expression of VSG up to once per 100 cell divisions (Morrison et al., 2005; Mugnier et al., 2016; Turner, 1999).

The kinetoplast is located at the posterior end of the cell. It is known to be the mitochondrial DNA that is associated with the base of the flagellum. This structure is significantly larger than the mitochondrial genomes in other eukaryotic cells. Hence it is prominently stainly with DNA-specific dyes. It comprises a series of intercatenated circular DNA molecules, including maxi-circles that encode a small proportion of the mitochondrial proteins and mini-circles that encode guide RNAs.
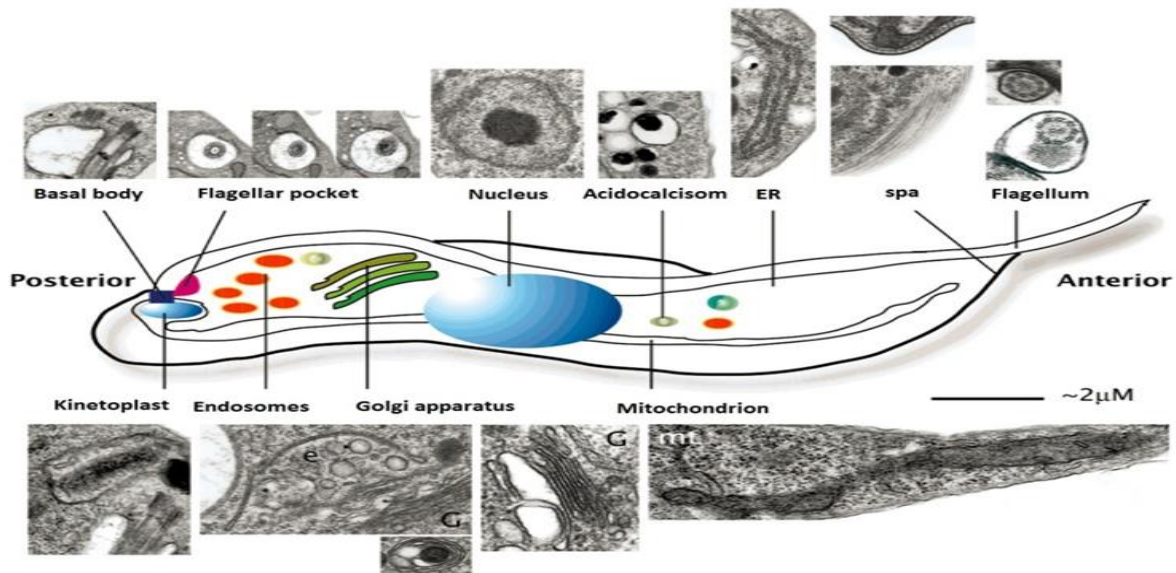
Figure 1.4: Morphologie of *Trypanosoma brucei*. The central image is a cartoon showing the location of the major organelles and structures. The endoplasmic reticulum (ER) has been omitted for clarity as this structure extends throughout the cell and forms the nuclear envelope. The structures shown are the basal body, the flagellar pocket, the nucleus, supellicular microtubular array (spa), the flagellum, the kinetoplast, endosomes, the Golgi apparatus, the mitochondrion, the endoplasmic reticulum (ER) and acidocalcisomes. Insets show examples of these structures as seen by thin section transmission electron microscopy (Field et al., 2004).

1.2.3 Life Cycle

Trypanosomes are transmitted by blood-feeding tsetse flies of the genus Glossinae (Figure 1.5). The life-cycle is relatively complex, with various stages of distinctive morphology, biochemistry and physiology in the mammalian hosts and in the insect vector (Figure 1.6). The transformation from bloodstream to insect forms includes degradation and finally loss of the variant surface glycoprotein (VSG) by coordinated action of a metalloprotease (named major metalloprotease B) MSP-B and the GPI-specific phospholipase C. Specifically, TbMSP-B seems to be responsible for the remodeling of VSG during differentiation (Donelson, 2003).

The procyclic form expresses a different type of surface protein that has been named procyclin (Roditi et al., 1989). Procyclic parasites replicate in the insect midgut before they migrate to the salivary gland. Here it differentiates to the epimastigote form that attaches with part of its flagellum to epithelial cells of the organ (Hendry and Vickerman, 1988; Vickerman et al., 1988).

The final differentiation step is the formation of the infectious free swimming metacyclic form, characterized by the acquisition of the protective variant surface glycoprotein coat (VSG). Trypanosomes contain several hundred VSG genes, out of which only one protein is expressed at a given time. This coat protects the parasite from the cellular immune system response and seems to inhibit complement reactions. The VSG coat is immunogenic and leads to the formation of specific antibodies that opsonize and eventually kill all parasites that carry this specific VSG type. However, due to antigenic variation, new populations appear spontaneously carrying a different coat formed from VSG switch variants and escape the destruction by the immune system. Thus, the trypanosomal infection is characterized by an oscillating population density in blood.

In addition to this host-induced density regulation, trypanosomes differentiate in blood from dividing long slender to a non-dividing stumpy form that is preadapted to survive in the insect's midgut. This differentiation depends on the slender population density and is induced by a secreted low-molecular-weight factor (stumpy inducing factor (SIF)) (Vassella et al., 1997) of so far unknown chemical identity that enriches in conditioned culture media (Hamm et al., 1990). SIF works like an autocrine mediator that is released from slender cells and induces slender cells to differentiate to the stumpy form, which cannot proliferate within the mammalian host but are needed for tsetse fly infection.

Metacyclic forms are injected during a tsetse blood-meal and trypanosomes, injected subdermally, initially proliferate at the site of injection, often forming a reaction at the location of the tsetse fly bite called chancre, but concomitantly they also appear in the blood and lymphatic vessel. It has been recently demonstrated that infective metacyclic trypanosomes can be acquired from the dermis inoculation site immediately after the initial transmission and that intradermal parasite expansion induced skin surface temperature elevation (Caljon et al., 2016).

In man, the life cycle of trypanosomes proceeds and ends with infection of the central nervous system (CNS). The parasite's progression from the bloodstream to the CNS will take a latency of weeks (Rhodesiense HAT) or months to years (Gambiense HAT). The parasite will travel to the brain either by crossing the blood-brain barrier (BBB) and settle down in the brain parenchyma (Grab and Kennedy, 2008; Mulenga et al., 2001), or by crossing the blood-CSF barrier (BCB) (Mogk et al., 2016). There still is considerable controversy by which way trypanosomes invade the CNS: across the BBB or across the blood-CSF barrier (BCB)? Following the literature on trypanosome brain invasion, there is much experimental evidence showing that trypanosomes cross the BBB via different mechanisms, but it has been demonstrated that trypanosomes could not survive in the brain parenchyma (Wolburg et al., 2012). It has been shown by electron microscopy studies that trypanosomes first appear in the choroid plexus by crossing the fenestrated endothelium cell layer of plexus vessels. Some of the parasites die within the plexus's stroma, but some trypanosomes make their way to the ventricle and move on to the sub-arachnoid space, where they finally settle between the cells of the pia mater (Wolburg et al., 2012). The pia mater is the innermost layer of the meninges (dura mater, arachnoidea mater

and pia mater), which surround the brain and the spinal cord. Trypanosomes cannot survive within the stroma of the plexus nor within the CSF as it contains a trypanocidal compound, the pia mater is safety place for living at all time of the infection (Wolburg et al., 2012).

Mogk et al., 2014, showed that trypanosomes repeatedly cross the BCB depending on their cell density in the blood. Thus, Mogk et coworkers suggested the existence of an additional distinct meningeal stage from where the trypanosomes can invade the brain via the Virchow-Robin space thereby bypassing the blood-brain barrier. This mechanism would lead to three instead of two steps: first, the haemolymphatic stage; second, the meningeal stage; third, the encephalitic stage characterized by the invasion of the CNS and the occurrence of encephalopathy (Mogk et al., 2016).
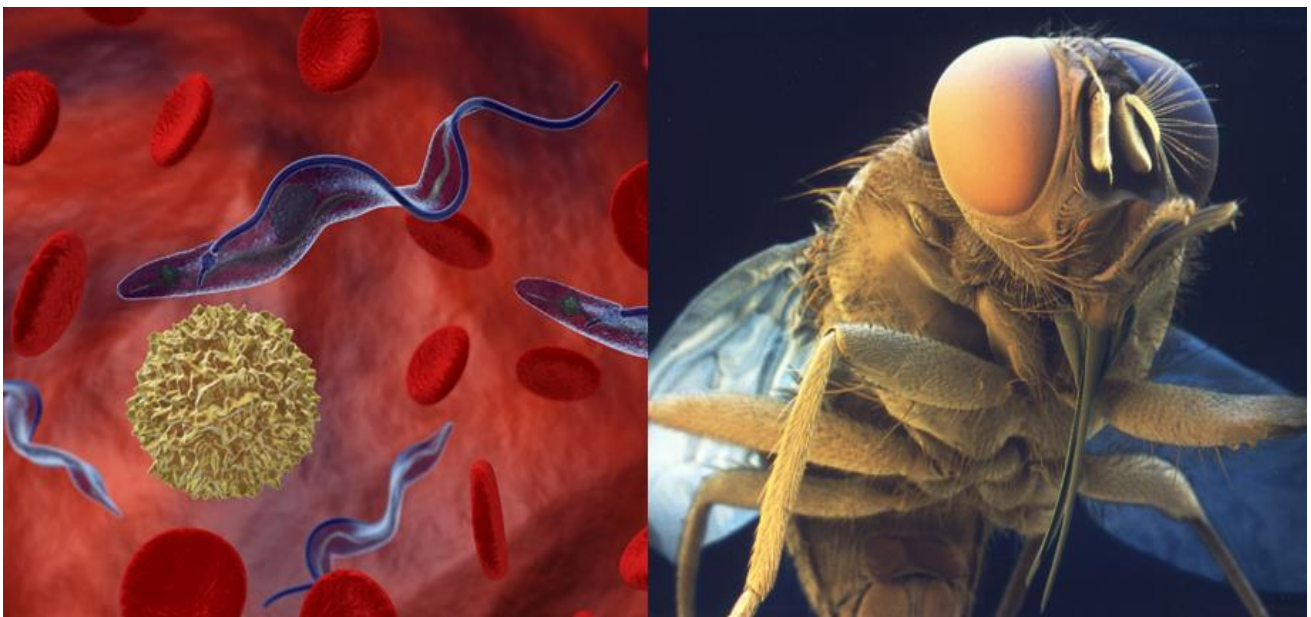
Figure 1.5: Trypanosomes within blood **(A)**, and **(B)** the tsetse fly vector (Michael Duszenko, University of Tübingen, Germany).
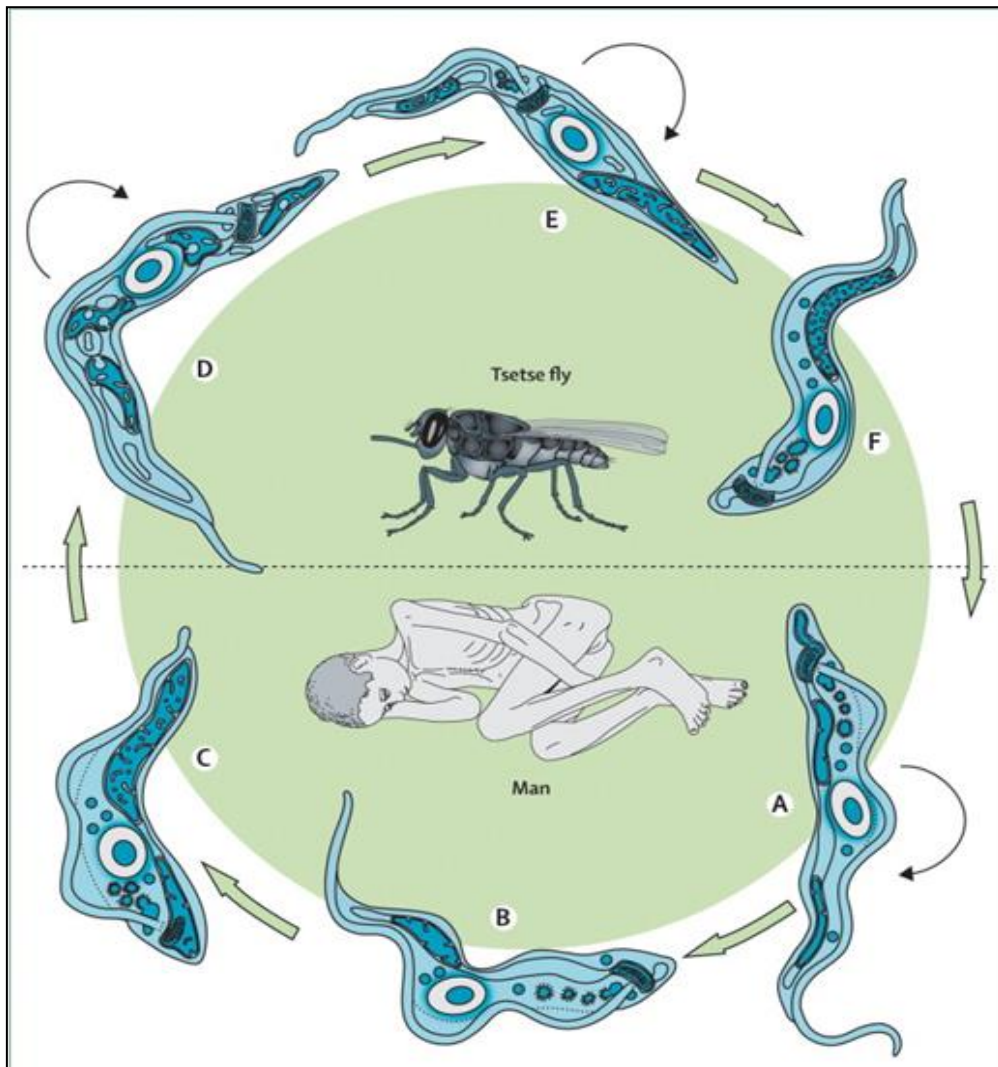
Figure 1.6: Life cycle of African trypanosomes: In man, the bloodstream form shows a polymorphism **(A)** dividing (black arrows) slender forms, **(B)** intermediate forms, and **(C)** stumpy forms. In the tsetse fly vector, the stumpy form transforms to **(D)** the dividing midgut form, then to **(E)** the migrating epimastigote form, which multiplies in the salivary glands to **(F)** the infective metacyclic form, which is injected during the next blood meal into the mammalian host (Barrett et al., 2007).

1.3 RNA interference in *Trypanosoma brucei*

Fire et al. first described RNA interference (RNAi) during their research with the nematodes worm *Caenorhabditis elegans* and described post-transcriptional gene silencing of a target gene sequence, mediated by double-stranded RNA (dsRNA) (Fire et al., 1998).

It has also been discovered to occur in *Trypanosoma brucei*. *T. brucei* transient expression, or electroporation of the dsRNA homologous to α-tubulin mRNA led to downregulation of α-tubulin synthesis because the

corresponding mRNA was degraded (Ngo et al., 1998). The silencing effect was not specific to α-tubulin mRNA but could be obtained with dsRNA homologous to other mRNAs (Ullu et al., 2002).

After that, RNAi has been intensively studied in many other organisms, including the plant *Arabidopsis thaliana*, the fruit fly Drosophila and the Zebrafish of the carp family. However, RNAi is notably absent in protozoans closely related to *T. brucei*, such as *T. cruzi* and *Leishmania major* (Motyka and Englund, 2004).

The existence of the RNAi system in *T. brucei* was confirmed by the identification of endogenous small interfering RNA (siRNAs) in *T. brucei* (Djikeng et al., 2001). Furthermore, two of the classical proteins required for the RNAi pathway namely, TbAGO1, a member of the Argonaute family of proteins (Kolev et al., 2011), and two Dicer-like homologs, TbDCL1 and TbDCL2 (Patrick et al., 2009; Shi et al., 2006) exist in *T. brucei*.

Mechanistically, RNAi is a two-step process (Figure 1.7). During the first step, the dsRNA that triggers the silencing response is cleaved into small interfering RNAs (siRNAs) of 21-25 nucleotides. It is accomplished by Dicer, an RNase-III-family nuclease. In the second step, siRNAs are incorporated into a targeting complex, known as RISC (RNA-induced silence complex), which destroys mRNAs that are homologous to the integral siRNA (Balaña-Fouce and Reguera, 2007). The result is a suppression of the respective gene expression. RNAi has become the method of choice to elucidate the function of individual genes in *T. brucei* (Tschudi et al., 2003). It is relatively easy to apply and a fast option as compared to knockout experiments, on which ablation eliminates all copies of the gene of interest.
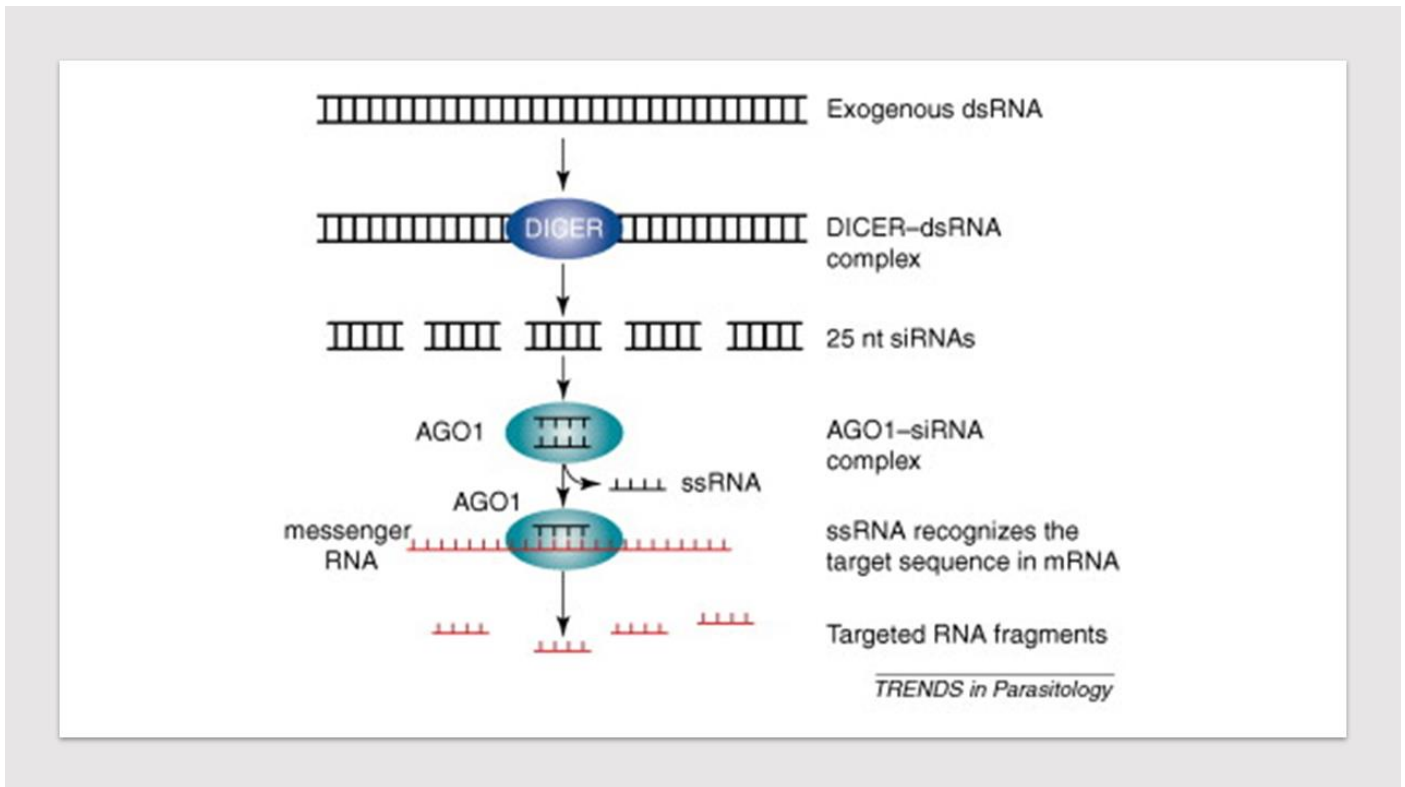
Figure 1.7: Representation of the RNAi pathway in trypanosomes (Balaña-Fouce and Reguera, 2007).

1.4 *In vivo* Protein Crystallization

Protein crystallization is a mainstream research technique for the elucidation of protein function and structure based drug design. Protein crystallization is a multi-parameter process that is very difficult to predict (McPherson and Gavira, 2014).

In the last decades great efforts have been made by structural biologists for developing crystallization tools or deciphering the mechanisms by which proteins crystallize and more to predict protein crystallizability based on the protein sequence.

The formation of well-ordered protein crystals is still a challenge in X-ray crystallography. This is, in particular, the case for glycoproteins, lipoproteins, membrane proteins and large protein complexes which are attracting increasing interest due to their vital roles in biological process (McPherson and Gavira, 2014).

The general procedures used to determine the structures of proteins involve many intricate and handling steps: 1) cloning the target gene; 2) expressing of the protein in a suitable expression system; 3) purifying a good yield of the pure protein for crystallization and structure determination. This so-called *in vitro* protein crystallography is the major source of protein crystal structures in PDB database. Typically, *in vitro*

crystallization requires optimization of various conditions, including unphysiological pH values as well as exposure to potent precipitating agents and salts (Kang et al., 2013).

It has been observed in the past that some proteins forms crystals *in vivo* (Doye and Poon, 2006). Prominent examples are (i) storage proteins in plant seeds, (ii) insulin in secretory granules of pancreatic ß-cells, (iii) alcohol oxidase in peroxisomes of methylotrophic yeast, (iv) insecticidal toxins in bacteria such as *Bacillus thuringiensis* and (v) polyhedrin in various types of baculoviruses (Doye and Poon, 2006). As indicated herein, intracellular crystallization is widely associated with cellular functions of protein storage and secretion, solid-phase catalysis as well as environmental protection (Doye and Poon, 2006). Nevertheless, crystallization (and protein aggregation) inside cells also appears to be linked to the pathology of several diseases, either as one of the causes or as a harmful side effect of the disease (Doye and Poon, 2006). For this reason, crystal formation *in vivo* has classically been perceived as an unusual or lucky event and was disregarded from structural biology (Axford et al., 2014; Doye and Poon, 2006).

Recently, *in vivo* crystallization has been observed several times as a result of heterologous overexpression, mostly within cell lines of insect or mammalian origin (Duszenko et al., 2015; Hasegawa et al., 2011). In this manner, the phenomenon of intracellular crystallogenesis has shifted more and more into scientific awareness. Nevertheless, the considerable small size of *in vivo*-grown crystals rendered them seemingly unsuitable for conventional X-ray analysis (Sanishvili et al., 2011; Schlichting and Miao, 2012).

Only the advent of new X-ray sources and new data-processing tools such us XFEL/SFX opened the way for protein structure determination from nano-micro-sized crystals. Numerous independent expert investigators have already demonstrated the applicability of theses techniques (Axford et al., 2014; Gallat et al., 2014; Gati et al., 2014a; Jakobi et al., 2016; Muniyappan et al., 2015; Redecke et al., 2013a; Sawaya et al., 2014), underlining the potential of *in vivo* crystals to become a feasible source of structural biology (Koopmann et al., 2012).

Despite great high technologie tools and increasing numbers of successful examples, the process of *in vivo* crystallization itself is not yet understood in detail. Principally, the underlying mechanism is assumed to be similar to crystal formation *in vitro* (Duszenko et al., 2015).

At first, a high local concentration of the recombinant protein is required to render crystallization thermodynamically favorable and, to some extent, by protein sorting into subcellular compartments offering only limited space (Duszenko et al., 2015). As a result of supersaturation, the equilibrium between liquid and solid phase is reestablished via displacement of protein surrounding water. This, in turn, will favor the formation of interprotein contacts, if suitably positioned interaction sites are accessible. Thereon, orderly associated protein molecules may act as nucleation centers providing surfaces for crystal growth progression. However, there are three examples known that challenge this presumption: (i) formation of *in vivo* crystals

from insecticidal Cry3A from *Bacillus thuringiensis* (Sawaya et al., 2014), (ii) insecticidal protein Cry1Ac from *Bacillus thuringiensis* (Evdokimov et al., 2014), and (iii) µNS viral protein in baculovirus-infected Sf9 cells (Schönherr et al., 2015). The authors reported that in the former two cases a sporulation-like process occurred, while the viral protein in the latter case was involved in virus production and initiated a nucleation process within the host cell.

So far, most examples of *in vivo* crystallization from heterologously expressed genes were obtained using the insect cell-baculovirus expression system (Duszenko et al., 2015).

This system utilizes site-specific transposition to introduce a foreign gene of interest into the polyhedrin locus of baculoviral DNA. Thereby, the newly inserted gene substitutes the open reading frame of viral polh, placing the transgene under direct control of the *polh* promoter. This polyhedrin promoter is very robust and efficient. It induces a high concentration of intracellular protein, one the major prerequisite for *in vivo* crystallogenesis, and spontaneous crystallization will take place within infected insect cells.

1.5   Structure determination from in vivo grown crystals

In conventional X-ray crystallography (beam size >10 µm), crystal sizes of at least 20-30 µm in all three dimensions are required to obtain interpretable diffraction patterns and to withstand the large radiation dose that accumulates during the collection of a complete rotation series from a single crystal (Holton and Frankel, 2010).

In the case of smaller crystal diameters, as obtained by *in vivo* crystallization, the X-ray beam may only partially hit the mounted crystal. Thus, the proportion of the beam that does not intercept the sample contributes anything but the background to the diffraction image, thereby reducing the signal-to-noise ratio and, effectively, the resolution limit. The only way to overcome this bottleneck, the beam size need to be decreased, placing a stringent demand on the technical set-up (Sanishvili et al., 2011). Furthermore, there is a proportional relationship between crystal volume and observable spot intensities (Holton and Frankel, 2010), forcing usage of a high radiation dose to obtain sufficiently strong diffraction signals from small crystals (Chapman et al., 2011; Sliz et al., 2003).

As a consequence thereof, the extent of radiation damage increases (Chapman et al., 2011; Sanishvili et al., 2011). Recently, three important strategies have been developed which can bypass these limitations.

Firstly, X-ray free-electron lasers (XFEL) combined with serial femtosecond crystallography (SFX) can provide high-resolution diffraction data from small crystals. The high-intensity beam obliterates the crystal after one exposure, but before the crystal is destroyed diffraction is collected. This avoids radiation damage by making use of the "diffraction-before-destruction" principle (Barty et al., 2013; Neutze and Moffat, 2012;

Schlichting and Miao, 2012). At this moment, a liquid jet of protein crystals at room temperature is continuously exposed to ultrashot X-ray FEL pulses, each of 10-100 fs duration (Neutze and Moffat, 2012) and with a 10^{12} times stronger peak intensity than obtained by synchrotron radiation (Fromme, 2015). Delivery of such high doses of photon energy ultimately destroys the sample. However, the pulse terminates before damage occurs, allowing to collect millions of diffraction pattern snapshots of the individual, randomly oriented crystals. Data sets are then applied to software algorithms for the three-dimensional structure model resolution. The shortcomings of XFEL are that the cost of the experiment is prohibitively high, instrument beam time availability is very low, and difficulties processing the large amount of data are considerable (Liu et al., 2016). Furthermore, recent studies indicate that even SFX data are affected by radiation damage (Nass et al., 2015). Additional complications arise from the variance in the exposed crystal volume during each shot and fluctuations in the pulse intensity. Scaling is achieved by merging the reflections originating from thousands of diffraction patterns (Kirian et al., 2010, 2011). In XFEL experiments, the sample delivery is commonly achieved via a nozzle that sprays grams of crystalline material at the diffraction beam. Therefore the sample requirement is high, and the delivery nozzle can quite frequently clog up, thus stopping the experiments (Liu et al., 2016).

Secondly, serial synchrotron crystallography (SSX) used a third-generation synchrotron microfocus beamline (beam size reduced to <10 μm) as X-ray source and cryogenic crystals mounted into a rotating loop are serially illuminated with somewhat higher-than-conventional flux densities. In contrast to SFX, multiple diffraction patterns of the same crystal are obtained, increasing the redundancy of the data set.

Thirdly, micro-electron microscopy diffraction (MicroED) is a recently developed method, which allows the collection of high-resolution diffraction data from tiny protein microcrystals using electron cryo-microscopy (cryo-EM) (Shi et al., 2016). MicroED has determined several protein structures. The first structure solved by still diffraction was that of lysozyme at 2.9 Å resolution (Shi et al., 2013) and 2.5 Å resolution by continuous rotation (Nannenga et al., 2014a). This was followed by the elucidation of the structures of catalyse at 3.2 Å resolution (Nannenga et al., 2014b) and of Ca^{2+}/ATPase at 3.4 Å resolution (Yonekura et al., 2015).

In late 2015, the toxic core of α-synuclein structure was determined at 1.4 Å resolution (Rodriguez et al., 2015), and recently the structures of four prion peptides were solved at 1 Å resolution and direct phasing methods (Sawaya et al., 2016).

1.6 Aims of this study

Trypanosoma brucei is an extracellular hemoflagellated kinetoplastid protozoon and the causative agent of HAT. The genome sequence of *T. brucei* revealed that approximately 50% of genes which are uncharacterized

for their biochemical or cellular functions are identified as hypothetical proteins with no homologs in the human host. The hypothetical or uncharacterized proteins validated as essential for parasitic survival and infectivity opens possibilities for new target identification and drug discovery. Previous experiments discovered that *T. brucei* produces PGD_2 PGE_2 and $PGF_{2\alpha}$ from exogenous arachidonic acid (Kubata et al., 2000, 2007).

It was also shown that PGD_2 is one of the best-characterized sleep-inducing substances and PGD_2 injected stereotactically into rat brain parenchyma induced directly sleep phenomenon (Hayaishi, 2000, 2002).

This data joins the Pentreath et al. publication, 1990, showing that a high concentration of PGD_2 is found in CSF of late stage sleeping sickness patients. This motivated us to analyze the prostaglandin biosynthetic pathways in detail and to search for biomolecules secreted by trypanosomes. Firstly, our group could show that PGD_2 induces an apoptotic cells death in stumpy parasites, thus being involved in the parasite's cell density regulation to sustain the infection within the host (Duszenko et al., 2006). Secondly, our group isolated, crystallized, structurally solved and enzymatically characterized the NADPH-dependent PGF synthase (TbPGFS) from *T. brucei* that catalyzes the reduction of PGH_2 to $PGF_{2\alpha}$ (Okano et al., 2002). Thirdly, we hypothesized that *T. brucei* might well possess a unique cyclooxygenase (COX)-like enzyme, developed by a co-evolution process, that is responsible for prostaglandins production. Based on literature searches, there is so far only one identified COX-like enzyme from *Entamoeba histolytica*, which also shows no clear structural similarity to other well-known cyclooxygenases in protein databases (PDB) (Dey et al., 2003).

In the meantime, a peroxidase activity was detected in our group using Amplex Red in total trypanosome lysates, and a positive signal was obtained by Western bot analysis of total trypanosome lysates using a polyclonal cyclooxygenase ovine antibody (Barth, 2013). The specific band was cut-off for SDS-PAGE and mass spectrometry analysis to identify the proteins recognized by the above polyclonal antibody. This lead us to a list of known and hypothetical genes as putative *T. brucei* genes encoding for a putative cyclooxygenase-like enzyme candidate (Barth, 2013).

Among them, one gene (Tb427.10.13790/Tb927.10.13790/Tb10.61.3130), internally named putative cyclooxygenase-like gene from *T. brucei*, is annotated as a hypothetical protein in *T. brucei* genome databases (TriTrydb, Genedb & NCBI gene). Homologs of this gene are conserved in all three major kinetoplastids (*T. brucei, T. cruzi* and *L. major*). This gene was chosen for further experimental investigation. So far, our bioinformatic analyses using Pfam, Prosite, Swiss-Pro, InterPro, TMHHM and NetPhos databases revealed no convincing homolog protein in any other organisms. Additionally, these analyses revealed that the respective protein in trypanosomes carries no known signal peptide and no transmembrane domain, while extensive coil-coiled structures and multiple putative phosphorylation sites showed up.

The main goals of this thesis were: 1) to clone and express this annotated hypothetical protein from *T. brucei* using *E. coli* and Sf9 insect cells as expression systems; 2) to investigate whether this annotated hypothetical protein could crystallize *in vivo* using Sf9 insect cells prior to structural analysis using serial-X-ray crystallography or free-electron laser (XFEL); 3) to investigate and validate the physiological function of the pTbCOX protein in the trypanosome SMB cell line using RNA interference; 4) to develop SMB trypanosomes expressing pTbCOX fused with GFP for localization studies. Our hope was that once identified and characterized, the pTbCOX protein may become a potential target for HAT therapy.

2 Research thesis description

2.1 Statement of the problem

Previous experiments on the prostaglandin (PG) metabolism have shown that trypanosomes produce PGD_2, PGE_2, and $PGF_{2\alpha}$ from exogenous arachidonic acid (Kubata et al., 2000, 2007).

Our group has previously shown that production of prostaglandin-like compounds was not inhibitable by the classical inhibitors of prostaglandin synthesis (NSAID) such as aspirin and indomethacin (Rawer, 2004; Duszenko, unpublished observation). PGD_2 is known to induce sleep in mammals (Hayaishi, 2000, 2002). Since PGD_2 is highly elevated in the cerebrospinal fluid of late stage sleeping patients (Pentreath et al., 1990), production of this molecule by trypanosomes would help to understand the sleeping induction mechanism which is one of the main symptoms observed during sleeping sickness.

It is also known and well demonstrated that PGD_2 induces a form of apoptosis in stumpy parasites for cell density regulation to sustain the infection within the host (Duszenko et al., 2006; Figarella et al., 2006).

However, in view of the prostaglandin metabolism, structure and function of the COX-like enzyme is still poorly understood, since blast analysis of mammalian cyclooxygenase in higher eukaryotes did not reveal any sequences with significant homology. This fact is easily understood since the invention of prostaglandin synthesis during evolution occurred after the appearance of protozoa. Based on our experimental data and the fact that trypanosomes produce prostaglandins from arachidonic acid, we hypothesized that *Trypanosoma brucei* may well possess a unique COX-like enzyme that is responsible for prostaglandin production. However, if the hypothetical conserved pTbCOX protein would appear not to be a COX-like enzyme, we will delete the gene of this protein in *T. brucei* using RNAi to investigate whether it is essential (or not) and is thus a suitable or credible target for inhibitory drugs development against HAT.

2.2 Justification

Arachidonic acid (AA) metabolites are potent lipid mediators of physiological and pathological processes in humans and animals. The enzymes that catalyze the metabolism of AA are scientifically interesting for two major reasons: First, they can be a target of chemotherapeutic agents (specific inhibitors) used to control response mechanisms during inflammation; second, *in vitro* studies of these enzymes may well shed light on the biochemical pathways of AA metabolism and physiological relevance of the AA metabolites, namely the control of cell death mechanisms.

Parasitic protozoa undergo complex transformations in specific environments during their life cycles. Such activities frequently involve an insect vector and a mammalian host.

The proliferation of the parasite within the mammalian host can cause disease and sometimes death. However, rapid death is not the preferred outcome of the infection, because the parasite depends on its host to complete its life cycle and propagate its progeny. Therefore, pathogenic parasites must have evolved mechanisms to regulate critical checkpoints in their developmental cycle and potentially modulate the local physiological response of the host.

Successful pathogens must have erected platforms that allow crosstalk between developmental regulatory molecules of the parasite and those that regulate host cellular and tissue function. For this to occur, the parasite should employ similar regulators with "built-in" unique features that allow it to evade the detection and ultimately subvert such host functions. Arachidonic acid metabolites, i.e., PG, are suited for such a role because they are known to be strong local regulators of host cells and tissue functions.

Despite PG association with the genesis of fever, somnolence, headache, ovarian dysfunction and immune suppression observed during parasitic protozoa infections, the etiologic agents have just recently been given a direct role in the production of these molecules.

Furthermore, the biochemical pathways of AA metabolism in mammalian cells do exist. However, these biochemical pathways have not been unequivocally demonstrated in parasitic protozoa. Indeed, the knowledge that parasites actively synthesize and release molecules like PGs that potentially modulate host functions ascribes to the pathogen a more active role in the pathophysiology of the disease. In fact, PG production appears first in sponges during evolution, but not in protozoa. Accordingly, PG synthesis in trypanosomes is a typical co-evolutionary process that was probably established because of its benefits for the parasites.

Hence, a better understanding of the basic biochemical pathways of the parasites may pave the road to establish new strategies for the development of more effective and less toxic drugs. The finding that PG-producing enzymes are distinct from their mammalian counterpart makes them a suitable drug target.

As soon as some of the enzymes involved in PG synthesis in this parasite are discovered, genetic manipulation will allow a definitive understanding of the role of theses enzymes respectively in the pathogenesis of sleeping sickness and the life cycle of *Trypanosoma brucei*.

The identification and purification of that putative COX-like enzyme from *T. brucei* would, therefore, be of great interest because it will bring new insights into the understanding of its role during the cell cycle, cell morphogenesis, and pathogenesis. On the other hand, as more crystal structures of this enzymatic system are determined, it will be possible to rationally design specific inhibitors and better drugs against sleeping sickness.

3 Materials and Methods

3.1 Materials

3.1.1 Bacteria strains

Bacteria strains	Supplier
BL21-DE3 E. coli	Invitrogen, Karlsruhe
NEB Turbo Competent E. coli (High Efficiency)	New England Biolabs, Frankfurt
One Shot Top 10 Competent E. coli	Invitrogen, Karlsruhe
Max Efficiency DH10Bac™	Invitrogen, Karlsruhe
Rosetta Competent Cells	Merck, Darmstadt

3.1.2 Trypanosoma strains

In this work, the monomorphic single marker bloodstream forms (BF SMB) strain EATRO 427 clone MITat 1.2 (**M**olteno **I**nstitute **T**rypanozoon **a**ntigenic **t**ype, Cambridge) with the VSG (Variable Surface Glycoprotein) antigen variant 221 (Cross, 1975) were used for the pTbCOX knockdown and pTbCOX-eGFP expression experiments. The bloodstream forms SMB cells line (BF SMB) was used as wild type strains to generate all the transgenic cell line during this PhD project.

The BF SMB/wild type strain and the transgenic cell line listed below have been named according to the *T. brucei* community nomenclature (Clayton et al., 1998). However, in some cases alternatives name will be used in this thesis to facilitate reading.

1. **BF SMB (WT)**

   Name according to nomenclature: MITat1.2 T7RNAP TETR NEO

   Selection marker: Geneticin (2 µg/ml)

2. **BF pTbCOX-Knockdown**

   Made by: Celestin Mudogo & Salesia Werner

   Name according to nomenclature: MITat1.2 T7RNAP TETR NEO RDNA::T7PRO[Ti] pTbCOX HYG

   Alternative name: pTbCOX-RNAi or pTbCOX-KD

   Plasmid name: p2T7Ablue

   Selection marker: Geneticin (2 µg/ml), Phleomycin (2.5 µg/ml)

3. BF pTbCOX eGFP

Made by: Celestin Mudogo & Danyang Xu

Name according to nomenclature:

MITat1.2 T7RNAP TETR NEO HYG RDNA::PGPEET^{Ti} pTbCOX-eGFPT7RNAP BLE

Alternative name: pTbCOX-pCO57

Plasmid name: pCO57

Selection marker: Geneticin (2 µg/ml), Phleomycin (2.5 µg/ml)

3.1.3 Spodoptera frugiperda (Sf9) insect cells

Insect cells Sf9 (fall armyworm) stabilates were bought from Invitrogen, Germany, stored at -70°C and propagated at 27°C in an incubator.

3.1.4 Antibodies

Antibodies	Supplier
Anti-rabbit IgG alkaline phosphate conjugate	Sigma-Aldrich, Steinheim
Anti-His-Tag (6-histidine) rabbit	Biomol, Hamburg

3.1.5 Plasmids

Plasmids	Supplier
pCR 2.1	Invitrogen, Karlsruhe
pProExHTa	Invitrogen, Karlsruhe
pFastBacHTb	Invitrogen, Karlsruhe
p2T7Ablue	George Cross, New York, USA
pCO57	George Cross, New York, USA

3.1.6 Primers/Oligonucleotides

Primers (oligonucleotides) were purchased from Invitrogen and stored as 100 µM stock solution at -20°C. For the polymerase chain reactions (PCR), the stock solution was used in a dilution of 1:10.

1. Primers for pTbCOX in pProExHTa expression in *E. coli*

Fw-BamHI-pTbCOX: 5´- GGATCCACCACGTTCTTTGGCATTTACTGA- 3´

Rv-HindIII-pTbCOX: 5´- AAGCTTTGGCATCAATTTTACCTACCC- 3´

2. Primers for pTbCOX in pFastBacHTb expression and *in vivo* protein crystallization in Sf9 insect cells

Fw-BamHI: 5´- GGATCCATGGCAACCATAGCGGAGT- 3´

Rv-HindIII: 5´- AAGCTTTGGCATCAATTTTACCTACC- 3´

3. Primers for pTbCOX RNAi experiments

Fw-XhoI-pTbCOX-KD: 5´- CTCGAGAGATACGGGGAACACACGAG- 3´

Rv-BamHI-pTbCOX-KD: 5´- GGATCCAACGTGGAGAGGAACAGTGG- 3´

4. Primers for qRT-PCR experiments

Fw-pTbCOX-qPCR: 5´- AGGATTTGGAGGACGCGAAG- 3´

Rv-pTbCOX-qPCR: 5´- TAAGCACCTCAAGCATCCGT- 3´

Fw-ß-Tubulin-qPCR: 5´- TTCCGCACCCTGAAACTGA- 3´

Rv-ß-Tubulin-qPCR: 5´ - TGACGCCGGACACAACAG- 3´

5. Primers for pTbCOXpCO57 or pTbCOX-eGFP expression in *T. brucei*

Fw-HindIII-pTbCOX: 5´- AAGCTTATGGCAACCATAGCGGAGT- 3´

Rv-PvuII-pTbCOX: 5´- CAGCTGACCTTCAACTCGCGCTAG- 3´

3.1.7 Enzymes

Enzymes	Supplier
BamHI	Thermo Fisher Scientific, Braunschweig
EcoRV	Thermo Fisher Scientific, Braunschweig
HindIII	Thermo Fisher Scientific, Braunschweig
PvuII	Thermo Fisher Scientific, Braunschweig
NotI	Thermo Fisher Scientific, Braunschweig
T4DNA Ligase	Qiagen GmbH, Hilden
DNase I	Thermo Fisher Scientific, Braunschweig
Accu Prime DNA Polymerase High Fidelity	Thermo Fisher Scientific, Braunschweig
HotStar Tag DNA Polymerase	Qiagen GmbH, Hilden
XhoI	Thermo Fisher Scientific, Braunschweig

3.1.8 General Chemicals

Chemicals	Supplier
Acetone	Sigma-Aldrich, Steinheim

Acetic acid	Carl Roth GmbH, Karlsruhe
Agar 100 Resin	Agar Scientific Ltd., Stansted (UK)
Agar-Agar	Carl Roth GmbH, Karlsruhe
Agarose	Biozym Scientific GmbH, Oldendorf
Ampuwa	Fresenius Kabi, Bad Homburg
10% APS	Carl Roth GmbH, Karlsruhe
L-Arginine	Sigma-Aldrich, Steinheim
Bathocuproinedisulfonic acid disodium salt (BCS)	Sigma-Aldrich, Steinheim
Benzyldimethylamine (BDMA)	Agar Scientific Ltd., Stansted (UK)
Bovine serum albumin (BSA)	Sigma-Aldrich, Steinheim
Bradford protein assay reagent	Bio-Rad, Munich
5-Bromo-4-chloro-3-indolyl phosphate (BCIP)	Sigma-Aldrich, Steinheim
Calcium chloride	Merck Eurolab GmbH, Darmstadt
Chloroform	Merck Eurolab GmbH, Darmstadt
Coomassie brilliant blue R-250	Serva, Heidelberg
L-Cysteine	Sigma-Aldrich, Steinheim
4´, 6-Diamidino-2-phenylindole (DAPI)	Sigma-Aldrich, Steinheim
DEAE-Sephacel	Sigma-Aldrich, Steinheim
Digitonin	Sigma-Aldrich, Steinheim
Dimethyl formamide	Sigma-Aldrich, Steinheim
Disodium hydrogen phosphate	Merck Eurolab GmbH, Darmstadt
Dipotassium hydrogen phosphate	Merck Eurolab GmbH, Darmstadt
6X DNA loading dye	Thermo Fisher Scientific, Braunschweig
Dodecenylsuccinic Anhydride (DDSA)	Agar Scientific Ltd., Stansted (UK)
Doxycycline hyclate	Sigma-Aldrich, Steinheim
Epon	Sigma-Aldrich, Steinheim
Ethylenediaminetetraacetic acid disodium salt (EDTA)	Carl Roth GmbH, Karlsruhe
Ethyleneglycol-bis (ß-aminoethyl ether)-N,N,N´, N´-tetraacetic acid (EGTA)	Sigma-Aldrich, Steinheim
Ethanol	Carl Roth GmbH, Karlsruhe
EX-CELL 420 serum free medium w/L-Glutamine	Sigma-Aldrich, Steinheim
Fetal calf serum (FCS)	Invitrogen, Karlsruhe
Formaldehyde (37%)	Sigma-Aldrich, Steinheim
GeneRuler 1 kb DNA Ladder	Invitrogen, Karlsruhe
O´Gene Ruler Ultra Low Range DNA Ladder	Thermo Fisher Scientific, Schwerte

Gentamicin	Sigma-Aldrich, Steinheim
Geneticin (G-418) (50 mg/ml)	Carl Roth GmbH, Karlsruhe
D-Glucose monohydrate	Sigma-Aldrich, Steinheim
L-Glutamine	Sigma-Aldrich, Steinheim
L-Glutamic acid	Sigma-Aldrich, Steinheim
Glutaraldehyde 25%	Carl Roth GmbH, Karlsruhe
L-Glutathione reduced (GSG)	Sigma-Aldrich, Steinheim
L-Glutathione oxidized (GSSG)	Sigma-Aldrich, Steinheim
Glycerin 87% or 100%	Sigma-Aldrich, Steinheim
L-Glycine	Sigma-Aldrich, Steinheim
Guanidine hydrochloride	Sigma-Aldrich, Steinheim
Haemin	Sigma-Aldrich, Steinheim
HEPES	Sigma-Aldrich, Steinheim
L-Histidine	Sigma-Aldrich, Steinheim
Hydrochloric acid	Merck Eurolab GmbH, Darmstadt
Hygromycin B (50 mg/ml)	Roche, Basel
Hypoxanthine	Sigma-Aldrich, Steinheim
Imidazole	Sigma-Aldrich, Steinheim
Iscove's Modified Dulbecco's Medium (IMDM)	Sigma-Aldrich, Steinheim
L-Isoleucine	Sigma-Aldrich, Steinheim
Isopropanol	Merck Eurolab GmbH, Darmstadt
Kanamycin	Merck Eurolab GmbH, Darmstadt
Leupeptin	Merck Eurolab GmbH, Darmstadt
L-Lysine	Sigma-Aldrich, Steinheim
Magnesium chloride	Merck Eurolab GmbH, Darmstadt
Magnesium sulphate	Merck Eurolab GmbH, Darmstadt
MEM vitamin solution	Sigma-Aldrich, Steinheim
MEM amino acids	Sigma-Aldrich, Steinheim
Mercaptoethanol	Merck Eurolab GmbH, Darmstadt
Methanol	Carl Roth GmbH, Karlsruhe
L-Methionine	Sigma-Aldrich, Steinheim
Methyl-5-norbronene-2,3-dicarboxylic anhydride (MNA)	Agar Scientific Ltd., Stansted (UK)
Midori Green Advance DNA Stain	Nippon Genetics, Düren
Monopotassium phosphate	Merck Eurolab GmbH, Darmstadt
N-Lauroylsarcosine sodium salt	Sigma-Aldrich, Steinheim

Nitro Blue tetrazolium (NBT)	Sigma-Aldrich, Steinheim
Nonidet P-40	Sigma-Aldrich, Steinheim
L-Ornithine	Sigma-Aldrich, Steinheim
Osmium Tetroxide	Carl Roth GmbH, Karlsruhe
Paraformaldehyde	Fluka, Buchs
Penicillin/Streptomycin	Sigma-Aldrich, Steinheim
Pepstatin	Sigma-Aldrich, Steinheim
Pepton aus casein	Carl Roth GmbH, Karlsruhe
Phenol red	Sigma-Aldrich, Steinheim
L-Phenylalanine	Sigma-Aldrich, Steinheim
Polyethyleneglycol 6000 (PEG)	Sigma-Aldrich, Steinheim
Potassium acetate	Merck Eurolab GmbH, Darmstadt
Potassium chloride	Merck Eurolab GmbH, Darmstadt
Potassium dihydrogen phosphate	Merck Eurolab GmbH, Darmstadt
Potassium hydroxide	Carl Roth GmbH, Karlsruhe
Prestained protein ladder	Thermo Fisher Scientific, Braunschweig
Protein molecular marker	Thermo Fisher Scientific, Braunschweig
L-Proline	Sigma-Aldrich, Steinheim
Propidium iodide	Sigma-Aldrich, Steinheim
Propylene oxide	Sigma-Aldrich, Steinheim
Protease Inhibitor Cocktail	Sigma-Aldrich, Steinheim
Pyruvate	Sigma-Aldrich, Steinheim
Roti® Load-1	Carl Roth GmbH, Karlsruhe
RNase away®	Thermo Fisher Scientific, Braunschweig
Sodium azide	Sigma-Aldrich, Steinheim
Sodium acetate	Sigma-Aldrich, Steinheim
Sodium cacodylate trihydrate	Sigma-Aldrich, Steinheim
Sodium chloride	Fuka, Buchs
Sodium bicarbonate	Sigma-Aldrich, Steinheim
Sodium citrate dihydrate	Carl Roth GmbH, Karlsruhe
Sodium dihydrogen phosphate	Merck Eurolab GmbH, Darmstadt
Sodium dihydrogen carbonate	Merck Eurolab GmbH, Darmstadt
Sodium dodecyl sulphate	Sigma-Aldrich, Steinheim
Sodium hydroxide	Sigma-Aldrich, Steinheim
RNase away	Fisher Thermo Scientific GmbH, Schwerte

Saccharose	Sigma-Aldrich, Steinheim
Serum Plus SLBG4295	SAFC Biosciences, Hampshire (UK)
10% SDS	Carl Roth GmbH, Karlsruhe
Sucrose	Sigma-Aldrich, Steinheim
TEMED	Carl Roth GmbH, Karlsruhe
Tetracycline	Sigma-Aldrich, Steinheim
L-Threonine	Sigma-Aldrich, Steinheim
Thymidine	Sigma-Aldrich, Steinheim
Tris-HCl	Carl Roth GmbH, Karlsruhe
Triton X-100	Carl Roth GmbH, Karlsruhe
L-Tryptophane	Sigma-Aldrich, Steinheim
Tween 20	Carl Roth GmbH, Karlsruhe
L-Tyrosine	Sigma-Aldrich, Steinheim
L-Valine	Sigma-Aldrich, Steinheim
Uranyl acetate	Plane GmbH, Wetzlar
Yeast extract	Sigma-Aldrich, Steinheim

3.1.9 Kits

Kit	Supplier
AccuPrime Tag DNA Polymerase high fidelity Kit	Invitrogen, Karlsruhe
Bac-to-Bac Baculovirus Expression System Kit	Invitrogen, Karlsruhe
HotStar Tag Master Mix Kit	Qiagen GmbH, Hilden
Dneasy Blood & Tissue Kit	Qiagen GmbH, Hilden
QIAquick gel extraction Kit	Qiagen GmbH, Hilden
QIAquick PCR purification Kit	Qiagen GmbH, Hilden
Qiagen Plasmid Midi Kit	Qiagen GmbH, Hilden
QIAprep Spin Miniprep Kit	Qiagen GmbH, Hilden
Power SYBR Green RNA-to C_T 1-step Kit	Thermo Fisher Scientific, Braunschweig
Rneasy Mini Kit	Qiagen GmbH, Hilden
TOPO TA Cloning Kit	Thermo Fisher Scientific, Braunschweig

3.1.10 Media

3.1.10.1 Media for bacteria cell culture

Luria-Bertani medium (LB-medium 2X) pH 7

Tryptone	20 g/l
Yeast extract	10 g/l
NaCl	20 g/l

Transformation medium for E. coli (TSS)

Supplemented in LB-medium

DMSO	5 %
$MgCl_2$	50 Mm
PEG 6000	10 %

SOB medium

Tryptone	20 g
Yeast extract	5 g
NaCl	0.5 g

Distilled water was added to above chemicals and mixed. The final volume of the solution was made to 1 liter and then autoclaved. Afterward, 10 ml of filter-sterilized 1M $MgCl_2$ and 10 ml of filter-sterilized 1M $MgSO_4$ was added to this solution before use.

SOC medium

To the autoclaved SOB medium, 1 ml of filter-sterilized 2M glucose was added to a final volume of 100 ml. Subsequently, aliquots of 5 ml of the medium were made and stored at -20°C till further use.

Ampicillin stock solution (1000X)

Ampicillin (50 mg/ml) was dissolved in 70% ethanol and stored at -20°C.

X-Gal stock solution (500X)

X-Gal (20 mg/ml) was dissolved in dimethylformamide and stored at -20°C.

Agar-Agar 2X

Agar-Agar	40 g/l

LB-Ampicillin Agar-culture plate

Agar-Agar 2X	0.5 ml/ml
LB-medium 2X	0.5 ml/ml

X-Gal (20 mg/ml)	2 µg/ml
Ampicillin (50 mg/ml)	1 µg/ml

3.1.10.2 Media for Sf9 cell culture

EX-CELL® 420 serum-free medium with L-glutamine (Sigma-Aldrich, Steinheim) was used for the insect cell culture after the addition of 5 ml/l of a penicillin/ streptomycin stock solution.

3.1.10.3 Media for *Trypanosoma brucei* cell culture

1. Basic medium pH 7.2

IMDM	35.4 g/l
Sodium Bicarbonate	3.02 g/l
H_2O distilled (d H_2O)	900 ml/l
Add 1 l d H_2O	

2. 1X HMI-9 Medium/Complete bloodstream culture medium (BF-medium) pH 7.4

Basic medium	890 ml/l
L-Cysteine (18.2 mg/ml in d H_2O)	11 ml/l
Pyruvate (110 mg/ml in d H_2O)	1.11 ml/l
Thymidine (39 mg/ml in d H_2O)	1.11 ml/l
Hypoxanthine (13.6mg/10ml with 0.1N NaOH)	10 ml/l
BCS (28.2 mg/ml in d H_2O)	1.11 ml/l
2-Mercaptoethanol	15.5 µl/l
Penicillin/Streptomycin (100X)	11 ml/l
FBS (Heat inactivated: 30 min. 56°C)	110 ml/l
Serum Plus (No overheated)	110 ml/l

The BF-medium was adjusted to pH 7.4 using NaOH. Afterwards, it was sterile filtered and stored at 4°C and can be used for up to 4 weeks.

3. Cytomix buffer

Cytomix buffer was prepared to be use for stable transfection in *T. brucei* experiments. At first, preparation of the Phosphate buffer (8.66 ml/100 ml dH_2O K_2HPO_4 (1M)/ 1.34 ml/100 ml dH_2O KH_2PO_4 (1M) pH 7.6).

Cytomix buffer:

EGTA	0.76 g/l
KCl	8.88 g/l
$CaCl_2$ x 2 H_2O	19.2 mg/l

MgCl$_2$ x 6 H$_2$O	1.01 g/l
Glucose	5.00 g/l
Bovine Serum albumin	100 mg/l
HEPES	5.96 g/l
K$_2$HPO$_4$/KH$_2$PO$_4$	100 mg/l
Hypoxanthine (1.36 g in 100 ml NaOH)	10 ml/l

Add 1 l dH$_2$O; adjust pH 7.6 and sterile filtration.

4. Trypanosome dilution buffer (TDB) pH 7.7

Na$_2$HPO$_4$ X 12 H$_2$O (18 mM)	6.45 g/l
NaH$_2$PO$_4$ X H$_2$O (2 mM)	0.28 g/l
KCl (5mM)	0.37 g/l
NaCl (80 mM)	4.67 g/l
MgSO$_4$ X 7 H$_2$O (1mM)	0.25 g/l
Glucose X H$_2$O (20 mM)	3.96 g/l

5. Freezing medium for stabilates (TDB-Glycerin)

77 ml/100 ml TDB

23 ml/100 ml Glycerin 87% (20% end concentration)

3.1.11 Buffers and solutions

3.1.11.1 Buffers for agarose gel electrophoresis

Agarose gel electrophoresis (1%)

0.5 g/50 ml Agarose

Add 50 ml TAE buffer (50X) pH 8.0.

Heat the mixture in the microwave till the solution become clear without any particle.

Add 2.5 µl/50 ml Midori Green Advance.

TAE- buffer pH 8.0 (50X)

Tris	242 g/l
Na$_2$EDTA	37.2 g/l
Acetic acid	57.1 ml/l
dH$_2$O	add to 1 l

3.1.11.2 Buffers and solutions for 10% SDS-PAGE and Gel staining

Running buffer pH 8.3

Tris	3.04 g/l
Glycine	14.42 g/l
SDS	1 g/l
dH$_2$O	add to 1 l

Resolving gel (for 4 gels)

1 M Tris-HCl (pH 8.8)	8.60 ml
dH$_2$O	6.60 ml
Acrylamide	7.60 ml
10% SDS	228 µl
10% APS	78 µl
TEMED	24 µl

Stacking gel (for 4 gels)

1 M Tris-HCl (pH 6.8)	1.50 ml
dH$_2$O	8.40 ml
Acrylamide	2.00 ml
10% SDS	120 µl
10% APS	60 µl
TEMED	12 µl

3.1.11.3 Coomassie staining

Staining solution

Coomassie Brilliant Blue R-250	1 g/l
Ethanol	400 ml/l
Acetic acid	100 ml/l
dH$_2$O	500 ml/l

Coomassie Brilliant Blue R-250 was dissolved in ethanol. Subsequently, other solutions were added after Coomassie was completely solubilized and the volume was made up to 1 liter.

Destaining solution

Ethanol	400 ml/l
Acetic acid	100 ml/l
dH$_2$O	500 ml/l

3.1.11.4 Siver staining

Fixation solution

Acetic acid	12%
Ethanol	40%
Formaldehyde (37%)	0.05%

Wash solution

| Ethanol | 50% |
| dH$_2$O | 50% |

Pretreatment

| Na$_2$S$_2$O$_3$ X 5H$_2$O | 0.2% |

Impregnation

| AgNO$_3$ | 0.2% |
| Formaldehyde (37%) | 0.075% |

Development

Na$_2$CO$_3$	6%
Na$_2$S$_2$O$_3$ X 5H$_2$O (10% in dH$_2$O)	0.004%
Formaldehyde (37%)	0.005%

Stop solution

| Ethanol | 40% |
| Acetic acid | 12% |

All Silver staining solutions were made in distilled water (dH$_2$O).

Gel drying solution

| Glycerol 87% | 2.3% |
| Ethanol | 25% |

The gel drying olution was made in dH$_2$O and volume made up to 1 liter.

3.1.11.5 Buffers and solutions for Western blot

Transfer buffer pH 9.2

Tris (48 mM)	5.82 g/l
Glycine (39 mM)	2.93 g/l
SDS (10%)	3.75 ml
Methanol (20%)	200 ml/l

Wash buffer pH 7.4

| Tris (10 mM) | 1.21 g/l |
| NaCl (150 mM) | 8.766 g/l |

Tween 20 (0.1%)	1 ml/l

Tris Buffered Saline (TBS) pH 7.4

Tris (25 mM)	5.82 g/l
KCl	0.2 g/l
NaCl	8 g/l

Blocking solution

Milk powder	10% in 2 X PBS

2X Phosphate Buffered Saline (PBS) pH 7.4

Na_2HPO_4 X $12H_2O$	7.26 g/l
KH_2PO_4	0.48 g/l
NaCl	16 g/l
KCl	0.40 g/l

Alkaline phospatase (AP buffer) pH 8.9

Tris (20 mM)	2.42 g/l
NaCl (150 mM)	8.77 g/l
$MgCl_2$ (10 mM)	2.03 g/l

Color development solutions

BCIP, Toluidine salt (fresh solution in 100% DMF) (0.38 Mm)	7 mg/250 µl
NBT (fresh solution in 70% DMF)	16.25 mg/500 µl

The BCIP and NBT solutions were dissolved in 50 ml AP buffer for each blot.

Primary antibody (Anti-His (6x histidine)) in TBS 1:1000

Secondary antibody (Anti-Rabbit IgG, alkaline phosphatase conjugated) in TBS 1:10 000

3.1.11.6 Buffers for transmission electron microscopy

Cacodylate buffer (2x)

Na-Cacodylate x 3 H_2O	4.28 g
Sucrose	8.00 g
dH_2O	add to 100 ml

Glutaraldehyde in cacodylate buffer

2% or 2.5% Glutaraldehyde in 1x cacodylate buffer

Osmium tetroxide in cacodylate buffer

3% OsO_4 1:1 in 2x cacodylate buffer

Osmium tetroxide solution (3%)

OsO_4	0.25 g
dH_2O	8.18 ml

Uranyl acetate (0.5%)

Uranyl acetate	5 mg
dH_2O	1 ml

Epon

Agar	2 g
DDSA	1 g
MNA	1.08 g
BDMA	0.04 g

3.1.11.7 Buffers for Inclusions bodies (IBs) isolation and solubilization

Lysis buffer pH 7.5

Tris-HCl	20 mM
EDTA	15 mM
Triton X-100	1%

IBs solubilization buffer pH 8

Tris-HCl	50 mM
GuHCl	4 M
BME	10 mM

Additives used for Refolding procedure

L-Arginine	0.4 M and 0.1 M
L-Glutathione reduced	3 mM
L-Glutathione oxidized	0.3 mM

3.1.11.8 Buffers for Ni-NTA affinity chromatography using AKTA-FPLC

Equilibration & Wash buffer pH 8

Tris-HCl	20 mM
NaCl	1 M

Binding buffer pH 8

Tris-HCl	20 mM
NaCl	150 mM
Imidazole	10 mM

Triton X-100	0.1%

Elution buffer pH 8

Tris-HCl	20 mM
Imidazole	500 mM

3.1.12 Consumables

Materials	Supplier
Balance Mettler PJ3000	Mettler-Toledo GmbH, Giessen
Balance OHAUS® Analytical plus	Ohaus Corporation, Giessen
Beem - Blocks	Plano GmbH, Wetzlar
Cover slip slides	Carl Roth GmbH, Karlsruhe
Cryotubes	Greiner Bio-One GmbH, Frickenhausen
Electroporation cuvette 0.2 cm	Bio-Rad Laboratories Inc., München
Eppendorf cups (1.5 ml and 2 ml)	Greiner Bio-One GmbH, Frickenhausen
Falcon tubes (15 ml and 50 ml)	Greiner Bio-One GmbH, Frickenhausen
Flask cell culture T-25, T-75, T-150	Greiner Bio-One GmbH, Frickenhausen
Grids	Plano GmbH, Marburg Brand, Wertheim
Hemocytometer (0.02 mm)	Brand, Wertheim
Hybond-ECL Nitrocellulose membrane	Amersham Biosciences, Freiburg
Nalgene Rapid-Flow 50 mm Bottle Top Filter	Thermo Fisher Scientific, Karlsruhe
Negative Film KODAK 4488/Caresteam	Plano GmbH, Wetzlar
Nitrocellulose Membrane	GE Healthcare, Dornstadt
Millex-PES-Filter (0.22 µm)	Carl Roth GmbH, Karlsruhe
Object slides	Carl Roth GmbH, Karlsruhe
Object Polylysine slides	Gerhard Menzel GmbH, Braunschweig
Parafilm	American Can Go, Chicago (USA)
PCR-Tubes	Greiner Bio-One GmbH, Frickenhausen
Petri dishes	Greiner Bio-One GmbH, Frickenhausen
Sterile pipette	Greiner Bio-One GmbH, Frickenhausen
Sterile filter (0.22 µm)	Carl Roth GmbH, Karlsruhe
UV-Cuvette, Mikro	Carl Roth GmbH, Karlsruhe
6/12/24/48 and 96 well platte	Greiner Bio-One GmbH, Frickenhausen
96-well reaction plate (0.1 ml)	Applied Biosystems, Fisher Scientific GmbH, Schwerte
Whatman paper	Whatman, Maidstone (USA)

3.1.13 Equipments

Equipments	Supplier
ÄKTA FPLC	GE Healthcare, München
Autoclave	Münchner Mechanik, Stadlern
Beckmann Centrifuge	Beckmann, München
Beckmann TI-100 Ultracentrifuge	Beckmann, München
Centrifuge Heraus Multifuge 1L-R	Heraus, Osterode
Centrifuge Sigma 3K12	Bachoder, Reutlingen
Incubator Hera Cell (37°C, 5% CO_2)	Heraus, Osterode
Incubator 37°C	Infos AG, Bottmingen
Inverted Microscope ID02	Zeiss, Oberkochen
Light Microscope Axiostar plus	Zeiss, Oberkochen
Light Microscope Leica DM IL LED	Leica Microsystems CMS GmbH, wetzlar
Fluorescence Microscope (AG Dodt and AG Jansen)	Carl Zeiss AG, Oberkochen
Fluorescence Microscope BH2 RFCA	Olympus, Hamburg
Microscope-Camera U-PMTVC	Olympus, Hamburg
Microprocessor pH-Meter	Bachofer, Reutlingen
Microwave	Panasonic, Wiesbaden
Micro centrifuge Pico17	Heraus, Osterode
Mini Centrifuge MiniStar Galaxy	VWR International GmbH, Erlangen
Nanodrop ND-1000 (AG Thilo Sthele)	PreqLab, VWR International GmbH, Erlangen
Oven drying machine	BINDER GmbH, Tuttlingen
Pressure Cooker	CS Solingen, Solingen
pH-Meter	WTW, Weilheim
Photometer Ultraspec 3000	Pharmacia Biotech, Wien
Power Supply EPS301 for Gel electrophoresis	Amersham pharmacia biotech, Freiburg
Pyramitome 11800	LKB Ultramicrotome Laboratory
Shaker	Brau, Melsungen
Spectrophotometer GeneQuant 1300	GE Healthcare, München
Sterilbank LaminAir HLB 2248 GS	Heraus, Osterode
SteOnePlus® Real-time PCR System	Applied Biosystems, Thermo Fisher Scientific, Braunschweig
Transmission electron microscope EM10	Zeiss, Oberkochen
Ultramicrotome OM U3C	Reichert, Wien

Vortex Mixer	NeoLab, Heidelberg
Water bath	Gesellschaft für Labortechnik, Burwedel

3.1.14 Databank and Softwares

Software	Supplier /Web site links
AxioVision LE v4.8.2.0	Carl Zeiss AG, Oberkochen
Blast Local Alignment Search Tool (BLAST) (NCBI)	https://blast.ncbi.nlm.nih.gov/Blast.cgi
DNAman	Lynnon Biosoft, Quebec (CA)
Endnote X7.3.1	Thomsom Reuters, New York (USA)
LOMETS V.4 (Local meta-threading-server for protein structure prediction)	http://zhang.compbio.ku.edu/LOMETS
FastGene® Gel Pic	Nippon Genetics, Düren
GeneDB	http://www.genedb.org
GNU Image Manipulation Program v2.8.4 (GIMP)	http://www.gimp.org
Image J	https://imagej.nih.gov/ij/
NetPhos 2.0 (Protein Phosphorylation Prediction Server)	http://www.cbs.dtu.dk/services/NetPhos/np.html
OriginPro 8	OriginLab, Northampton (USA)
Pfam database	http://pfam.xfam.org
Primer 3 v0.4.0	http://www.bioinfo.ut.ee/primer3-0.4.0/
Primer-BLAST (NCBI)	http://www.ncbi.nlm.nih.gov/tools/primer-blast/
PubMed Central (NCBI)	http://www.ncbi.nlm.nih.gov/pmc/
SnapGene Viewer v2.8.2	GLS Biotech LLC, Chicago (USA)
StepOne Software v2.2	Applied Biosystems, Thermo Fisher Scientific, Braunschweig
TriTrypDB	http://www.tritrypdb.org/tritrpdb/
TrypanoFan	http://trypanofan.bioc.cam.ac.uk/trypanofan/main/
Zotero	https://www.zotero.org/

3.2 Methods and Protocols

3.2.1 Standard protocols for molecular biology

3.2.1.1 Extraction of genomic DNA from *T. brucei* bloodstream form (BF221)

Genomic DNA from *T. brucei* BF221 was extracted using a DNeasy Blood & Tissue Kit QIAGEN (Hilden, Germany). The extraction procedure was accomplished according to the manufacturer's instructions as follows: Per column 1×10^6 cells were added, the cells were centrifuged at 3000g for 5 min at 4°C. DNA was eluted with 100 µl elution buffer per column and stored at -20°C.

3.2.1.2 Polymerase chain reaction (PCR)

The full length pTbCOX gene (Tb427.10.13790/Tb927.10.13790/Tb10.61.3130) was amplified from *T. brucei* BF221 bloodstream form genomic DNA using AccuPrime Tag DNA Polymerase High Fidelity (Thermo Fischer Scientific, Germany). The AccuPrime PCR reaction mixture and program used for the pTbCOX amplification are described below:

AccuPrime™ PCR reaction mixture		AccuPrime™ PCR -Program			
10xAccuPrime™ PCR Buffer	5.00 µl	Denaturation	94°C	30 sec	1X
Fw-pTbCOX Primer, 10 µM	1.00 µl	Denaturation	94°C	30 sec	
Rv-pTbCOX Primer, 10 µM	1.00 µl	Annealing	56°C	30 sec	30X
T. brucei gDNA (28 ng/µl)	1.00 µl	Elongation	68°C	2 min	
AccuPrime™ DNA Polymerase (5 U/µl)	0.20 µl	Cooling	4°C	24 h	1X

3.2.1.3 Agarose gel electrophoresis

The pTbCOX PCR product as well as products obtained by restriction digestion were subjected in 1% agarose (w/v) (Biozym Scientific, Germany) dissolved in 1x TAE buffer (50x TAE: 242,0 g/l, 57,1 ml/l acetic acid, 37,2 g/l EDTA). After heating in the microwave until the solution became clear, Midori Green Advance DNA stain (Nippon Genetics, Germany) was added to a ratio of 5 µl/100 ml gel. Samples were mixed with an appropriate volume of 6x DNA Gel Loading Dye (Thermo Fischer Scientific, Germany) to reach an end concentration of 1x DNA Gel Loading Dye. For size reference, 1 kb Gene Ruler (Thermo Fischer Scientific, #SM0311, Germany) was used. Depending on the gel size, electrophoresis was performed for 45 min or 1 hour at 80-100 V. The gel was visualized using LED illuminator.

3.2.1.4   DNA Gel Extraction and DNA concentration

After detection of the pTbCOX PCR product in Agarose gel electrophoresis, the product of interest was extracted using the QIAquick Gel Extraction Kit (Qiagen) according to the manufacturer's protocol.

The DNA concentration of isolated pTbCOX PCR product was measured using a Nanodrop ND-100 (PeqLab, AG Stehle). The quotient E_{260nm}/E_{280nm} was utilized to determine protein contaminations. Pure DNA has an E_{260nm}/E_{280nm} quotient of 1.8.

3.2.1.5   Ligation into pCR2.1®-TOPO® TA vector

A TOPO TA Cloning Kit was used for subcloning the pTbCOX amplified PCR product into pCR 2.1 plasmid vector. The *Taq* DNA polymerase used for PCR as described above contains a non-template-dependent terminal transferase activity that adds a unique deoxyadenosine (A) to the 3' ends of PCR products. The pCR2.1®-TOPO® TA vector has single 3´-thymidine (T) overhangs. Therefore, PCR inserts can ligate efficiently with the vector and are covalently attached to it by topoisomerase I. Ligation was performed using following reaction mixture:

Ligation pTbCOX into pCR 2.1 reaction mixture

pCR 2.1 vector (25 ng/µl)	2 µl
T4 DNA Ligase	2 µl
10X T4 DNA Ligase buffer	1 µl
pTbCOX PCR product (50 ng/µl)	1 µl
Ampuwa water	4 µl
Total Volume	10 µl

The reaction mixture was performed overnight in a thermocycler repeating the following temperature steps: 2 h at 22°C, 1 h at 16°C and 1 h at 4°C (Lund et al., 1996).

3.2.1.6   Ligation into the donor plasmid pFastBacHTb

Both DNA Strands (subcloning/target vector) fragments, respectively the pTbCOX fragment as well as the donor plasmid pFastBacHTb previously digested with BamHI and HindIII restriction enzymes, were used for sticky-end ligation. Both clones were ligated in a 1:1 and a 1:3 ratio of the target gene and target vector. The

ligation mixture for the proportion 1:1 was set up for a total volume of 20 µl, whereas the ligation mixes for the ratio 1:3 were prepared for a total volume of 30 µl (see description below).

Components	Volume for 1:2 ratio	Volume for 1:3 ratio
Vector pFastBacHTb	5 µl	5 µl
pTbCOX	5 µl	15 µl
10X T4 DNA Ligase buffer	2 µl	3 µl
T4 DNA Ligase	1 µl	1 µl
Ampuwa water	7 µl	6 µl
Total Volume	20 µl	20 µl

The reaction was performed overnight in a thermocycler, repeating the following temperature steps: 2 h at 22°C, 1 h at 16°C and 1 h at 4°C (Lund et al., 1996).

3.2.1.7 Transformation of chemically competent *E. coli*

Immediately after ligation, the freshly ligated DNA construct was transformed into NEB® Turbo Competent *E. coli* (New England Biolabs, Germany) or One Shot Top10 *E. coli* (Invitrogen, Germany) and in expression grade BL21-DE3 competent cells using a protocol from Stratagene. The tubes of competent cells were thawed on ice for 10 min. Then, 10 µl ligation product was gently added into pre-chilled 100 µl tubes of competent bacteria cells. The tubes were incubated on ice for 30 min.

Afterward, a heat shock was applied for 30 sec at 42°C, using a prewarmed water bath. The duration of the heat shock was critical for maximum efficiency. Thereon, the cells were supplemented with 200 µl of prewarmed SOC medium and incubated for 1 h at 37°C at 225 rpm in a shaking incubator.

Finally, the cells were plated on LB agar plates containing appropriate antibiotic (and containing X-gal and IPTG if blue-white screening was desired) for selection purposes.

After overnight incubation at 37°C, single colonies were picked and screened for true uptake of the transgene by colony PCR, plasmid purification, and restriction digestion. Colonies validated to carry the desired construct were used to prepare long-term cryostock stabilates.

3.2.1.8 Bacterial colony PCR

The PCR was performed using HotStarTaq® Master Mix Kit (Qiagen). A single bacterial colony was picked with a sterile pipette tip and transferred into the prepared PCR mix.

The components of the PCR reaction mixture and the Master mix PCR program ran in the thermocycler are shown below:

PCR reaction mixture		Master mix PCR-Program			
HotStarTag®Master Mix (5 U/µl)	10.00 µl	Activation	95°C	15 min	1X
Fw-pTbCOX Primer, 10 µM	1.00 µl	Denaturation	94°C	1 min	
Rv-pTbCOX Primer, 10 µM	1.00 µl	Annealing	56°C	1 min	30X
Bacteria from single colony	-	Elongation	68°C	2 min	
Ampuwa water	0.20 µl	Final Extension	4°C	24 h	1X

3.2.1.9 Plasmid purification from *E. coli*

Plasmid mini-preparation

After transformation, the colonies were selected and inoculated with a sterile pipette tip into respective 6 ml LB medium with appropriate selective antibiotics (i.e. 50 mg/ml ampicillin). The cultures were propagated at 37°C with shaking at 225-250 rpm. After overnight incubation (17 h), the plasmid purification was done using QIAprep Spin Miniprep Kit (Qiagen, Germany). The starter culture was harvested by centrifugation at 13000 rpm (Amicon microcentrifuge MC13) for 2 min. The supernatant was discarded, and the pellet was re-suspended in 250 µl P1 buffer, incubated for 5 min at room temperature. The re-suspended cells were lysed by adding 250 µl alkaline P2 buffer, gently inverting the solution 4-6 times and stand for 5 min. The solution was neutralized with 350 µl N3 buffer.

The precipitate was spun down at 13000 rpm for 10 min. The supernatant was transferred to a QIAprep spin column and centrifuged at 13000 rpm for 1 min. The column was washed with 0.5 ml buffer PB and 0.75 ml buffer PE. DNA bound to the column was eluted with 50 µl H_2O or elution EB buffer and stored at -20°C.

Plasmid midi-preparation

For plasmid midi-preparation, the QIAprep Spin Midiprep Kit (Qiagen, Germany) was utilized. 50 ml *E. coli* overnight culture at 37°C respectively inoculated with the colonies and under specific antibiotics selection pressure were centrifuged at 6000g for 15 min at 4°C and then the bacterial pellet resuspended in 4 ml P1

buffer (add RNase A solution to buffer P1 before to use, mix, and store at 2-8°C). The resuspended cells were lysed by adding a 4 ml P2 buffer, mix thoroughly by vigorously inverting 4-6 times, and incubated for 5 min at room temperature. The solution was neutralized with 4 ml prechilled P3 buffer, mix thoroughly by vigorously inverting 4-6 times, and incubated for 15 min on ice. The precipitate was spin down at 14000-18000g for 10 min at 4°C.

At the same time, the QIAGEN-tip column was equilibrated by applying 4 ml QBT buffer. The supernatant was gently transferred to the QIAGEN-tip column and allowed it to enter the resin by gravity flow.

The column was washed 2 times with 10 ml QC buffer, and the DNA was eluted with 5 ml QF buffer into a clean 15 ml vessel. The DNA was precipitated by adding 3.5 ml isopropanol at room temperature to the eluted DNA and spin down by centrifugation at 15000g for 30 min at 4°C. The supernatant was carefully discarded, and the pellet was washed with 70% ethanol at room temperature, centrifuged down at 15000g for 10 min. The supernatant was again discarded and the pellet was air-dry or dried with a SpeedVac Vacuum Concentrator and resolved in 150 µl appropriate buffer (e.g. sterile Ampuwa water, TE buffer, pH 8.0, or 10 mM Tris-Cl, pH 8.5).

3.2.1.10   Bacmid purification for Sf9 transfection (Minipreparation)

The bacmid purification was performed using the DNA Purification Kit (Qiagen). White colonies from DH10Bac transformation were grown overnight at 37°C in 6 ml 1x LB under antibiotic selection (kanamycin, 50 µg/ml; gentamycin, 7 µg/ml; tetracycline, 10 µg/ml). On the next day, the bacterial suspension was centrifuged at 17000g for 3 min. The supernatant was discarded, whereas the cell pellet was resuspended in 300 µl P1 buffer. By the addition of 300 µl P2 lysis and incubation at room temperature for 2-5 min, lysis was induced. 300 µl N3 buffer was used to neutralize and, thus, to stop the lysis.

After 10 min incubation on ice, the sample was centrifuged at 17000g for 10 min. Bacmid precipitation was achieved by mixing the supernatant with 800 µl 100% isopropanol. After 10 min incubation on ice, centrifugation at 17000g for 10 min was performed. Further on, the pellet was washed with 500 µl 70% ice-cold ethanol and dried at room temperature. Finally, the dry bacmid pellet was resuspended in sterilized water, and the DNA concentration was measured at Nanodrop ND-1000 (PeqLab, AG Stehle). This experiment produced a high yield of bacmid DNA (> 1000 ng/µl) which was stored at -20°C till further used.

3.2.1.11   Restriction digestion analysis

Different restriction enzymes and respective buffers were used to digest the pTbCOX-pCR 2.1 subcloning (BamHI and HindIII), pTbCOX-pFastBacHTb constructs (BamHI and HindIII), pTbCOX-KD-pCR 2.1 subcloning (XhoI and BamHI) and pTbCOX-pCR 2.1 subcloning (HindIII and PvuII). According to required

analysis, the plasmid and plasmid constructs with the gene of interest (pTbCOX) were checked for suitable restriction enzyme using DNAMAN software. The reaction mixture consisted of full DNA plasmid constructs, a respective buffer for each enzyme, restriction enzyme and elution buffer to make up a volume of 35 µl. The reaction mixture was incubated for 1 h or overnight at 37°C. Afterwards the restriction products were analyzed by agarose gel electrophoresis and purified according to the instruction of the QIAquick gel extraction kit.

The reaction mixture as an example for the restriction digestion using BamHI and HindIII was done as described below.

Double restriction digest with BamHI & HindIII

DNA (subcloning/target vector)	15.0 µl
10x Buffer BamHI	3.5 µl
BamHI (10 U/µl)	0.5 µl
HindIII (10 U/µl)	1 µl
Ampuwa water	15.0 µl
Total Volume	35 µl

3.2.1.12 DNA sequencing

The isolated plasmid constructs after verification on agarose gel electrophoresis and DNA concentration were sent for sequencing to Eurofins Genomics or GATC Biotech in the concentration of 30-100 ng/µl.

The results of sequenced DNA were analyzed with DNAMAN software or NCBI blast by alignment with the gene of interest or plasmid sequence.

3.2.2 Cultivation and handling of organisms

3.2.2.1 Escherichia coli

3.2.2.1.1 Cultivation on agar plates

The bacterial cells were cultivated on agar-agar with LB-medium and ampicillin. LB-medium was prepared as 2X stock solution and mixed with pre-warmed 2X agar-agar under sterile conditions. After cooling to room temperature, ampicillin (1 ml/l) and X-gal (2 ml/l) were immediately added and poured into culture plates. The plates were left to solidify. When the agar was solidified, the plates were packed under sterile conditions and stored at 4°C till further use.

3.2.2.1.2 Preparation of competent *E. coli* cells (Chung et al., 1989)

Competent *E. coli* cells were inoculated into 5 ml LB-medium with specific antibiotics selection pressure and incubated at 37°C with shaking at 225 rpm for overnight (17 h). After the overnight incubation, 1 ml of the starter culture was inoculated into 100 ml LB-medium with the right antibiotics selection and propagated at 37°C with shaking at 225 rpm till the absorbance reached 0.8 at 600 nm.

Then the cells were harvested at 5000 rpm for 5 min at 4°C, and the cell pellet was re-suspended in 10 ml TSS medium. Subsequently, 100 µl aliquots were made in cryogenic vials which were immediately frozen in liquid nitrogen and stored at -80°C.

3.2.2.1.3 Preparation of long term storage of *E. coli* – Cryostabilates

The new starter culture of tested clones and sterile 50% glycerol were added in volumes of 700 µl and 300 µl, respectively in cryotubes. The tubes were immediately shock-frozen in liquid nitrogen and stored in the liquid nitrogen tank.

3.2.2.2 Spodoptera frugiperda (Sf9 insect cells)

Insect cells Sf9 (fall armyworm) were bought from Novagene, Germany as frozen vials, stored in the liquid nitrogen tank and propagated in adherent and suspension culture at 27°C in an incubator.

These cells were used for protein expression by following the Bac-to-Bac® Kit manual (Invitrogen, Germany) as the basis for the cultivation, transfection of Spodoptera frugiperda (Sf9) insect cells and *in vivo* protein crystallization experiments.

3.2.2.2.1 Culturing Sf9 insect cells

A cryo-stabilate of 2×10^7 Sf9 insect cells was removed from the nitrogen tank and rapidly defrosted at 27°C in a water bath. After the external disinfection of the cryotube, it was opened under a sterile bank and transferred to a 25 cm² cell culture flask. Subsequently, 10 mL of pre-warmed EX-CELL 420 Serum-Free Medium was added drop-by-drop. After an incubation period of one hour at 27°C, the vital cells had accumulated to form a monolayer at the bottom of the cell culture flask so that the medium with the non-adherent cells and the medium could be removed. Subsequently, a further 10 mL pre-warmed EX-CELL 420 Serum-Free Medium was carefully added to the cell culture flask. After that incubation was carried out at 27°C until the monolayer had a confluence of about 90%. Then the culture could be used to start and maintain a Sf9 insect cells suspension culture.

Cultivation of Sf9 insect cell monolayer culture

Monolayers of adherent insect cells were grown in different-sized culture flasks with sterile filter covers at a temperature of 27°C. Once a confluence of the cells of about 90% had been achieved, the old medium was removed, and fresh medium was added. Subsequently, the monolayer was detached from the floor by rinsing with a pipette or by careful scraping with a cell scraper and brought into suspension. The vitality of the insect cells could be examined microscopically, and the cell density was determined using a Neubauer hematocytometer. After that, the Sf9 insect cell culture could be diluted and transferred into a new culture flask with a larger volume:

Type of Culture Flasks	Number of cells	Volume of Medium
25 cm^2 Flask	1 x 10^7	10 mL
75 cm^2 Flask	3 x 10^7	20 mL
150 cm^2 Flask	6 x 10^7	40 mL

Cultivation of Sf9 insect cell suspension culture

To be able to cultivate higher cell densities, suspension cultures with an initial cell concentration of 8 x 10^5 cells/ml could be generated from monolayers, which had previously been passed at least twice. These suspension cultures were shaken at 100 rpm and incubated at 27°C. The same culture flask was used for the suspension cultures as in the cultivation of monolayers.

During the cultivation, the culture flask stood at a 45° angle on the shaker. It is important in the case of suspension cultures, that there is a good supply of oxygen to the cells, so that a sufficiently large vascular volume may be selected for the respective cultures.

The cell density of the suspension culture was determined twice a week using a Neubauer hematocytometer, and the cells were kept between 1 x 10^6 and 8 x 10^6 cells/ml. When the cells density reached the upper limit, cell density was adjusted to 1 x 10^6 cells/ml by dilution. The passage numbers should not exceed 30.

Preparation of Sf9 insect cell stabilates

Cells with a low passage number were frozen as reserves. After the absolute cell number of a suspension culture was determined, this was centrifuged, and the insect cells were adjusted to a concentration of 4×10^6 cells/ml in a fresh EX-CELL 420 Serum-Free Medium. The Sf9 cells were then cooled to a temperature of 4°C, and the same volume of pre-cooled medium was added with the addition of 20% (v/v) DMSO. Then, 4 x 10^6 cells/ml insect cells were distributed to each cryotube for 12 hours at -20°C, then overnight at -80°C, and finally stored as stabilate in the nitrogen tank.

3.2.2.2.2 Transformation in DH10Bac competent cells

The purified validated pTbCOX-pFastBacHTb plasmid was used for transformation of DH10Bac *E. coli* competent cells (Thermo Fisher Scientific). Aliquots of 100 µl competent DH10Bac *E. coli* (stored at -80°C) were thawed on ice. Then, 5 µl of the pTbCOX-pFastBacHTb construct were added, followed by 30 min incubation on ice.

Next, a heat shock was applied for 45 sec at 42°C using a pre-warmed water bath. Thereon, cells were supplemented with 200 µl SOC medium. After 4 h incubation at 37°C, while shaking, the cells were plated on LB-agar plates. The agar was previously prepared with various antibiotics (kanamycin, 50 µg/ml; gentamycin, 7 µg/ml; tetracycline, 10 µg/ml); as well as X-Gal (100 µg/ml) and IPTG (40 µg/ml) which allows selection of recombinant *E. coli* cells. The plates were incubated for 48-72 h at 37°C. Afterward, the white DH10Bac colonies were used for Bacmid purification (see 3.2.1.10).

3.2.2.2.3 Transfection of Sf9 insect cells

The recombinant bacmid purified (see 3.2.1.10) and validated by Bacmid PCR analysis (Bac-to-Bac® Kit manual) was used to transfect the Sf9 insect cells. The X-tremeGENE HP DNA Transfection Reagent (Sigma-Aldrich, Germany) was used for the transfection of Sf9 insect cells experiments.

The transfection was performed by Bac-to-Bac® Kit manual (Invitrogen, Germany) with some minor modifications. The numbers and volume given here are sufficient to transfect two wells of a standard 6-well plate and to prepare two wells as negative controls.

The cell density of a Sf9 suspension culture was determined using a Neubauer hematocytometer. The first requirement is that the cells should grow in the log-phase ($1.5\text{-}2.5 \times 10^6$ cells/ml) with greater than 95% viability). Next step, the cell density was adjusted to 8×10^5 cells/ml (10 ml in total, use medium without antibiotics), and 2 ml/well were seeded thereof into four wells of the six-well plate. The cells were allowed to attach for 15-45 min at room temperature.

In the meanwhile, the lipofection mixture was prepared: X-tremeGENE HP DNA Transfection Reagents was carefully mixed, and 6-8 µl of this reagent were transferred into 100 µl of EX-CELL 420 serum-free medium (without antibiotics). Thereupon, the mixture was briefly vortexed and kept at room temperature.

Next step, 5 µl recombinant bacmid DNA (1 µg DNA) was added to 100 µl of EX-CELL 420 serum-free medium (without antibiotics) and gently mixed. Both, X-tremeGENE in medium and DNA in the medium were then combined to give a total volume of ~209 µl. After the expiration of a 15-30 min incubation period at room temperature, 150 µl of the mixture were added dropwise onto the cells in the first well. The remaining 50 µl were used to transfect the second well equally. Control wells were treated with the same volumina (150

µl and 50 µl) of the serum-free media. The plate was incubated for 4 h at 27°C, but before, it was slightly wiggled to ensure even distribution of the DNA.

As soon as the incubation period was finished, the transfection mixture was carefully removed by pipetting and subsequently replaced by 2 ml EX-CELL 420 serum-free medium (with or without antibiotics optionally). After 72 h incubation at 27°C, the cells were daily inspected under a light microscope for signs of viral infection, such as swollen cell bodies, increased cellular granularity, and reduction of confluence.

3.2.2.2.4 Isolation of virus stock

After the Sf9 cells had been transfected with the pTbCOX bacmid, the first virus generation (P1) was isolated approximately 7-10 days post transfection, as soon as about 90% of the cells were lysed. Therefore, the medium of infected cells was carefully collected, transferred into a sterile 15 ml tube and centrifuge at 3500 rpm for 5 min. The supernatant, now representing P1 viral stock, was then moved to a new tube, protected from light, and stored at 4°C. Further virus stock generations were obtained in the same way.

The P1 viral stock will be used for the virus stock amplification as described in the protocol of Bac-to-Bac® Kit manual (Invitrogen, Germany) by the manufacturer's instructions.

3.2.2.2.5 Determination of the virus titer using the Reed-Muench method

The infectivity of the generated virus stock (plaque-forming units/ml) was estimated using an endpoint dilution assay method developed by Reed and Muench (Reed and Muench, 1938), using adopted equations as described by O'Reilly et al. (1994). In a 96 well plate, Sf9 insect cells were prepared monolayer cultures of 200 µl/well by letting the cells attach for 30 min.

The virus stock, whose titer should be determined, was diluted to achieve final concentrations of 10^{-3}, 10^{-4}, 10^{-5}, 10^{-6} and 10^{-7}. For each dilution stage, seven technical replicates were prepared, and the monolayer cells were infected. As a negative control, seven wells were left uninfected. The plate was incubated at 27°C. After incubation of seven days, the cells were analyzed by light microscopy. Each well was assessed for signs indicating a viral infection and based on this; it was scored either as infected (+ sign) or uninfected (- sign). The total number of uninfected and infected cells were determined by summed up over all uninfected wells of higher virus concentration (corresponding to lower dilution) ("top-down"). We assumed that all wells uninfected at that dilution would also have stayed uninfected at all higher dilution rates (less virus). Conversely, the total number of infected wells was obtained by summing up over all infected wells of lower virus concentration (corresponding to higher dilution) ("bottom-up"), assuming that these wells would equally have been infected at all lower dilutions. Further, the total percentage of infected wells for each dilution were calculated.

Therefore, we estimated the dilution, which would give rise 50% infected cultures, by linear interpolation. In doing so, we determined the next dilution above to 50% (termed A) and the next below 50% (termed B). Then, calculation of the proportionate distance (PD) between these two dilutions (A and B) was done according to equation **(1)**.

$$(1) \qquad PD \; = \; \% \; \text{in A} \; - \; 50\%/\% \; \text{in B}$$

The dose that would have given a 50% response (50% tissue culture infective dose, $TCID_{50}$) is then calculated using equation **(2)**.

$$(2) \qquad TCID50 \; = \; 10((\text{Exponent of dilution in A}) - PD)$$

The $TCID_{50}$ was converted to plaque forming units (pfu) per milliliter. According to Poisson distribution, the mean distribution of infectious units at 50% infection rate is equal to $\ln(2) = 0.69$.

$$(3) \qquad \text{Virus titer} \; = \; 1/TCID50 \; x \; \ln(2) \; x \; 1000 \; \mu l/ml/\mu l \; \text{of virus/well}$$

Equation **(4)** was used to assess the number of particles that were available per cell (multiplicity of infection, MOI) in retrospect.

$$(4) \qquad MOI \; = \; \text{virus inoculum x virus titer / number of cells}$$

For further used of the stock, the inoculum required to infect cells at a certain MOI was calculated according to Equation **(5)**.

$$(5) \qquad \text{Inoculum (ml)} \; = \; \text{MOI (pfu/cell) x number of cells / virus titer (pfu/ml)}$$

3.2.2.2.6 *Trypanosoma brucei*

Cultivation of monomorphic bloodstream form trypanosomes (SMB cell line) *in vitro*

Single marker bloodstream form (SMB) stored in the liquid nitrogen were used for axenic cultures of parasites. The stabilates were quickly thawed under warm water; the thawed parasite suspension was then transferred to a falcon tube containing 10 ml cold HMI-9 medium and then centrifuged (1500 g, 10 min, 4°C). The supernatant was eliminated, and the cellular pellet was resuspended in 500 µl – 1 ml bloodstream medium (HMI-9 medium) to determine cell density using a Neubauer hemocytometer. The cell suspension preculture was started by adjusting the cell density to $1 \; x \; 10^5$ parasites per ml with pre-warmed bloodstream medium (10-50 ml HMI-9 medium). The cultivation of trypanosomes was carried out at 37°C in a water-saturated atmosphere containing 5% CO_2. After the 8-16 h incubation period, the cell density of the preculture was determined again to verify that the cells had entered the logarithmic growth phase. If the cells reached $2.5 \; x \; 10^5$ cells/ml, the culture was adjusted by dilution to $1 \; x \; 10^5$ cells/ml to be sure that the cell will not exceed the critical value of $8 \; x \; 10^5$ cells/ml after 24 h incubation time. Approximately after 24 h post incubation, the

started preculture was counted for the growth curves, cells doubling timing and maintained by daily dilution to 1 x 10^5 and 1 x 10^6 cells/ml.

Depending on the daily cell counting results, the cells were placed in standard and synchronized cells density for growth curves experiments. Others cell cultures vessels were maintained or prepared to reach the high cell density cultivation required for further investigations. Geneticin G-418 2 µg/ml was systematically added to the SMB trypanosomes cell line to prevent the loss of the T7 RNAP and encoding TetR genes. The stable transfected SMB trypanosomes cells were cultivated with additionally selection pressure of 2 µg/ml Hygromycin.

Stable electroporation of SMB trypanosomes cells

SMB trypanosomes at a cell density between 2.5 and 4 x 10^7 cells/ml were harvested by centrifugation (1500 g, 10 min, RT). The supernatant was decanted, and the pellet was resuspended in 25 ml Cytomix. The resuspension cell-Cytomix was centrifuged at 1500g for 10 min at room temperature, and the supernatant was carefully discarded. The cell pellet was resuspended in 500 µl Cytomix.

The cell density of this suspension was dissolved in 1:100 dilution, counting using Neubauer hemocytometer to prepare the required cells concentration for the transfection.

For each transfection approximately 1 x 10^7 cells/ 400 or 440 µl in Cytomix were transferred into a sterile cuvette together with 10 µg linearized plasmid DNA (1µg/µl). The electroporation was performed with Gene Pulser Xcell using a single pulse at 1400 V, 25 µF, ∞ Ω for 0.3 ms. The number of surviving cells was determined by counting in 1:100 dilution. After electroporation, cells were transferred immediately into 36 ml pre-warmed HMI-9 medium, cells counted again and the culture was incubated for 6 h at 37°C in a water-saturated atmosphere containing 5% CO_2. 6 hours after incubation of the transfection the selection marker was added in the appropriate concentration.

For the knockdown induction experiment, Geneticin (2 µg/ml) and Hygromycin (2 µg/ml) or Phleomycin (2.5µg/ml) were used for the pTbCOX-pCO57 expression in SMB trypanosomes experiments. After added those respective selective antibiotics to the 36 ml cells culture, the culture was distributed in 1 ml per well into 24-well plates and then incubated at 37°C and 5% CO_2. After 4-6 days, the transfectants were usually analyzed by light microscopy and counting surviving cells. Later, positive clonal transfectant cells were pooled and transferred to large culture volume for subsequent experiments and production of transgenic stabilates for long-term storage in liquid nitrogen.

3.2.3 Quantitative Real-time PCR (qRT-PCR)

3.2.3.1 RNA isolation

The first requirement before proceeding with RNA isolation, the RNA bench surfaces and equipment were cleaned with potassium hydroxide (10 M) and RNase away®. Only the certified RNase-free materials and chemicals were used and stored in separate RNA bench cabinets. The samples were always kept on ice during all the practical steps procedure.

Isolation of the RNA from *Trypanosoma brucei* was carried out using the QIAGEN Rneasy kit according to the manufacturer's instructions. 5×10^7 trypanosomes cells/ml were harvested by centrifugation (1500 g, 5 min, 4°C) and washed once with 20 ml TDB buffer. The supernatant was completely removed and the cell pellet resuspended in 350 µl of buffer RLT (lysis buffer). For the completion of the lysis of the cells, the samples were vortexed for about 1 min. 350 µl of 70% (v/v) ethanol was then added, and the lysate was transferred to Rneasy ion exchange columns. After 15 seconds of centrifugation at 13000 rpm, the columns were washed once with 700 µl of buffer RW1 and twice with 500 µl of buffer RPE.

The elution was done using 30 µl of RNase-free water. 3 µl of the eluates were transferred to PCR tubes for RNA concentration determination. The RNA concentration determination was carried out on a Nanodrop ND-1000 against RNase-free water as a blank.

The ratio 260/280 nm of the isolated RNA should be in the range between 2.0-2.2 to ensure a sufficiently high degree of purity. The remaining 27 µl of the eluates were stored at -80°C for further experimentations.

3.2.3.2 DNAsing of RNA

To ensure that the RNA used for the qRT-PCR had no DNA contamination, the freshly isolated RNA (see 3.2.3.1) was digested with DNase I (Thermo Fisher Scientific, Germany). The DNAsing of RNA was performed following the reaction mixture DNase I digestion: 25 µl of RNA eluate (Qiagen RNeasy Kit), 3 µl of 10x reaction buffer, 1.5 µl of DNase-free water and 0.5 µl of DNase I (1 U/µl). The control was prepared with 25 µl instead of RNA eluate which served as a blank for later RNA concentration determination. All samples DNasing were incubated for 30 min at 37°C. Finally, 1.5 µl EDTA (50 mM) was added, and the enzyme was inhibited by heating at 65°C for 10 min. The RNA concentration of the samples was determined again as described above (see 3.2.3.1).

3.2.3.3 Quantitative Real-time PCR (qRT-PCR)

The Power SYBR® Green RNA-to-CTTM 1-Step Kit from Applied Biosystems (Thermo Fisher Scientific, Schwerte) was used for quantitative RT-PCR. The reference gene for the quantification of the mRNA level of

the putative TbCOX gene (pTbCOX) was β-tubulin (TbTub) as housekeeping gene. Since the 1-Step Kit already contains all reagents required for reverse transcription and subsequent PCR, the isolated RNA (see 3.2.3.1) could be used directly as a template. The RNA concentrations of all samples were adjusted to 20 ng/µl by appropriate dilution with RNase-free water. A total of 60 ng RNA per reaction batch was used. Primer stock solutions (100 µM) were diluted 2:100 with RNase-free water and adjusted to a final concentration of 2 µM. To ensure that the levels of all components (primers, enzymes, SYBR fluorescent dye) were identical in all approaches, the next master mixes were prepared according to the manufacturer's instructions. This indicated quantity (52x) is sufficient for the investigation of 11 samples in triplicates in a total volume of 10 µl (including dilution series and negative controls).

	Mix 1 (pTbCOX)	Mix 2 (TbTub)
2x SYBR® Green RT-PCR-Mix	260,00 µl	260,00 µl
fw-Primer (2µM)	52,00 µl	52,00 µl
rv-Primer (2µM)	52,00 µl	52,00 µl
RT Enzyme Mix	4,16 µl	4,16 µl

A 96-well reaction plate (Applied Biosystems) was charged with 7 µl of the master mixes. Subsequently, 3 µl of DNase I-digested RNA (20 µg/ml) were added each time, so that the final volume per well was 10 µl. To the negative controls, 3 µl of RNase-free water was added instead of the RNA. Each RNA sample was measured in triplicate in master mix 1 (amplification of pTbCOX mRNA) and also as triplicate in master mix 2 (amplification of β-tubulin mRNA).

An RNA sample (SMB, not transfected) was diluted in a dilution series by a factor of 1:5 to determine the efficiency of the qRT-PCR (see 3.2.3.4), and the resulting amounts of RNA were added to both master mixes.

The reaction plate was sealed with an adhesive film and briefly centrifuged before the start of the reaction. The reaction was carried out in a StepOnePlus™ Real-Time PCR System from Applied Biosystems.

The temperature profile is shown in the table below. The data were evaluated using the StepOne software v2.2 (see 3.1.14)

Cycles	Programm	Temperature	Ramp Rate [°C/s]	Time
1X	Reverse Transcription	48°C	4,4	30 min

1X	Activation	95°C	4,4	10 min
	Denaturation	95°C	4,4	15 s
40X	Annealing/Elongation	60°C		1,5 min
	Measurement of fluorescence	72°C	4,4	10 s

Melting curve

1X	Denaturation	95°C	4,4	5 s
1X	Annealing	60°C	2,2	1 min
1X	Measurement of fluorescence	95°C	0,11	-
1X	Cooling	40°C	2,2	30 s

Melting curve analysis was used to verify the specificity of the PCR products. Also, agarose gel electrophoresis in a 5% TAE agarose gel (see section 2.3.2.2) was used to determine whether the fragments produced in the batches had the expected sizes of 165 bp (pTbCOX amplicons) or 76 bp (TbTub amplicons).

3.2.3.4 Determination of qRT-PCR efficiency

The analysis of the measured data was carried out with the help of the manufacturer software StepOne Software v2.2 (Applied Biosystems). The software automatically calculates a CT value (threshold cycle) for each sample – this value indicates the number of cycles at which the fluorescence of the sample increases significantly over the background fluorescence (baseline) for the first time. The relative determination of the transcript quantity was performed according to the efficiency-corrected relative quantification model according to Pfaffl (Pfaffl, 2001, 2004).

1. For the determination of the qRT-PCR efficiency E, the CT values of the two-dilution series were first plotted against the nanoprobes and subsequently logarithmized RNA quantity. E is obtained from the slope m of the compensating straight line according to the following formula:

$$(\textbf{6}) \quad E_{Gen} = 10^{-\frac{1}{m}}$$

2. The differences in the CT values (ΔCT) between induced samples and control samples (non-transfected SMB cells) were calculated by differentiation according to the formula (**7**). To compensate for fluctuations due to pipetting inaccuracies, the mean CT values of all three replicates of a sample were used for these calculations.

$$(7) \quad \Delta C_{T,Gen} = \overline{C_{T,Control}} - \overline{C_{T,induced}}$$

3. The relative expression difference was calculated by the formula **(8)**, which correlates the PCR efficiencies and the ΔCT values of the target gene (pTbCOX) and reference gene (TbTub).

$$(8) \quad R = \frac{E_{TbCOX}^{\Delta C_{T,TbCOX}}}{E_{TbTUB}^{\Delta C_{T,TbTUB}}}$$

The values calculated in this way are to be understood as arbitrary units.

3.2.4 DAPI staining of Trypanosoma brucei cells

DAPI is a fluorescent dye that specifically binds to AT-rich regions of DNA. Its absorption maximum is in the ultraviolet range; the emitted light has a blue color (maximum emission 453 nm) (Kapuscinski, 1995). As DAPI can easily pass through an intact cell membrane, it was used to stain the nucleus and Kinetoplast of noninduced and induced pTbCOX knockdown trypanosomes cells at different time post doxycycline induction. Approximately 1×10^6 cells/ml were harvested by centrifugation (1500g, 5 min, RT). The cell pellet was washed twice with TDB buffer and then resuspended in 100 µl of TDB buffer. 50 µl of the cell suspension were coated on a slide and dried in the air for 15-30 min. Subsequently, the cells were fixed by gently dropping 2-3 drops of ice-cold methanol (-20°C). After incubation at -20°C of the slide for 10 min, 50 µl of DAPI staining solution (1 µg/ml) were dropped, distributed on the entire surface by pivoting the slide and incubated for 5 min at RT in the dark.

The staining evaluation was carried out on an Olympus BH2 fluorescence microscope, equipped with a ColorView12 digital camera and the analysis software from Soft Imaging System GmbH (Münster), by counting Kinetoplast and nuclei from at least 100 cells.

3.2.5 Electron Microscopy

3.2.5.1 Transmission electron microscopy (TEM)

For TEM, SMB trypanosomes at a cell density between 2×10^7 and 1×10^8 cells/ml were harvested after different induction time (0 h, 6 h, 18 h, 24 h, 42 h) by centrifugation (1500g, 10 min). The supernatant was removed, and the cell pellet was washed once with TDB or MEM salts. The cell pellet was fixed in 2% glutaraldehyde (cross-linking fixative, dissolved in 1 x sodium cacodylate buffer, v/v) for 1 h at 4°C.

After washing four times (10 min each incubation on ice and termination by centrifugation 30 sec, RT, Beckmann Microfuge E) and storage overnight in 1 x cacodylate buffer, cells were postfixed in osmium tetroxide (1.5%, w/v) and stained with 0.5% uranyl acetate at RT for 60 min and washed with distilled water.

The fixed cells were dehydrated using ethanol solutions of increasing concentrations (50%, 70%, 95%, 100%, 5 min incubation, then 1 min centrifugation in Beckmann Microfuge E, RT) and washed 3 times 10 min each with propylene oxide. The samples were incubated with Epon: propylene oxide (1:1, 60 min, RT), infiltrated with pure Epon (60 min, RT) and transferred to Beem®-cups. The polymerization was carried out for 12 h at 45°C and 24 h at 60°C.

After polymerization, the sample was removed from the Beem®-cups using a scalpel and was trimmed into trapezium shape on LKB 11800 Pyramitone. The sample was sectioned using an Ultramicrotome OM U3 and fished with the copper grids. The grid was contrasted on a 100 µl 0.5% uranyl acetate drop (60 min, RT, face down) (Lewis and Knight, 1977). The grid was washed with distilled water and incubated in lead citrate solution (30 sec, RT) and again washed and dried.

TEM images were collected at a Zeiss EM 10 transmission electron microscope, and the photographs were developed using an automated Konica SRX-101A developer machine.

3.2.5.2   Scanning Electron Microscopy (SEM)

The SEM procedures were used to prepare the pTbCOX *in vivo* micro-sized crystals with Sf9 insect cells and pTbCOX SMB knockdown trypanosomes ($5 \times 10^7 - 2 \times 10^8$ cells/ml) post-induced with doxycycline (1 µg/ml) at the different time point (0 h, 6 h, 24 h). TEM procedures above described were followed for SEM pTbCOX micro-sized crystals with Sf9 insect cells samples preparation. For the pTbCOX SMB knockdown trypanosomes, SEM sample was fixed using 4% (w/v) glutaraldehyde and 4% (w/v) paraformaldehyde in 1 x cacodylate buffer overnight at 4°C. After washing four times (10 min each incubation on ice and termination by centrifugation 30 sec, RT, Beckmann Microfuge E), the cells were treated with 1.5% (w/v) osmium tetroxide with 70 Mm $HgCl_2$ in 1 x cacodylate buffer for 1 h at 4°C. Next step, the cells were washed one time with 1 x cacodylate buffer and three-time with distilled water. SEM samples were dehydrated up to 70% ethanol and stored overnight at 4°C. The subsequent steps for the preparation of SEM samples as well as SEM picture were carried out by Mrs. Meinert in the laboratory of Prof. Oliver Betz (Institute of Evolution and Ecology, University of Tübingen).

3.2.5.3   Negative staining

Approximately 5×10^7 cells (absolute) from a main culture in the logarithmic growth phase were harvested by centrifugation (1500g, 5 min, 4°C). The resulting cell pellet was washed twice in TDB (1500g, 5 min, 4°C) and subsequently resuspended in 0.2-1 ml TDB.

The cell density was examined by light microscopy. Depending on this, approximately 10-100 µl of the cell suspension were pipetted onto the bright side of a mold-coated copper grid. For this and all subsequent steps, a petri dish lined with parafilm served as a support. The grid was dried for at least 10 min at room temperature and then transferred to a drop of PEME + Nonidet P-40 (1%) with the shiny side facing downwards. After 2 min incubation, it was transferred to a drop of PEME + glutaraldehyde (2%) and incubated to fix the cells for 5 min. Subsequently, the grid was dried by carefully dabbing the liquid on filter paper and immediately transferred to a drop of 0.5% uranyl acetate for 30 s.

The preparation was terminated by washing in 3-5 drops of distilled water. After complete drying of the grids, they were analyzed and photographed on the Zeiss EM10 transmission electron microscope.

3.2.6 Standard protocols for protein biochemistry

3.2.6.1   Expression of rpTbCOX in BL21-DE3 *E. coli* strains as inclusion bodies

The pTbCOX-pProExHTa construct was transformed into the BL21-DE3 strain of *E. coli*. A 100 ml culture using LB medium containing ampicillin (50 µg/ml) and chloramphenicol (34 µg/ml) in the ratio of 1:1000 was grown overnight shaking at 37°C and used to inoculate 500 ml or 1 L of LB medium in a 2L flask.

The experiments on isopropyl ß-D-1-thiogalactopyranoside (IPTG) concentration and induction time were performed for better expression of the rpTbCOX. It was found that addition of 2Mm IPTG at a culture optical density (600 nm) of 0.6 – 0.8 and subsequent culturing for 4 hours at 37°C yielded the highest expression of the putative rpTbCOX in bacterial inclusion bodies (IBs). The cells were harvested by centrifugation at 10000 rpm or 4500g at 4°C for 10 min and stored frozen at -20°C.

3.2.6.2   Isolation of inclusion bodies and dialysis for protein refolding

Cells were resuspended in 25 ml or 50 ml of lysis buffer (20 mM Tris-HCl, pH 7.5, 15 mM EDTA, 1% Triton X-100 with the addition of Complete Protease Inhibitor Tablet (Roche)).

The cells were mechanically disrupted by sonication using short pulses of 20 seconds on ice in a Sonifer cell disruptor B-30. Protein refolding by stepwise dialysis was performed with slight modifications following the protocol developed by Buchner and Rudolph (Buchner and Rudolph, 1991) for refolding Fab fragment and by Tsumoto (Tsumoto et al., 1998) for the refolding of two scFv constructs. The inclusion bodies were isolated

from the cell supernatant by centrifugation at 10000 rpm at 4°C for 20 min. Inclusion bodies were solubilized in resuspension buffer (50 mM Tris-HCl, pH 8, 4 M GuHCl, 10 mM BME), incubated 10 min on ice, to allow denaturation and solubilization, and then centrifuge again at 10000 rpm at 4°C for 20 min to remove any residual insoluble material.

The resuspended protein solution was dialyzed against buffers containing decreasing amounts of guanidine hydrochloride (GuHCl) by stepwise dialysis, as well as adding additives like L-Arginine and the redox pair of oxidized and reduced glutathione (3 mM reduced glutathione (GSH)/ 0.3 mM oxidized glutathione (GSSG)) during 4 days.

The resuspended protein was dialyzed overnight at 4°C in snakeskin dialysis tubing against 1 L (10 ml vol. protein solution) or 2 L (30-40 ml vol. protein solution) of buffer # 1 (50 mM Tris-HCl, pH 8, 2 M GuHCl). The following day the dialysis buffer was changed to 1 or 2 L of dialysis buffer # 2 (50% dilution buffer # 1 with water, 0.4 M L-Arginine, 3 mM GSH, 0.3 mM GSSG) for overnight dialysis at 4°C.

The following day the dialysis buffer was diluted 50% with water (buffer # 3), and dialysis continued overnight. Any insoluble material was centrifuged at 10000 rpm at 4°C for 20 min and the protein solution dialyzed overnight at 4°C against 1 L or 2 L of buffer # 4 (50 mM Tris-HCl, pH 8, 300 mM NaCl, 0.1 M L-Arginine, 3 mM GSH, 0.3 mM GSSG) to remove the remaining GuHCl. The following day, the protein solution was centrifuged at 3000 rpm for 10 or 20 min to remove any insoluble material and then run a 10% SDS-Page and Western blot analysis. The remaining final protein solution after step-wise dialysis was stored at 4°C and ready to be used for Ni-NTA purification under AKTA-FPLC system.

3.2.6.3   Purification of (His)6 – tagged rTbCOX by Ni-NTA affinity chromatography

The final dialyzed protein solution (5 ml) was loaded onto a Protino® Ni-NTA (Macherey-Nagel, Germany) His-tag affinity column pre-equilibrated with an equilibration buffer (20 mM Tris-HCl, pH 8, 1 M NaCl) using an AKTA-FPLC system. The column was loaded with binding buffer (20 mM Tris-HCl, pH 8, 500 mM NaCl, 10 mM Imidazole, 0.1% Triton X-100) followed by a wash with equilibration buffer to remove the Triton X-100 for 30-45 min. The pTbCOX was eluted and collected in 1 ml different fractions from the resin column using a 100% linear gradient (0-500 mM) elution buffer (20 mM Tris-HCl, pH 8, 500 mM Imidazole). The equilibration-washing and elution steps were done respectively at a flow rate of 0.2 ml/min and 0.5 ml/min. Each eluted fraction was quickly analyzed by SDS-PAGE, gel silver staining and western blot analysis to identify the target fraction after the one step Ni-NTA affinity chromatography. Those fractions containing the eluted pTbCOX were pooled, dialyzed overnight at 4°C against 20 mM Tris-HCl, pH 8, 300 mM NaCl and concentrated using centricon filter MWCO 10 kDa.

3.2.6.4   Radioactive thin layer chromatography (TLC) cyclooxygenase activity assay

To determine the activity of the purified pTbCOX thin layer chromatography and C-14 arachidonic acid (2.5 µCi) as substrate were used. For this purpose, the solvent system containing 98.5:1:0.5 vol/vol/vol Diethyl ether/Methanol/Acetic acid was prepared and allowed to stand in a close chromatography tank at -20°C. Then 497 µl of the purified rTbCOX (200 ng) was incubated with 3 µl C-14 arachidonic acid (2.5 µCi) in COX activity buffer (see 3.1.11.3) at room temperature for 1 h. The reaction mixture was stopped by the addition of 100 µl of 1 M HCl and cold ethyl acetate. After vortex for 10 sec, the reaction mixture was centrifuged at 1000g at 4°C for 10 min. After that, the aqueous phase and the ethyl acetate phase were clearly separated from one another.

The ethyl acetate phase was transferred to an Eppendorf vessel, and the aqueous phase was extracted again with ethyl acetate. The collected extracted samples were then dried in speed vacuum centrifuge. The pellet was dissolved in 50 µl of ice-cold ethanol and place on ice for 30 min.

10 µl of sample was applied to the thin layer chromatography on a silica gel plate (20x20 cm) under an air stream and placed directly into the chromatography tank containing the solvent system at -20°C. After 45 min, the dry silica plate was exposed to X-ray film (KODAK MR Film) and radioactive products will be visualized after 7 days by autoradiography.

3.2.6.5   Protein concentration determination using Bradford assay

The protein concentration was determined by Bradford protein assay (Bradford, 1976). Therefore, Bio-Rad Protein Assay was utilized and diluted 1/5 with deionized water. The diluted reagent was pipetted in a volume of 900 µl in each cuvette. As a reference, 100 µl deionized water for standards or buffer for samples was used.

All measurements were performed in duplicate. The reaction mixtures were incubated for 5 min in the dark at room temperature, and then the protein concentration was determined by photometric measurement at 595 nm. The protein concentration was determined by comparison of the measured extinction values to a standard curve.

3.2.6.6   SDS-Polyacrylamide gel electrophoresis (SDS-PAGE)

At first, the glass plates, assembly, comb, and spacers were cleaned with ethanol. The glass plates with spacers were fixed inside the assembly. As mentioned above in section 3.1.11.2, separating gel mixture was poured carefully in between glass plates taking care not to let air bubbles in the solution and the gel was polymerized (polymerization time was for 30 min) with an overlay of deionized water. After the gel had polymerized, stacking gel mixture was poured above the gel carefully and immediately added comb on top of it till completely immersed between plates.

The polymerization time was 45 min, and during this time, protein samples were prepared after protein estimation from Bradford method from 10 to 60 µg protein concentration per sample. The reducing sample diluting buffer was added to samples and adjusted the volume accordingly. The samples were heat denatured by boiling at 100°C for 5 min and loaded into respective wells with Page Ruler Prestained Ladder as molecular protein marker.

The water cooling system was attached to the assembly, and running buffer was added in upper and lower reservoir.

The electrodes were attached accordingly into the power supply, and SDS-PAGE was run at the voltage of 80 V, and then after the sample has moved into the stacking gel, the voltage was increased to 160 V till the bromophenol boundary reached the bottom of the gel. The gel was removed carefully from the plates and placed in Coomassie solution for 1 h and then destained or in fixation solution for silver staining (see 3.1.11.3 and 3.1.11.4) or followed immediately for Western blotting.

3.2.6.7   Western blot analysis

The protein samples were resolved in SDS-PAGE and immediately blotted. The gel was placed on an anode plate in Semi-Dry apparatus.

It was overlaid onto blotting paper (Hybond-ECL nitrocellulose membrane) sandwiched between three layers of Whatman filter papers soaked with transfer buffer (see 3.1.11.5) on each side respectively. It was carefully assembled to remove any air bubbles in between the membrane, gel and filter papers. The electrotransfer was carried out at about 20 V (400 mA) for 45 min.

After that protein transfer from SDS gel to a nitrocellulose membrane, the membrane was blocked with 10% milk powder in 2 X PBS for 1 h at room temperature or overnight at 4°C with gentle shaking.

After the blocking step, the membrane was washed 5 times for 5 min in washing buffer and then incubated the first antibody diluted in TBS (1:1000) for 1 h at room temperature in new disposable bags with gently shaking. The membrane was washed again as above and incubated with the second antibody (coupled with alkaline phosphatase) diluted in TBS (1:10000) for 1 h at room temperature. After that, the membrane was washed 5 times for 5 min with gently shaking using TBS. Finally, the developing solution containing BCIP and NBT was added to the membrane and color development was observed carefully. When the bands appeared, the reaction was stopped with PBS and blot was scanned after drying on filter paper.

3.2.6.8   Gel staining

Following the SDS-PAGE run, the gels were stained with 1 mg/ml Coomassie blue R for at least 1 h at room temperature or overnight at 4°C. The gels were destained in destaining solution (10% acetic acid, 40% ethanol) till the respective bands appeared clear on the gels.

Silver staining also was performed as more sensitive than the staining by Coomassie blue dye. The gels were fixed in fixative solution (see 3.1.11.4) for 10 min at room temperature, washed with 50% ethanol 3 times for 10 min and then incubated in impregnation solution (see 3.1.11.4) for 3 min at room temperature with gently shaking.

The gels were washed 3 times for 1 min with water and then incubated with silver stain solution for 20 min (in the dark). The gels were further washed 2 times for 2 min with water. After that, the gels were soaked in developing solution (see 3.1.11.4) until the bands or protein spots appeared.

The gels were treated with stop solution (see 3.1.11.4) for 10 min at room temperature and were washed with 50% ethanol for 20 min. Later the gels were preserved by "sandwiching" the gels between two sheets of wet cellophane in gel storage solution (gel drying system) (see 3.1.11.4). Excess solution and air bubbles between the cellophane sheets and the gels were expelled by applying pressure using a ruler.

3.2.7 Biophysics Methods

3.2.7.1   Second Order Nonlinear Imaging of Chiral Crystals (SONICC)

Second order nonlinear imaging of chiral crystals (SONICC) was used to detect the isolated pTbCOX crystals. Using the SONICC method, the isolated pTbCOX crystals are irradiated with a 1064 nm fs laser pulse, which leads to a frequency doubling of the photon in the case of a chiral crystal.

The resulting signal of this second harmonic generation (SHG) process can thus be detected at a wavelength of 532 nm. The experiments were done using SONICC benchtop device (formatrix) with an SHG exposure time of 30 seconds. SONICC measurement, Dynamic Light Scattering (DLS) and CD spectroscopy on the pTbCOX crystals samples were carried out as cooperation project in the laboratory of Prof. Christian Betzel (Institute of Biochemistry and Molecular Biology, DESY – Hamburg).

3.2.8 In vivo crystallization in Sf9 insect cells

3.2.8.1   pTbCOX crystals production and isolation

The pTbCOX P3 virus stocks with respectively MOI 0.1 pfu/cell and 0.2 pfu/cell were used to infect the Sf9 insect cells for crystals production. For this experiment, 1×10^6 Sf9 cells/ml (monolayer culture, 60%

confluent) were infected in 6-well plate or 10 ml in T-flask 25 cm^2 for crystals production (virus dilution 1:1000). The infected Sf9 insect cells were incubated at 27°C for 2-3 weeks. The cells and crystals were visualized using an optical light microscope.

The produced pTbCOX crystals were isolated in principle by separation of crystals and cells by centrifugation. The Sf9 insect cells and crystals suspensions were centrifuged at 1500g for 10 min. The supernatant was collected and check for crystals under the light microscope.

The supernatant containing the tiny pTbCOX crystals was overnight dialyzed against water at 4°C using membrane filter 12-14 kDa cut-off membrane. The next day the crystals sample was visualized and counted under the light optical microscope using Neubauer chamber.

The crystals samples were concentrated using 10 kDa centricon (Millipore) at 15000g at room temperature until the desired concentration is reached.

The concentrated pTbCOX samples were then solubilized with sodium acetate pH 3.6 for SDS-PAGE and Western blot analysis.

4 Results

4.1 Description of the pTbCOX gene (Tb427.10.13790/Tb927.10.13790/Tb10.61.3130) and pTbCOX protein

The genome database of *T. brucei* contains the annotated gene Tb927.10.13790/Tb427.10.13790 that encodes a hypothetical conserved protein and is located on chromosome 10. This gene showed up in our search for a putative cyclooxygenase like enzyme in *Trypanosoma brucei* using Western blot analysis with a polyclonal anti-cyclooxygenase antibody from ovine, an enzyme assay for peroxidase activity with Amplex Red reagent, mass spectrometry analysis of the protein bands detected by Western blotting and a bioinformatic search (Barth, 2013). It was selected and postulated as a putative cyclooxygenase-like enzyme from *Trypanosoma brucei* (pTbCOX) to be further characterized in this thesis. The pTbCOX gene has a length of 2043 base pairs (bp) and has ortholog and paralog genes within the kinetoplastid family, however, all of them are still annotated as hypothetical conserved proteins. The pTbCOX gene encodes a pTbCOX protein which contains 680 amino acids and has a predicted molecular weight of 74.68 kDa. Bioinformatic analyses using Pfam, Prosite, Swiss-Pro, InterPro, TMHMM, Signal P, LOMET and NetPhos did not reveal any putative signal peptide or a transmembrane domain and no convincing homolog proteins in any other organism. The analyses revealed, however, the presence of α-helices, ß-strands and considerable coiled-coil structures and a large number of putative phosphorylation sites (Ser/Thr/Tyr) (Figure 4.1 and Figure 4.2).

Furthermore, the hydrophobicity or hydrophilicity of pTbCOX was evaluated using the Expasy ProtScale software. The Kyte-Doolittle scale revealed the hydrophobic amino acid within the pTbCOX sequence (Figure 4.3).

MATIAELQQAIRDEKEKHEQAMEELRSQRESLASVVAEQQQYTQDIIMRVSELRGRKSQQ
CCHHHHHHHHHHHHHHHHHHHHHHHHHHHHHHHHHHHHHHHHHHHHHHHHHHHCCHHHH
123456789012345678901234567890123456789012345678901234567890

MLAGNAAPNFAEIDTGCKAVDDILYSIEEGLETSTGKSSVVLGKILAAAVQAVVPGGDKK
HHHHCCCCCEEECCCHHHHHHHHHHHHHHCCCCCCCCCHHHHHHHHHHHHCCCCCCCCCC
123456789012345678901234567890123456789012345678901234567890

PSTLSSSSSATRTTDVVVISRNEIRGTHEWVKKHCKKCTACGELNGRPRPWEPPKKTDKG
CCCCCCCCCCCCCCCEEEECHHHHHHHHHHHHHHHHHHHHHHHHHCCCCCCCCCCCCCCCC
123456789012345678901234567890123456789012345678901234567890

KSIKGNASAPNLRCIPGKNFRSLSLCFRREPCSGTVLELMRISAVVNVQGQSGEQITNPR
CCCCCCCCCCCHHCCCCCCHHHHHHHHHCCCCCCEEEEEEEEEEEEEECCCCCCCCCCHH
123456789012345678901234567890123456789012345678901234567890

EVAAKITALVVEWVRKEMENAREAAKKAPWCEDGEDGQKFAVAVEMLLHNIDTRVEVFVI
HHHHHHHHHHHHHHHHHHHHHHHHHHHHCCCCCCCCCCHHHHHHHHHHHHHHCCCCEEEEEC
123456789012345678901234567890123456789012345678901234567890

PPKNGGNVGGSNHVPMKINVFVVSPLFLSTLQPFVELWGNERDREYMLQGLIKPAIKRIA
CCCCCCCCCCCCCCEEEEEEEEECCHHHHHHHHHHHHHCCHHHHHHHHHHHHHHHHHHHHH
123456789012345678901234567890123456789012345678901234567890

KLFGVDGVVDHGITVGLKAVDALVRMTKGKHFFEPTSPVKSKSGRPSASQPEQLIGFMHS
HHHCCCHHHHHHHHHHHHHHHHHHHHHHHCCEECCCCCCCCCCCCCCCCCCHHHHHHHHHH
123456789012345678901234567890123456789012345678901234567890

VILAMSLLGTRIELECAVPDLGDLKDLEDAKRSAFNIAKAFLQRLLPPRQDVAVSLTDPA
HHHHHHHHCCEEEEEEEECCCCCCCCHHHHHHHHHHHHHHHHHHHHHCCCCCCCCCCCCCC
123456789012345678901234567890123456789012345678901234567890

AADAVLWLRRMPTRMLEVLNNAFSSNSRLPSSLRTGVIDHLASPRLKINYALKNFSEIVI
HHHHHHHHHCCHHHHHHHHHHCCCCCCCCCCCCHHHHHHHCCCHHHHHHHHHHHHHHHHE
123456789012345678901234567890123456789012345678901234567890

DIFRPYAPNSGMMTVEEKHKGEKARIGACAPVVDIPRDIVRASAEAAAWAKDMQQELLKR
HHCCCCCCCCCEEEEECCCCCCCCCCCCCCCCCCCCHHHHHHHHHHHHHHHHHHHHHHHCC
123456789012345678901234567890123456789012345678901234567890

EAAGVNTKEGEDAVNVVLERTKGDEIMANFLKEMQDLRLEVVELLEFGCDVCLPFGVAMQ
HHHHHHHHHHHHHHHHHHHHCCCHHHHHHHHHHHHCCEEEEEEEEEEEEEEECCCCCC
123456789012345678901234567890123456789012345678901234567890

NGTTQPSEIIYARVEGVRNA
CCCCCCCCEEEEEEEEECCC
12345678901234567890

H – helix, E – strand, C - coil

Figure 4.1: pTbCOX 680 amino acids sequence and protein structure prediction using LOMETS V.4 (Local Meta-Threading-Server) software. This analysis revealed the presence of Helix, ß strand and more coiled-coil structure within the pTbCOX protein sequence.

NetPhos 2.0: Predicted Phosphorylation sites in the pTbCOX sequence
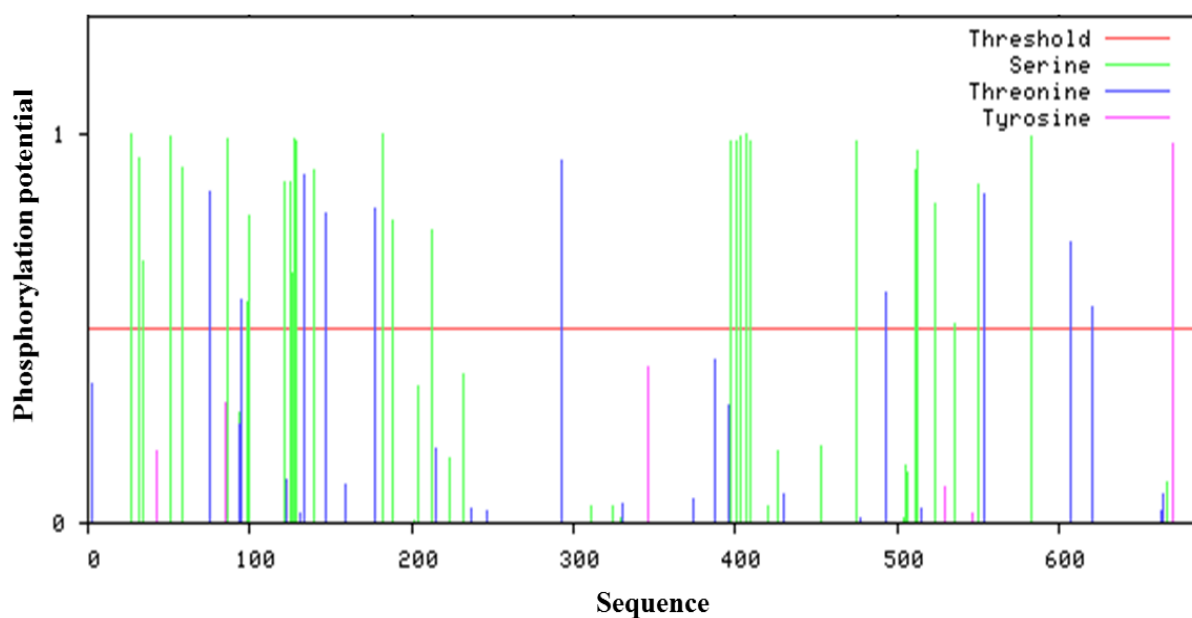
Phosphorylation site predicted : Ser : 29   Thr : 11   Tyr : 1

Figure 4.2: Phosphorylation sites prediction in pTbCOX sequence. The image is showing the numbers and position of Serine-Threonine-Tyrosine phosphorylation sites within the pTbCOX amino acid sequence using the NetPhos 2.0 bioinformatic software tool.
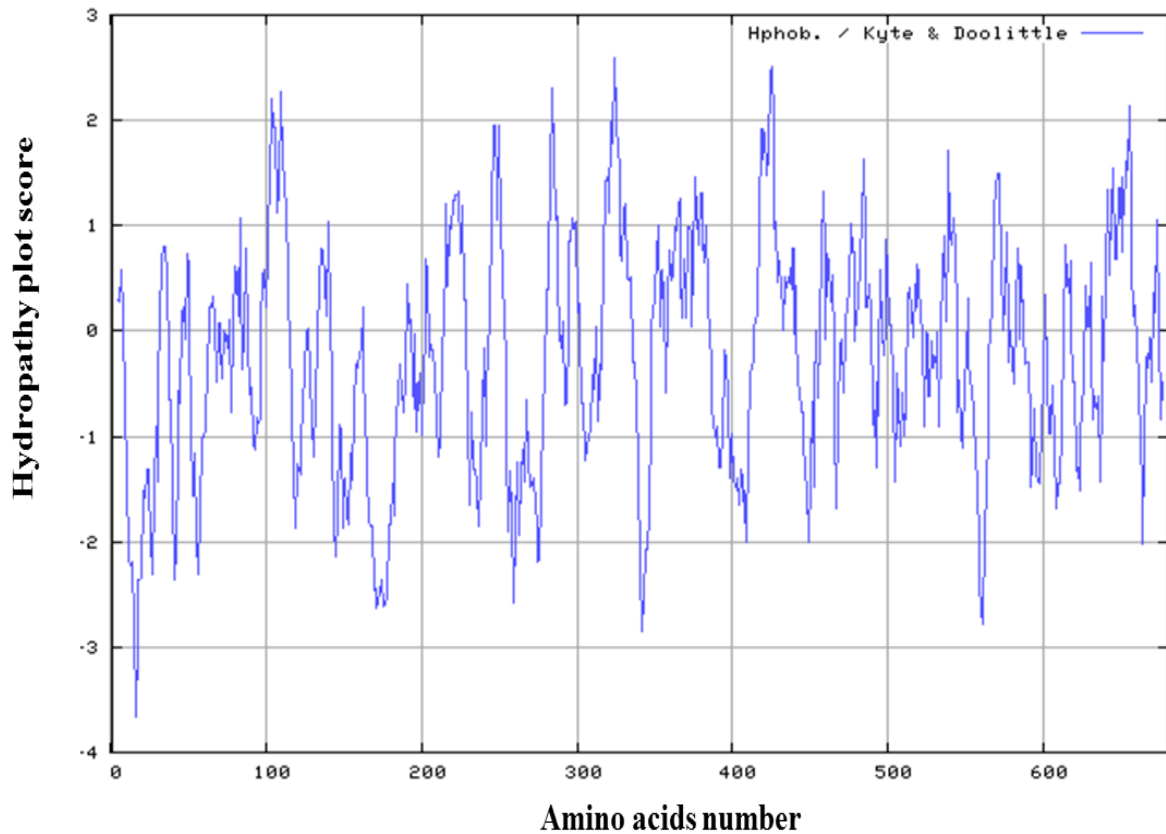
Figure 4.3: Kyte-Doolittle-Hydropathy Plot for pTbCOX. The hydropathy score is plotted on Y-axis and the amino acids number on X-axis. The positive score of the hydropathy indicated the hydrophobic segment within the pTbCOX protein sequence.

4.2 Expression, refolding and purification of pTbCOX

Following the T. Barth dissertation, the pTbCOX gene was successfully cloned into a pProExHTa plasmid (Invitrogen). This plasmid was introduced into the *E. coli* strain BL21(DE3) for heterologous protein expression as a recombinant His-tagged protein (rpTbCOX).

The rpTbCOX was found almost entirely in an insoluble form inside inclusion bodies (IBs) after gene induction with isopropyl ß-D-1-thiogalactopyranoside (IPTG) (see details in section 3.2.6.1). I first solubilized the inclusion bodies using N-lauroylsarcosine detergent. However, many different attempts to purify this rpTbCOX by a native purification strategy or by using a lauroylsarcosine-triton X-100 mix in the buffer system throughout the purification were not successful. The inclusion bodies were finally solubilized using 4 molar guanidine hydrochloride (GuHCl) and the protein was re-folded step-wise by GuHCl gradient dialysis with

the introduction of a redox agent (reduced and oxidized glutathione) and L-arginine, following the protocol described in section 3.2.6.2. Following the refolding procedure, rpTbCOX was subjected to 10% SDS-PAGE and Western blot analysis using the ovine anti His-tag antibody (Figure 4.4 and Figure 4.5).
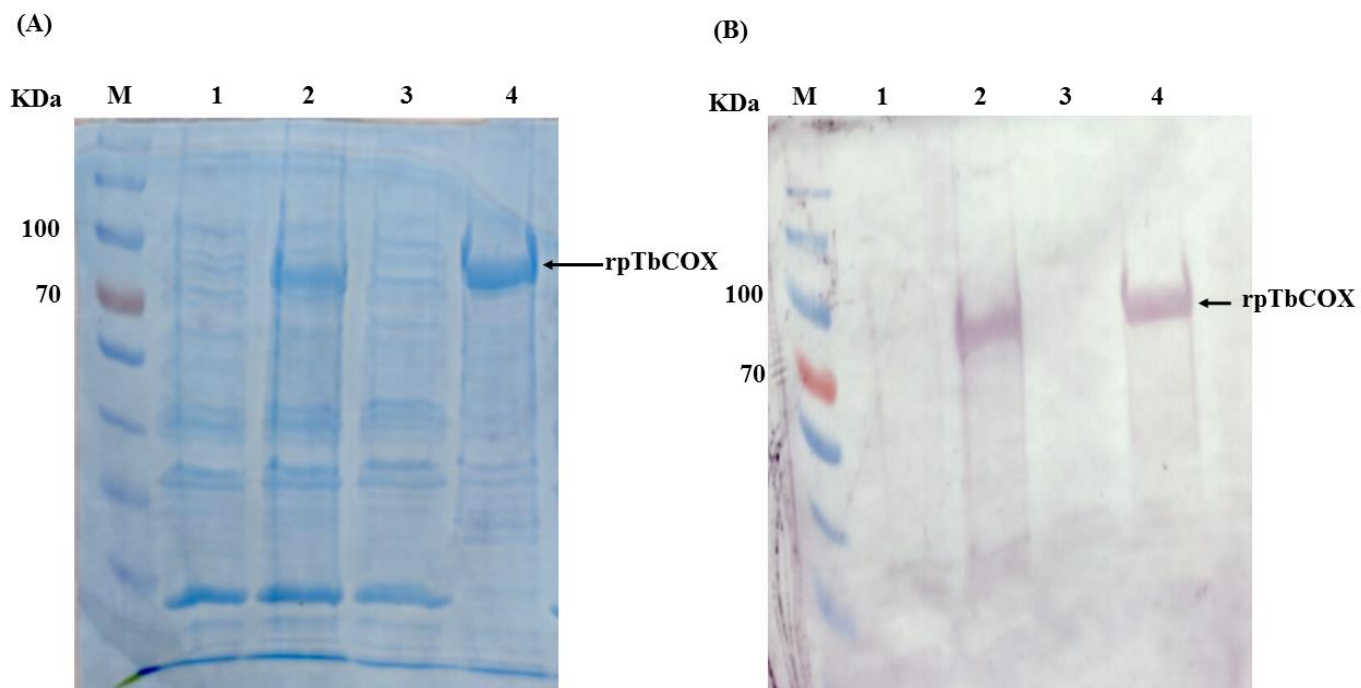

Figure 4.4: rpTbCOX expression in *E. coli* strain BL21 (DE3) and inclusion body preparation with lauroylsarcosine.

(A) Following induction with IPTG, the bacteria were lysed by sonication and the cell supernatant was separated from the pellet by centrifugation. Shown is the 10% reducing SDS-PAGE analysis of uninduced and induced cell lysates. The subsequent pellet fractions were used for inclusion body preparation with lauroylsarcosine. Lane M: prestained molecular weight marker; lane 1: pellet fraction from uninduced cells; lane 2: pellet fraction from induced cells; lane 3: supernatant fraction from inclusion body preparation with lauroylsarcosine; lane 4: inclusion body preparation with lauroylsarcosine. The gel was stained with Coomassie Brilliant Blue.

(B) Shown is the Western blot analysis of the former SDS PAGE gel using the antiHis-tag antibody. Upon addition of IPTG (+), the cells efficiently express the rpTbCOX protein. Lane M: prestained molecular weight marker; lane 1: protein extract from uninduced cells; lane 2: protein extract from induced cells; lane 3: supernatant from inclusion body preparation with lauroylsarcosine; lane 4: inclusion body preparation with lauroylsarcosine.
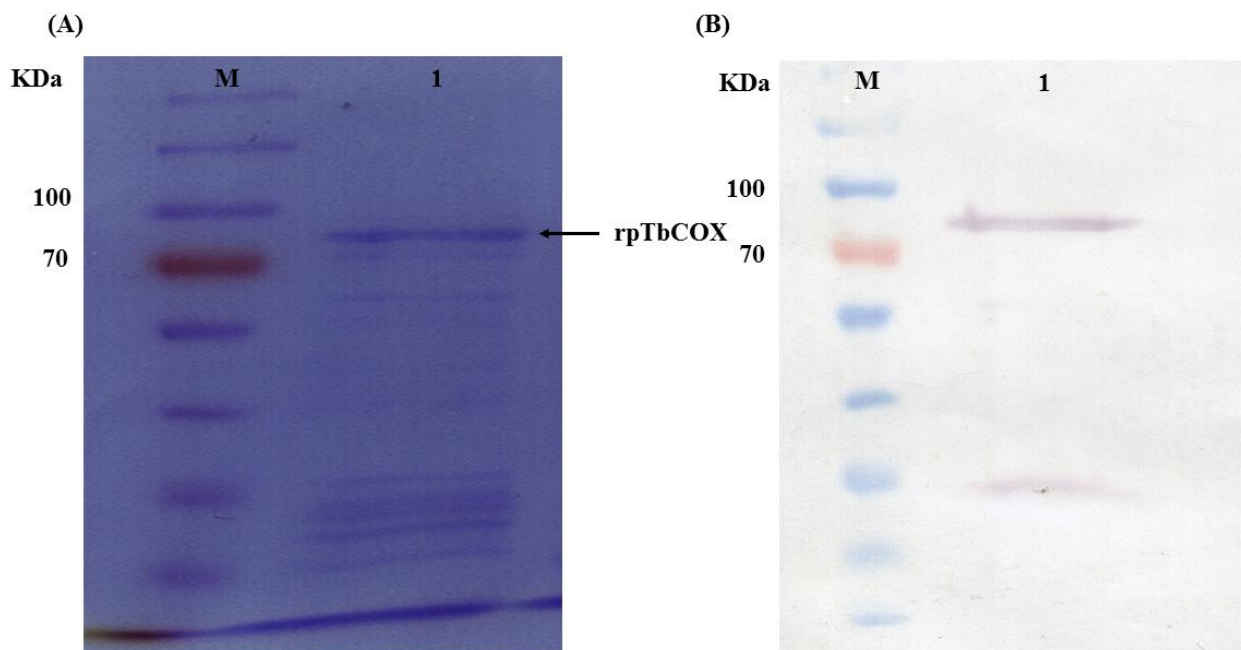
Figure 4.5: SDS-PAGE and Western blot analysis of rpTbCOX after the redox refolding procedure to determine the approximate size and yield. The recombinant rpTbCOX was quite stable to be load onto a Ni-NTA column after the refolding procedure under ÄKTA-FPLC. Lane M: protein molecular weight marker; lane 1: inclusion bodies solubilized with GuHCl, ß-mercaptoethanol and step-wise dialysis with GSH/GSSH plus L-arginine.

The rpTbCOX was successfully purified by one-step affinity chromatography using a Ni-NTA column on the ÄKTA-FPLC system following the protocol described in section 3.2.6.3. The protein profile (of the rpTbCOX) as eluted from the Ni-NTA column after the ÄKTA-FPLC run is presented in Figure 4.6. The flow through and elution fractions were immediately analyzed by SDS-PAGE and silver staining (Figure 4.6 **B**). Mass spectrometry confirmed the identity of the purified protein.
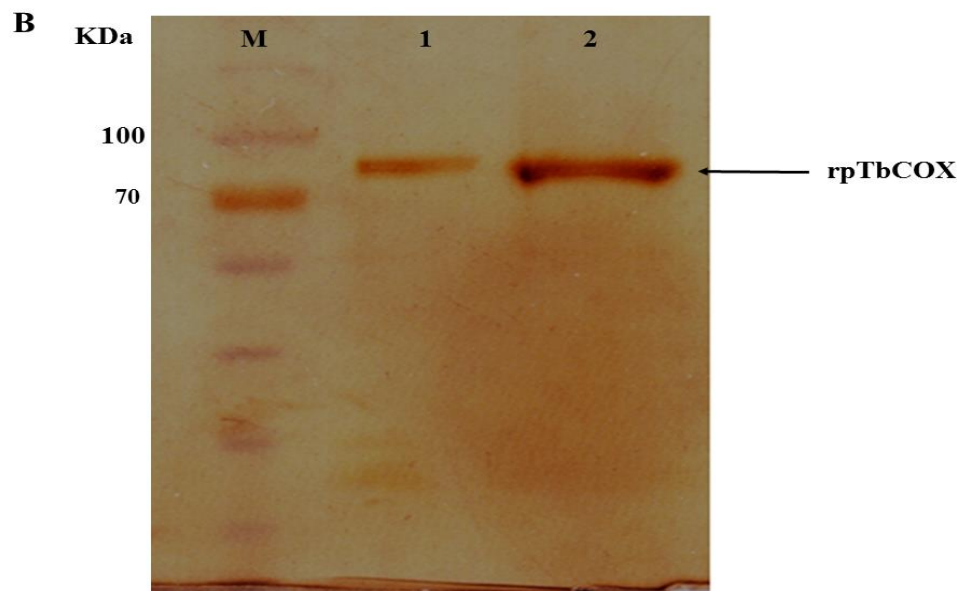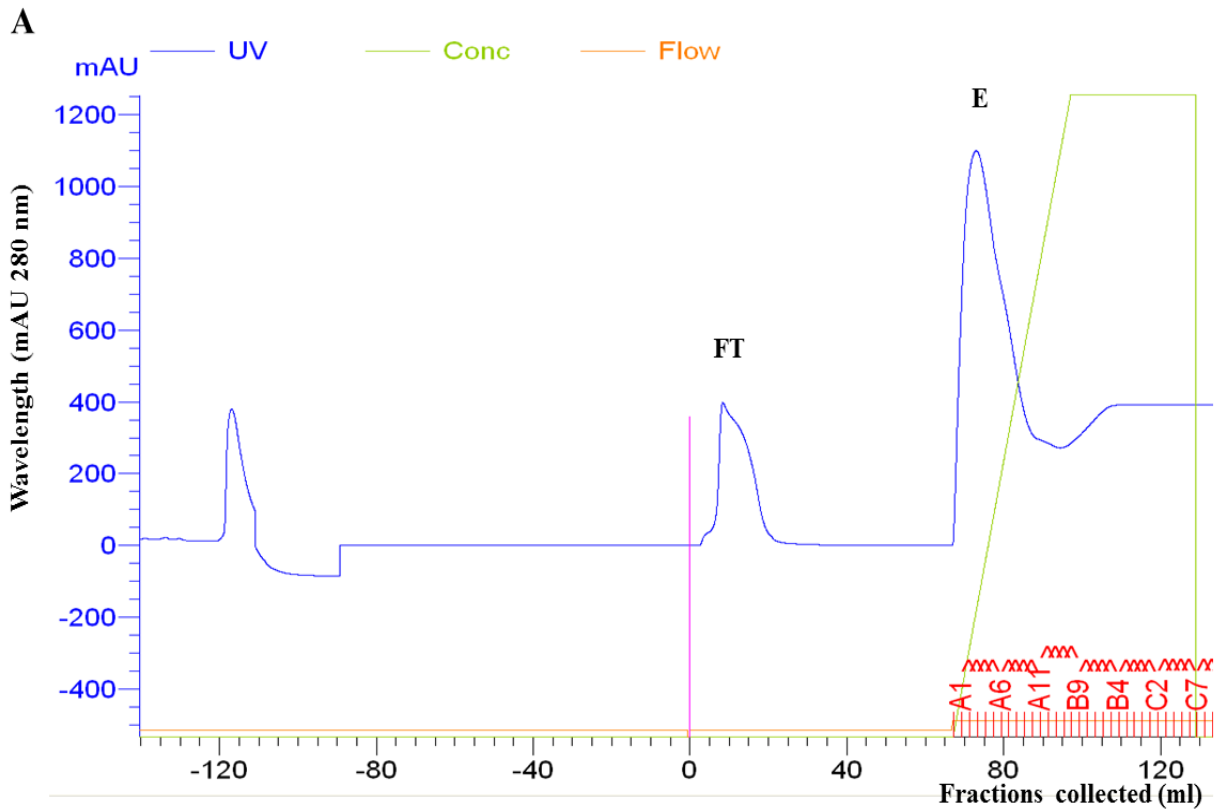
Figure 4.6: IMAC purification of the GuHCl-denatured rpTbCOX after refolding of the protein from inclusion bodies. **(A)** Chromatogram of the Ni-NTA chromatography illustrating the flow through (FT) and the Elution peak (E) of rpTbCOX. The Y-axis shows arbitrary absorbance units at 280 nm; the X-axis shows different fractions collected. The green solid line represents the imidazole gradient from 0 to 500 mM, passing through the elution peak (E).

The fractions A_1 to A_{12} were pooled and loaded onto the gel as shown in Figure 4.4 B. **(B)** Silver stained SDS-PAGE gel, indicating the identity of the purified rpTbCOX. Lane M: protein molecular weight marker; lane 1: pooled eluted fractions A_1 to A_{12}; lane 2: pooled eluted fractions A_1 to A_{12} after concentration using centricon with a molecular weight cut-off (MWCO) of 10 kDa (Millipore).

The pooled and concentrated elution fractions did not show any cyclooxygenase activity after performing a thin layer cyclooxygenase activity assay (section 3.2.6.4) (data not shown).

4.3 Cloning and expression of pTbCOX in Sf9 insect cells and *in vivo* protein crystallization

The pTbCOX gene sequence (Tb427.10.13790/Tb927.10.13790) was obtained from the *T. brucei* genome databank (Tritrypdb or Genedb). For PCR amplification of the pTbCOX, specific forward and reverse primers with BamHI and HindIII restriction sites were designed using Primer 3 software (see section 3.1.6). The pTbCOX gene was amplified by PCR using the above primers, AccuPrime Tag DNA polymerase (Invitrogen) and the trypanosome genomic DNA as a template (see section 3.2.1.1), following the protocol described in section 3.2.1.2. The TbCOX gene was successfully amplified and visualized in 1% agarose gel electrophoresis. The expected size of the TbCOX PCR product was 2079 bp and a band was seen at 2 kb. The respective gel is presented in Figure 4.7.
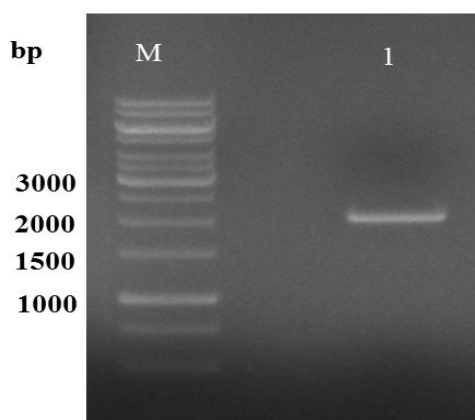

Figure 4.7: PCR amplification of the pTbCOX gene from Trypanosome genomic DNA using Accu Prime Tag DNA Polymerase. A 1% (w/v) agarose gel electrophoresis confirming the correct pTbCOX gene amplification. Lane M: molecular marker, 1 kb Gene Ruler; lane 1: pTbCOX PCR

product at 2 kb.

The pTbCOX PCR product was excised and extracted from the agarose gel and the DNA concentration was determined following the protocol described in section 3.2.1.4. The excised PCR product was first ligated into pCR 2.1-TOPO TA as a subcloning vector (see section 3.2.1.5) and then transformed using chemically competent *E. coli* cells (see section 3.2.1.7). The pTbCOX-pCR 2.1 recombinant clone was digested with BamHI and HindIII restriction enzymes (see section 3.2.1.11) and validated to be the correct construct by DNA sequencing analysis (see section 3.2.1.12).

The sample obtained by restriction digestion analysis was loaded on a 1% (w/v) agarose gel and subjected to electrophoresis. The result is shown in Figure 4.8.
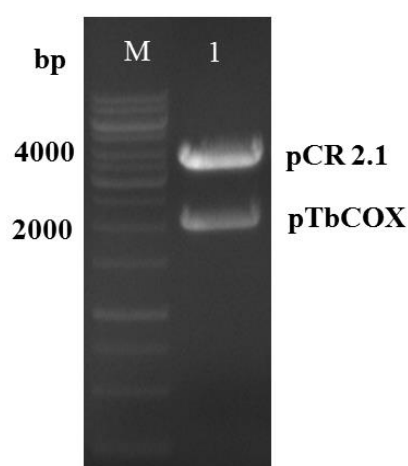

Figure 4.8: Agarose gel electrophoresis after digestion of the pTbCOX-pCR 2.1 recombinant clone with BamHI and HindIII. Lane M: Molecular weight marker, 1 kb Gene Ruler; lane 1: sample run, the upper band corresponds to the size of the vector pCR 2.1 (3929 bp), the lower band corresponds most likely to the size of pTbCOX (2079 bp).

The digested product was then ligated into the target vector pFastBacHTb previously prepared and digested with the same restriction enzymes (BamHI and HindIII). Formation of the pTbCOX-pFastBacHTb construct was done following the protocol described in section 3.2.1.6.

After ligation of the excised DNA into the donor plasmid pFastBacHTb, each ligation product was used for transformation of competent *E. coli* cells (see section 3.2.1.7). The clones were analyzed by bacterial colony PCR (see section 3.2.1.8) using specific pTbCOX primers. The clone containing the pTbCOX insert was subjected to restriction digestion analysis using BamHI and HindIII after plasmid mini-preparation (see section 3.2.1.9) and submitted for DNA sequencing. The sequencing results were analyzed with the NCBI

blast 2 sequence program, which showed that the sequence of pFastBacHTb was correct and that pTbCOX-pFastBacHTb had no mutations.

Figure 4.9 shows the result of the agarose gel electrophoresis for the pTbCOX-pFastBacHTb recombinant clones after digestion with BamHI and HindIII restriction enzymes.
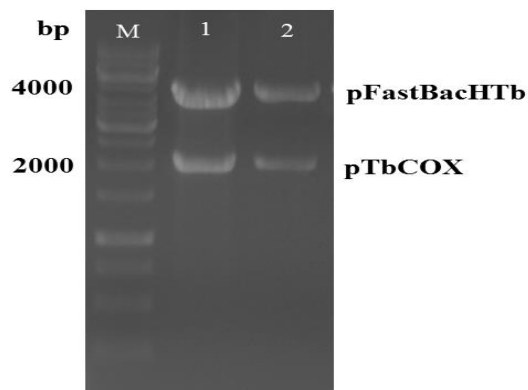

Figure 4.9: Agarose gel electrophoresis after digestion of pTbCOX-pFastBacHTb recombinant clones with BamHI and HindIII. Lane M: Molecular marker, 1 kb Gene Rule; lane 1 and 2: sample run, the upper band corresponds to the size of the vector pFastBacHTb (3930 bp), the lower band corresponds most likely to the size of pTbCOX (2079 bp).

In the next step, DH10Bac *E. coli* cells were transformed with pTbCOX-pFastBacHTb recombinant clones to generate a recombinant bacmid following the protocol described in section 3.2.2.2.2. After transformation, 4 white clones of the putative TbCOX-pFastBacHTb vector were picked and used for overnight cultures. Bacmid PCR analyzed the selected clones with M13 reverse and forward primers for the right clone selection containing the recombinant bacmid. Bacmid PCR was done following the Bac-to-Bac baculovirus expression system manual (Invitrogen, Germany). Figure 4.10 shows the results of the Bacmid PCR product analyzed with agarose gel electrophoresis. Obviously, the pTbCOX-pFastBacHTb clones contained the recombinant bacmid, since a band appeared at the expected size of 4509 bp (2430 bp + 2079 bp).
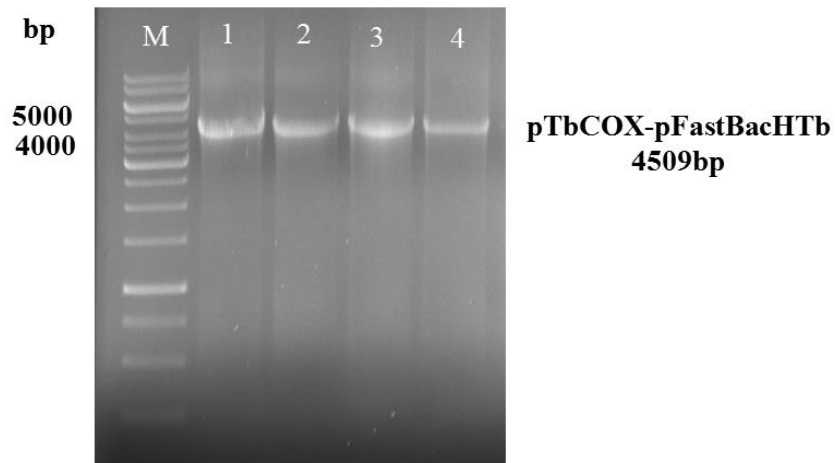
Figure 4.10: The results of the 1% (w/v) agarose gel electrophoresis showing the presence of the recombinant bacmid band at the expected size of about 4500 bp (4509 bp) in all four pTbCOX-pFastBacHTb clones analyzed by Bacmid PCR.

In the next step, the recombinant bacmid was isolated from overnight cultures of pTbCOX-pFastBacHTb clones following the protocol described in section 3.2.1.10. Then, the isolated bacmid containing the inserted pTbCOX encoding gene was used for the transfection of Sf9 insect cells (see section 3.2.2.2.3) and consecutive infections to produce three virus generations (P1, P2, P3). Sf9 insect cells showed first signs of infection 72 h after the transfection (increased cell diameter, bigger cell nuclei). 120 h or 5 days after transfection, late signs of infection in 80% of Sf9 insect cells were apparent (cessation of cell growth, granular appearance, detachment from substrate, cell lysis).

The pTbCOX-pFastBacHTb P1 viral stock was isolated and used to generate a high titer P2 stock. 120 h after infection 80% of Sf9 cells showed late signs of the infection. Therefore pTbCOX-pFastBacHTb P2 viral stock was isolated and used to generate a high titer P3 virus stock. The above process of virus stock isolation and amplification was performed following the protocol described in section 3.2.2.2.4. Afterward, the virus titer of the P3 virus stock was determined using the Reed-Muench method (section 3.2.2.2.5).

In the next experiment, Sf9 insect cells in 6-well plates were infected with a pTbCOX P3 virus with a MOI of 0.1 pfu/cell and 0.2 pfu/cell for crystal production and pTbCOX protein expression (section 3.2.8.1). Figure 4.11 showing the pTbCOX microcrystal structure obtained after 14 days post infection with pTbCOX P3 virus stock.
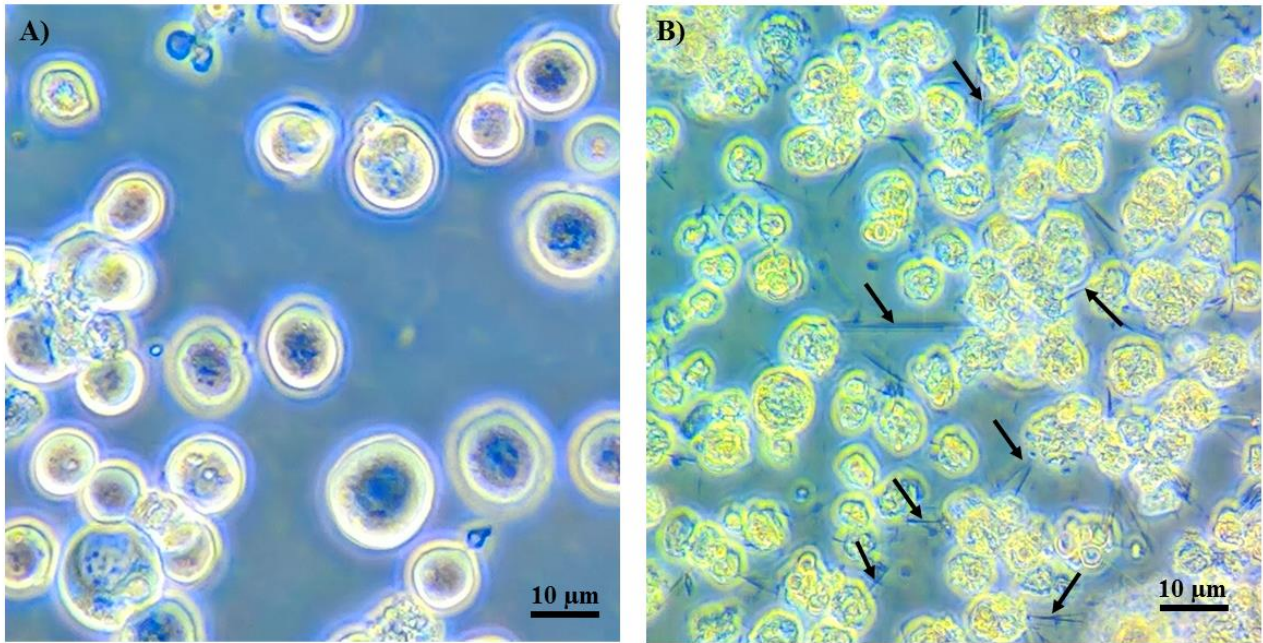
Figure 4.11: Light micrograph of Sf9 insect cells showing **A)** non-infected Sf9 cells as a negative control and **B)** P3 infected Sf9 cells containing pTbCOX microcrystals 14 days post infection. (Black arrows: needle shaped pTbCOX microcrystals).

The pTbCOX crystals were isolated by centrifugation (section 3.2.8.1), concentrated (3×10^6 crystals/ml), solubilized using sodium acetate pH 3.6 (section 3.2.8.1) and identified by Western blot analysis using Anti-His Tag antibody (section 3.2.6.7) and scanning electron microscopy (section 3.2.5.2) (Figure 4.12 and Figure 4.13).
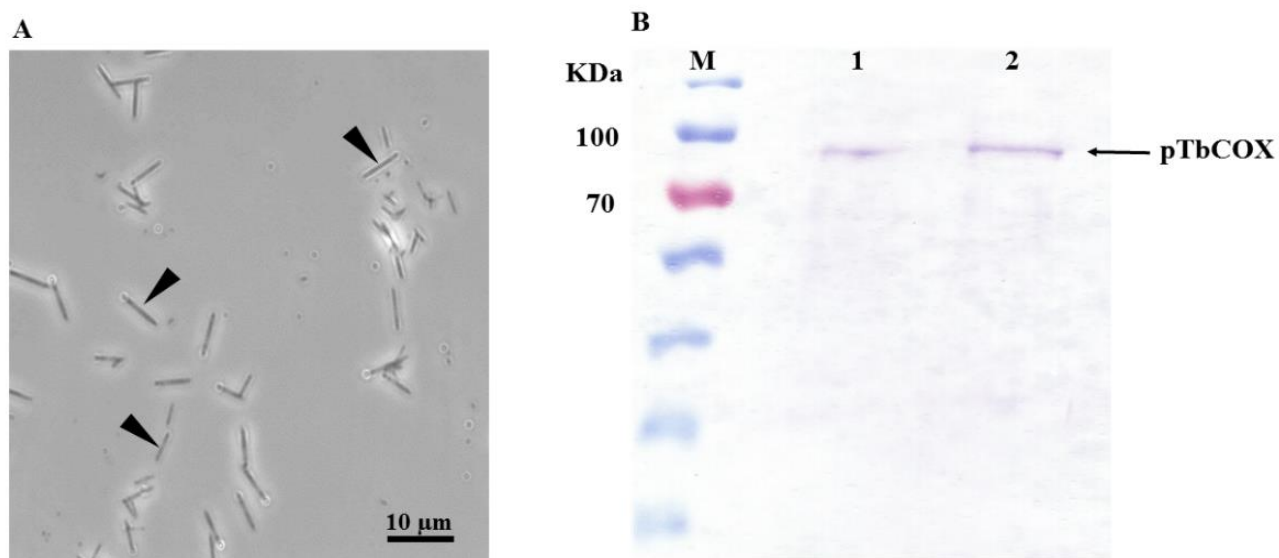
Figure 4.12: Images are showing: **(A)** phase contrast microscopy picture of pTbCOX isolated and concentrated crystals (arrowhead indicates pTbCOX crystals) and **(B)** Western blot analysis of pTbCOX solubilized crystals at ca. 74.68 kDa. Lane M: protein molecular weight marker (Page Ruler Prestained from Thermo Scientific); lane 1: pTbCOX crystals isolated non-concentrated; lane 2: pTbCOX crystals isolated and concentrated using centricon 30 kDa (Millipore).
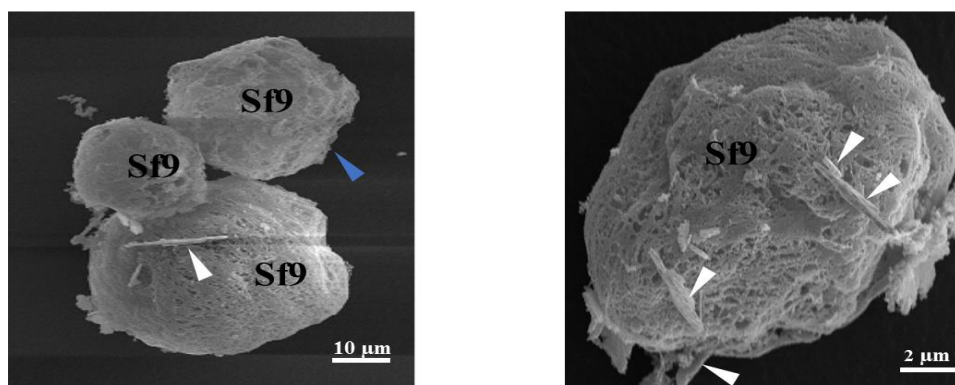
Figure 4.13: Scanning electron micrograph images of pTbCOX *in vivo* crystals protruding in /out Sf9 insect cells. Blue arrowhead indicates normal Sf9 insect cells without crystals, and the white arrowhead indicates pTbCOX *in vivo* crystals.

The pTbCOX isolated crystals (1 x 10^6 crystals/ml) were analyzed by second order nonlinear optical imaging of chiral crystals (SONICC), based on second harmonic generation (SHG) microscopy as an approach for

detection and characterization of protein crystals (section 3.2.7.1). Figure 4.14 presenting the results of SONICC and conventional optical methods for protein crystal detection of pTbCOX.
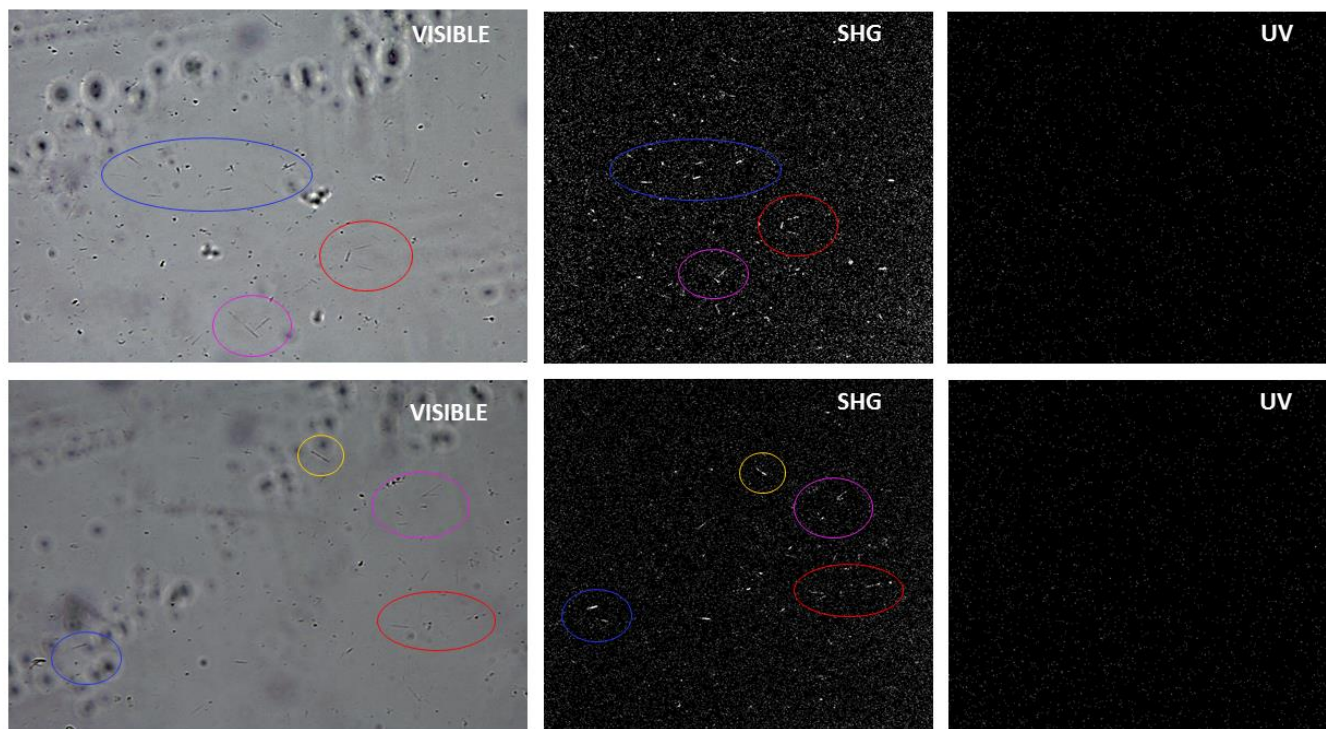
Figure 4.14: Analysis of pTbCOX crystals by SONICC. From left to right: Comparison of visible, second harmonic generation (SHG) and conventional UV-excited fluorescence (UV). The resulting signal of this second harmonic generation (SHG) process can be detected at a wavelength of 532 nm with SHG exposure time of 30 second. The tiny pTbCOX crystals and signal of SHG are shown inside the different circle.

A. Lysozyme nanocrystals
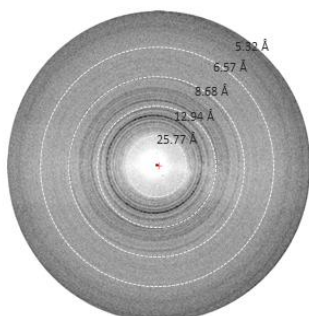
B. pTbCOX *in vivo* crystals

Exposure: 5 min
Resolution: 4.484 Å
Δphi: 3°
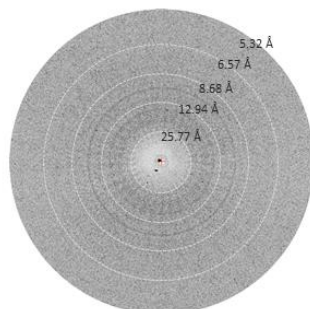
Exposure: 1 min
Resolution: 4.484 Å
Δphi: 1°
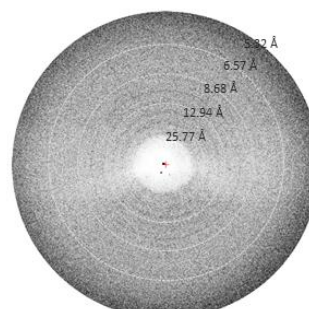
Exposure: 5 min
Resolution: 4.484 Å
Δphi: 3°

Figure 4.15: X-ray powder diffraction analysis of pTbCOX crystals. The pTbCOX crystals showed diffraction patterns using powder diffraction. Lysozyme nanocrystals were used for comparison and control.

The pTbCOX isolated *in vivo* crystals were solubilized with 200 µl 50 mM sodium acetate at pH 3 and concentrated using centricon 30 kDa centrifugal filter units (Millipore) at a centrifugation speed of 15000g at room temperature till approximately 30 µl volume was left. Immediately afterwards, the DLS measurement and CD spectroscopy were performed using Spectro Light 300 (Xtal-Concepts, Hamburg, Germany) and CD spectrometer J-815 (Jasco, UK) at DESY – Hamburg (Prof. Christian Betzel Laboratory). DLS measurement was performed with 15 µl at 20°C for 20 times 30-second measurements and CD spectroscopy was done over a wavelength area of 190-260 nm (15 measurements were accumulated and the buffer signal subtracted).

The DLS measurement of sample 1 performed after pTbCOX crystals solubilization with 200 µl 50 mM sodium acetate pH 3.6 using a sample concentration of 6 mg protein per ml showed highly aggregated protein molecules (R_h around 300 nm) (Figure 4.16).
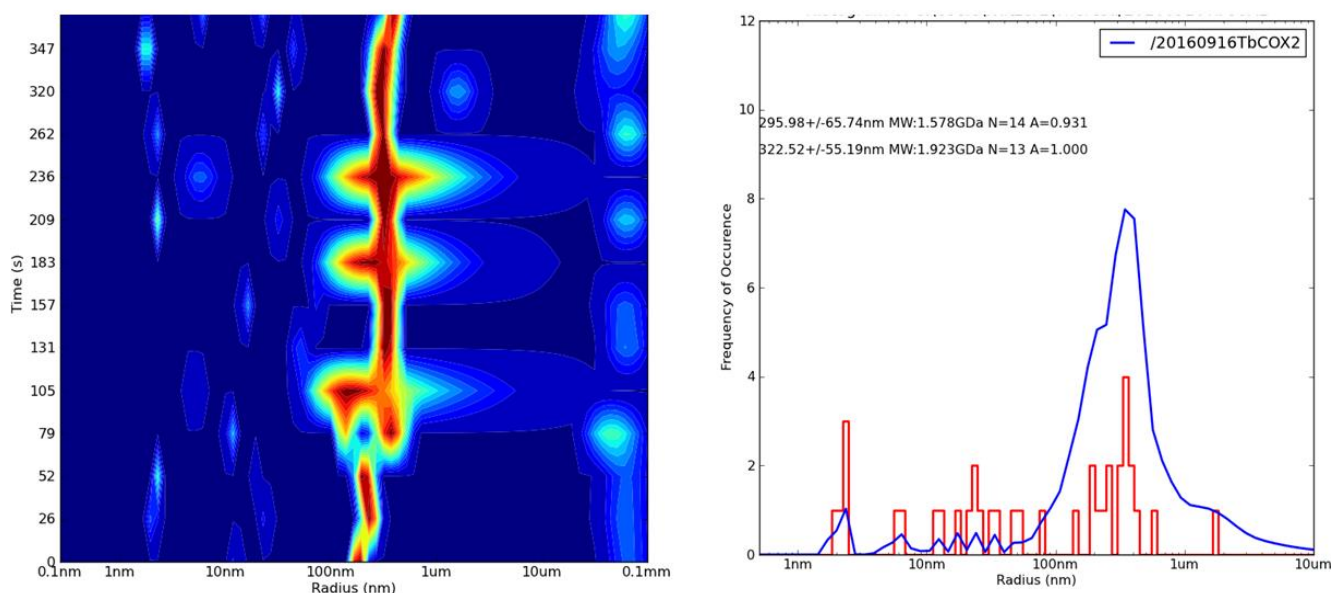
Figure 4.16: DLS measurement of pTbCOX crystals solubilized with 50 mM sodium acetate at pH 3.6 and the respective histogram plot showing highly aggregated pTbCOX protein, R_h ca. 300 nm and MW between 1.923GDa to 1.578GDa. Sample concentration: 6 mg/ml.

The DLS measurement of sample 2 was done by resolving pTbCOX crystals with 200 µl 50 mM sodium acetate at pH 3.6 using the same purification procedure as before until a volume of 30 µl was left. Then 300 µl of 5 mM sodium acetate buffer (1:10 dilution of 50 mM sodium acetate buffer in bidistilled water) was added. The above sample was centifuged again at 15000g at RT using the centrion until a volume of 30 µl left and then diluted 1:10 with bidistilled water. The final solution containing the pTbCOX crystals in 0.5 mM sodium acetate at pH 3.6 was transferred to a new Eppendorf vessel and centrifuged for 1 h at 15000g to get rid of any remaining precipitate. The final sample concentration was 1 mg protein per ml and showed monomeric protein molecules with R_h 4.30 ± 0.50 nm and a MW of approximately 89 kDa (Figure 4.17). The CD spectroscopy was performed by resolving the pTbCOX crystals in 50 mM sodium acetate pH 3.6 after 1:3 dilution with bidistilled water (16.7 mM sodium acetate pH 3.6). The CD spectra showed that pTbCOX protein is stable and properly folded in the above optimal buffer condition (Figure 4.18 **A**). The pTbCOX protein secondary structure estimated by using Yang's reference (Yang et al., 1986) revealed 25.7% helix, 27.7% beta sheet, 16.4% beta turn and 30.2% random (Figure 4.18 **B**).
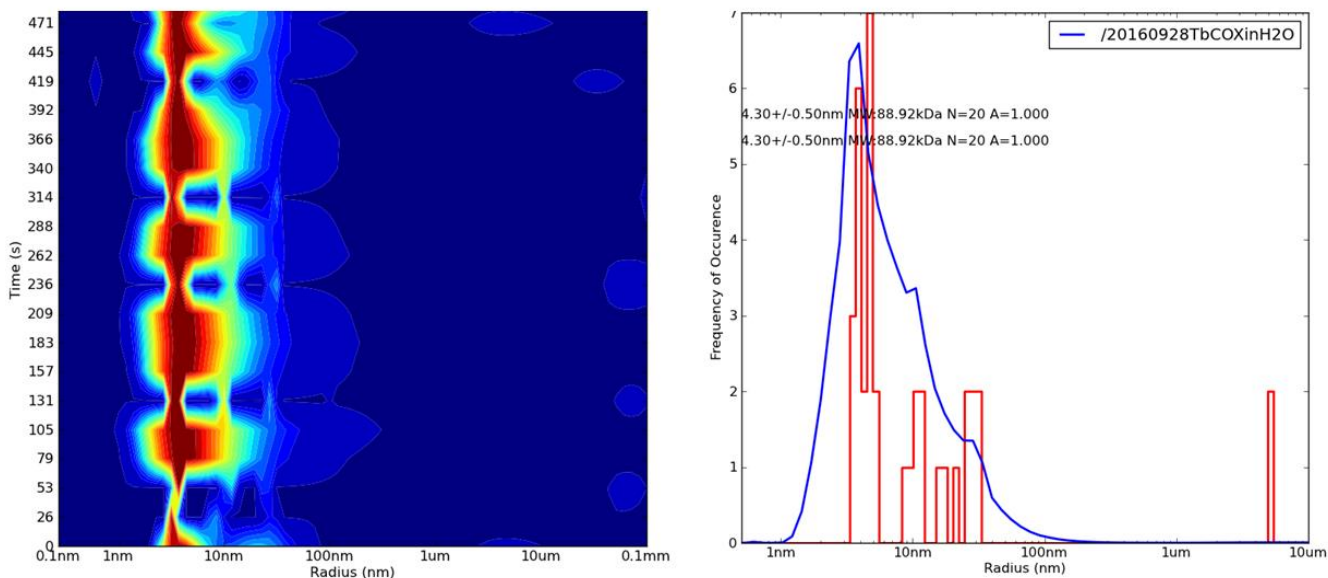
Figure 4.17: DLS measurement of pTbCOX crystals solubilized with 0.5 mM sodium acetate at pH 3.6 and the respective histogram plot showing monomeric protein molecules with R_h 4.30 ± 0.50 nm and a MW of approximately 89 kDa. Sample concentration 1 mg/ml.

Helix	25.7 %
Beta	27.7 %
Turn	16.4 %
Random	30.2 %
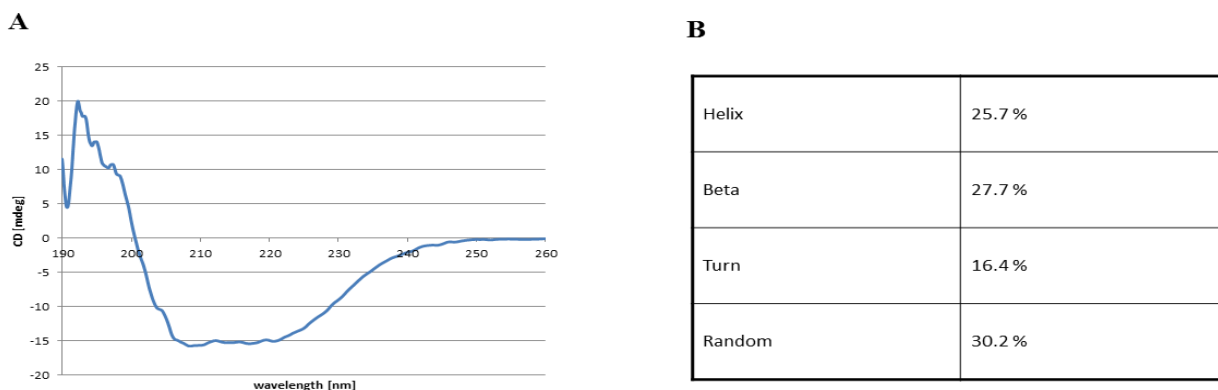
Figure 4.18: Circular Dichroism spectra of the pTbCOX crystals resolved in 16.7 mM sodium acetate pH 3.6. **(A)** CD spectrum of pTbCOX and **(B)** Secondary Structure Estimation of pTbCOX using Yang's reference (Yang et al., 1986).

4.4 pTbCOX RNA interference (RNAi) studies and phenotypes analysis

To investigate and validate the physiological function of the pTbCOX hypothetical protein (Tb427.10.13790) in *T. brucei*, a pTbCOX-knockdown (pTbCOX-KD) fragment of the encoding gene (position 427 bis 991, size: 565 bp) was cloned into an RNAi expression vector (p2T7Ablue) (Figure 4.21 A) which contained two opposing promoters and allowed transcription of the double-stranded RNA upon doxycycline or tetracycline induction.

For PCR amplification of the pTbCOX-KD fragment, specific forward and reverse primers with XhoI and BamHI restriction sites were designed using TrypanoFAN (*Trypanosoma brucei* Functional Genomic Project) (see 3.1.14).

The pTbCOX-KD fragment was amplified by PCR using the above primers, high proofreading AccuPrime Tag DNA polymerase (Invitrogen) and the trypanosome genomic DNA as a template following the protocol described in section 3.2.1.2.

The pTbCOX-KD fragment was successfully amplified and visualized by 1% agarose gel electrophoresis. The expected size of the TbCOX-KD PCR product is 577 bp. The results of the gel for pTbCOX-KD fragment amplification from trypanosome genomic DNA as template are presented in Figure 4.19.
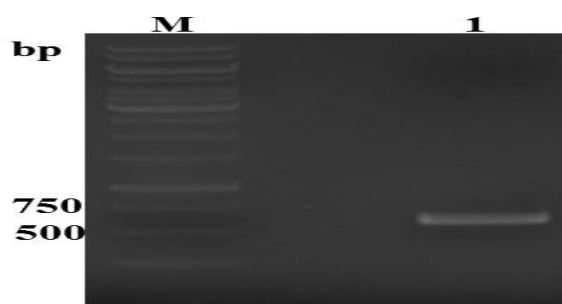
Figure 4.19: PCR amplification of a pTbCOX-KD fragment from trypanosome genomic DNA using Accu Prime Tag DNA Polymerase. A 1% (w/v) agarose gel electrophoresis suggesting the pTbCOX-KD fragment amplification. Lane M: Molecular marker, 1 Kb Gene Ruler (Thermo Fisher Scientific); lane 1: pTbCOX-KD PCR product sized range of about 577 bp.

The pTbCOX-KD fragment was excised and extracted from the agarose gel and the DNA concentration was determined following the protocol described in section 3.2.1.4.

The pTbCOX-KD PCR product was first ligated into pCR 2.1-TOPO TA as a subcloning vector (see section 3.2.1.5) and transformed using chemically competent *E. coli* cells (see section 3.2.1.7). The pTbCOX-KD-

pCR 2.1 recombinant clones were digested with XhoI and BamHI restriction enzymes (see section 3.2.1.11) and validated to be the correct construct by DNA sequencing analysis (see section 3.2.1.12).

The sample from the restriction digestion was analyzed by agarose gel electrophoresis. Figure 4.20 shows the result of the agarose gel electrophoresis.
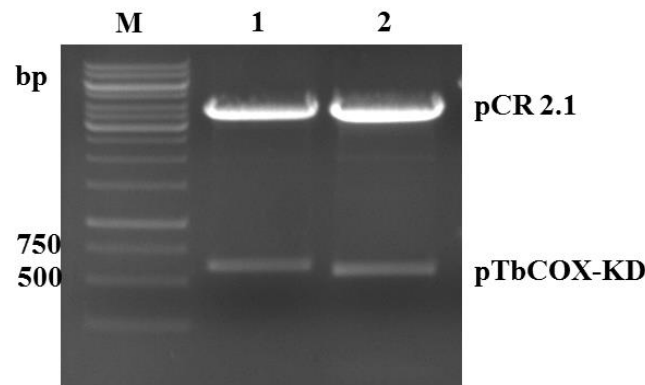
Figure 4.20: Agarose gel electrophoresis after digestion of the pTbCOX-KD-pCR 2.1 recombinant clones with XhoI and BamHI. Lane M: Molecular marker, 1 Kb Gene Ruler (Thermo Fisher Scientific); lane 1: Clone 1; lane 2: Clone 2. The upper band corresponds to the size of the vector pCR 2.1 (3929 bp), and the lower band corresponds to the size of pTbCOX-KD (577 bp).

The pTbCOX-KD digest product was then ligated into the RNAi vector p2T7Ablue (6740 bp) (see Figure 4.21) previously prepared and digested with the same restriction enzymes (XhoI and BamHI). The production of the pTbCOX-KD-p2T7Ablue construct was done following the protocol described in section 3.2.1.5. After ligation of the pTbCOX-KD fragment into the RNAi vector p2T7Ablue, each ligation product was used for transformation of competent *E. coli* cells (see section 3.2.1.7) and the clones were analyzed by bacterial colony PCR (see section 3.2.1.8) using specific pTbCOX-KD fragment primers (Figure 4.21).

The clone that contained the pTbCOX-KD insert was subjected to restriction digestion analysis using XhoI and BamHI after plasmid mini-preparation (see section 3.2.1.9) (Figure 4.21) and submitted for DNA sequencing. The results were analyzed with the NCBI blast 2 sequence program. The pTbCOX-KD-p2T7Ablue construct contained one single point mutation, which was not relevant for the further experiments in respect to RNAi mechanisms consisting of the depletion of mRNA of the target gene using the RNAi enzymatic machinery to cleave the translated dsRNA into small interfering RNA (25 nt).
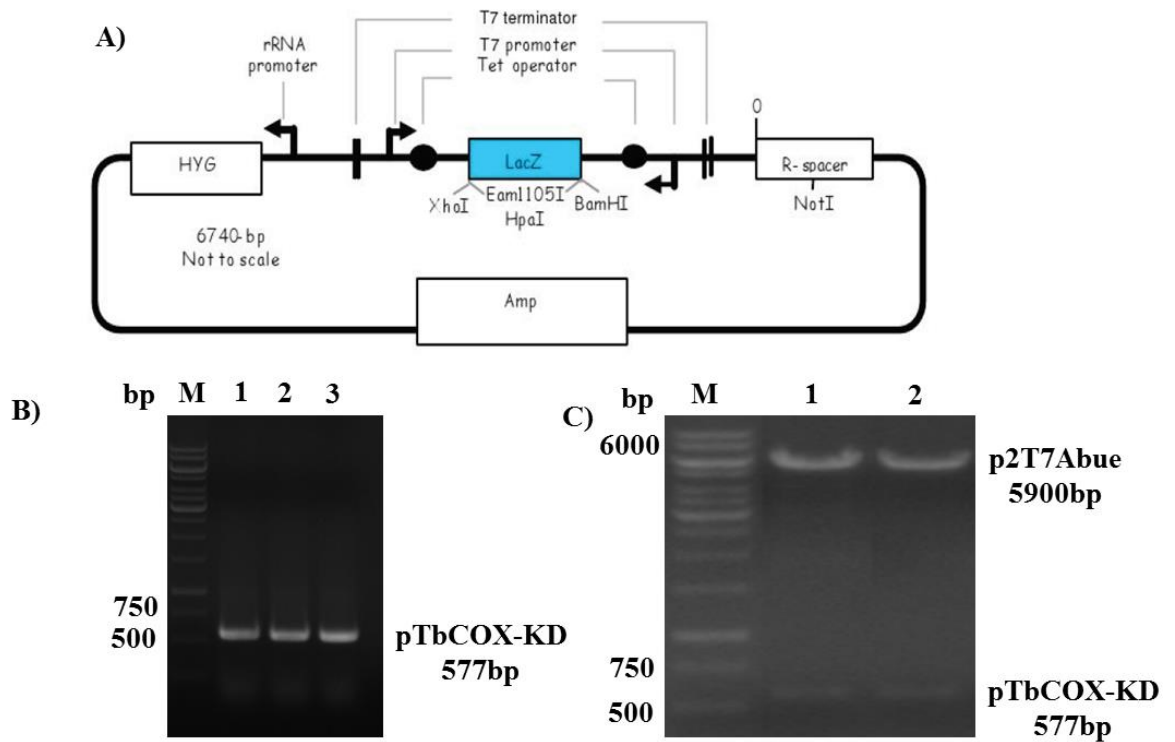
Figure 4.21: A) p2T7Ablue RNAi vector (6470 bp) picture from TrypanoFan; **B)** Validation of the pTbCOX-KD-p2T7Ablue construct by colony PCR; and **C)** Restriction analysis of the pTbCOX-KD-p2T7Ablue construct using XhoI and BamHI. A 1% (w/v) agarose gel electrophoresis confirms the pTbCOX-KD-p2T7Ablue. Lane M: Molecular marker, 1 Kb Gene Ruler (Thermo Fisher Scientific); Lanes 1, 2 and 3 represent different pTbCOX-KD-p2T7Ablue recombinant clones.

After the cloning strategy of the pTbCOX RNAi construct (pTbCOX-KD-p2T7Ablue construct) was successful, bloodform SMB trypanosomes were prepared in cell culture as described in section 3.2.2.2.6. SMB trypanosomes were transfected with the pTbCOX-KD-p2T7Ablue construct (10 µg), afore linearized with NotI restriction enzyme, by electroporation following the SMB transfection protocol (see 3.2.2.2.6).

The NotI linearization of pTbCOX RNAi construct was confirmed and visualized by agarose gel electrophoresis (Figure 4.22).
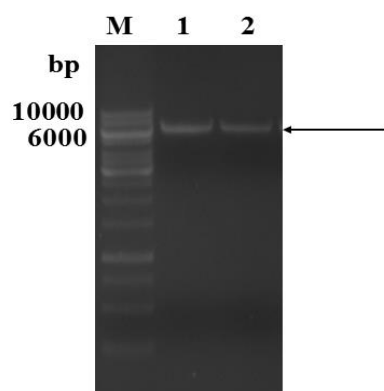
Figure 4.22: NotI linearization of the pTbCOX-KD-p2T7Ablue construct visualized by agarose gel electrophoresis. Black narrow shows the 6473 bp size expected of the recombinant pTbCOX-KD-p2T7Ablue construct after NotI single digestion.

The transfected pTbCOX-KD SMB cells were selected and maintained by *in vitro* cultivation as described in section 3.2.2.2.6 under Geneticin (2 µg/ml) and Hygromycin (2 µg/ml) antibiotics selection pressure for further experiments. During this investigation, two different clones of pTbCOX-KD SMB cells were generated and cryopreserved, named pTbCOX RNAi clone T1.1 and pTbCOX RNAi clone T2.2, respectively. Both cell lines were picked from different electroporation experiments 2 and 5 days post electroporation.

After selection of transgenic clones, post-transcriptional silencing of the pTbCOX target gene was validated and confirmed by quantitative real-time PCR (qRT-PCR) as a standard gold method for measuring the steady state of mRNA levels (see 3.2.3). For the qRT-PCR experiments, specific primers were designed respectively for pTbCOX (target gene-sized 165 bp) and for ß-tubulin (reference gene-sized 76 bp) using Primer 3 and Primer NCBI blast software (see 3.1.6).

The "Power SYBR® Green RNA-to-CTTM" 1-Step Kit from Applied Biosystems, which combines reverse transcription and qPCR in a buffer system, was used to perform the qRT-PCR as described in section 3.2.3.3.

Since the SYBR® Green fluorescence signal, which is used to quantify the amplified amount of DNA, does not allow any conclusions to be drawn about the quality and specificity of the qRT-PCR amplification, these parameters had to be examined separately.

The specificity and the degree of purity of the PCR products were carried out immediately following the qRT-PCR by melting curve analysis. The melting curve showed symmetrical peaks with identical peak maxima.

This symmetrical peak is an indication of the quality of primers and confirms the emergence of a single PCR product. The resulting qR-PCR products were validated for pTbCOX (target gene) and ß-tubulin (reference

gene) by gel electrophoresis analysis. The observed bands (Figure 4.23) are approximately the same as the expected product sizes.

Therefore, these results suggested the correct and specific amplification of the designated cDNA sequence regions for both the β-tubulin (reference gene) and the pTbCOX (target gene).
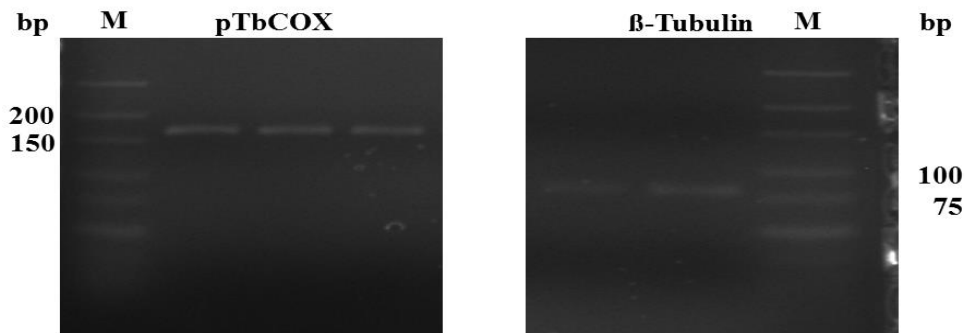
Figure 4.23: 5% (w/v) agarose gel electrophoresis for validation of the qRT-PCR products. Lane M: O'GeneRuler Ultra Low Range DNA Ladder. Expected product sizes were 76 bp for ß-tubulin and 165 bp for the pTbCOX.

The evaluation of the qRT-PCR was carried out as described under 3.2.3.4, according to the method of Pfaffl (2001). From the CT values of the dilution series, a standard curve was created for each primer pair (Figure 4.24).

The qRT-PCR amplification efficiency could be determined from the resulting slope of the compensating straight lines. For pTbCOX, the efficiency was E pTbCOX of 2.11, and for β-tubulin, an E β-tubulin of 2.16 was obtained.
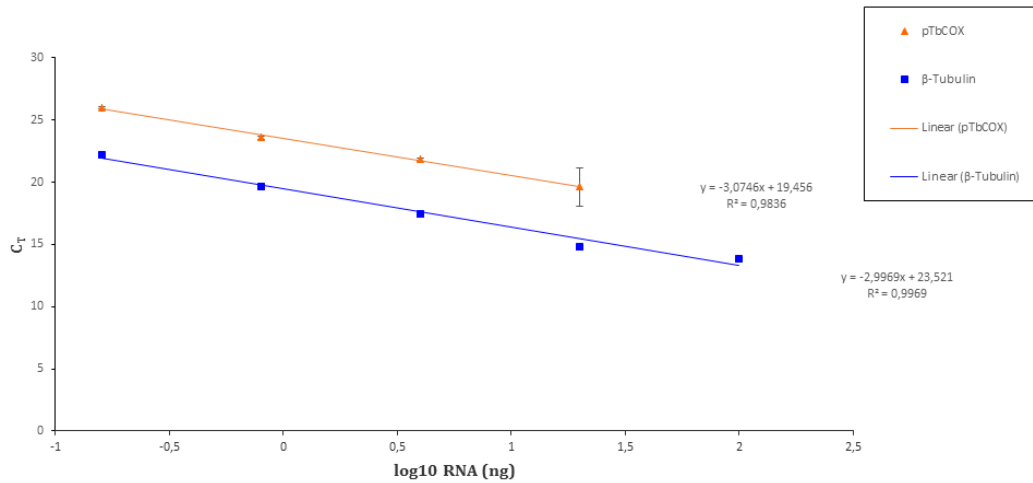
Figure 4.24: Standard curves for qRT-PCR amplification efficiency.

Figure 4.25 presents the results of pTbCOX mRNA levels following 18 h, 42 h and 66 h of RNAi induction of the pTbCOX RNAi clone T1.1 and pTbCOX RNAi clone T2.2. The concentration of pTbCOX-mRNA decreased in both clones to approximately 50% after 18 h and 42 h post-induction by doxycycline and in clone T2.2 to about 25% 66 h post-induction in comparison to the 100% SMB non-transfected cells.
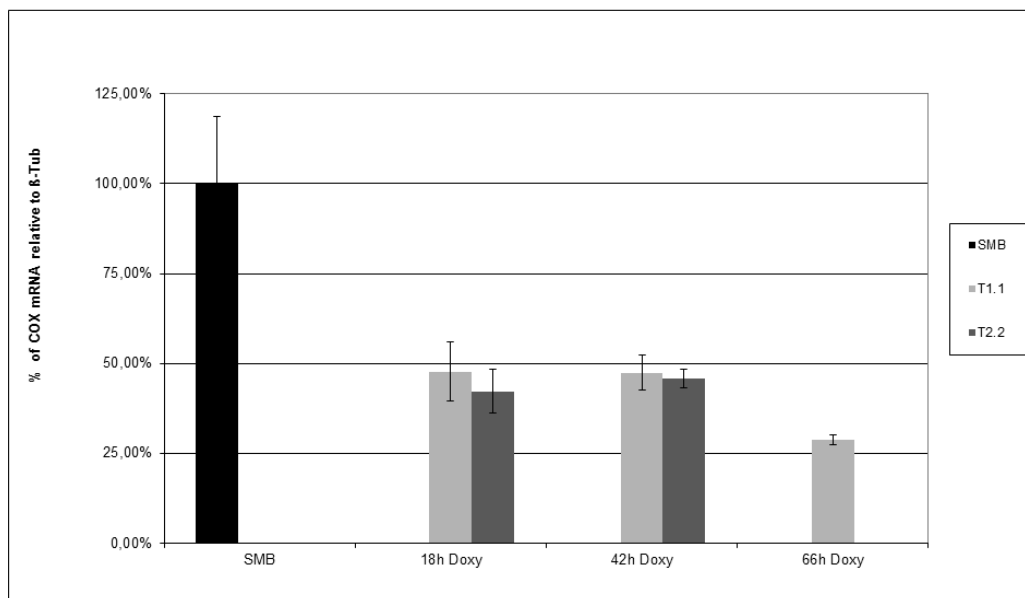
Figure 4.25: qRT-PCR analysis of pTbCOX mRNA levels after 18 h, 42 h and 66 h of RNAi induction by doxycycline, 1 µg/ml. Data were normalized to ß-tubulin mRNA expression. Data represent the means ± SD of three independent experiments.

Next, both clones (T1.1 and T2.2) were characterized individually to assess the effects of the pTbCOX gene depletion on the proliferation of *T. brucei* bloodstream forms.

RNAi was induced by addition of doxycycline (1 µg/ml), and the cell growth was monitored daily using a hemocytometer (Neubauer). Cells culture densities were maintained between 2.5 x 10^4 and 1 x 10^6 cells/ml for keeping the cell growing by daily dilution. The results shown in Figure 4.26 reveal that the pTbCOX RNAi progressively decreases the proliferation of *T. brucei* bloodstreams forms in both, clone T1.1 and T2.2, as compared to the non-transfected SMB trypanosomes (WT).
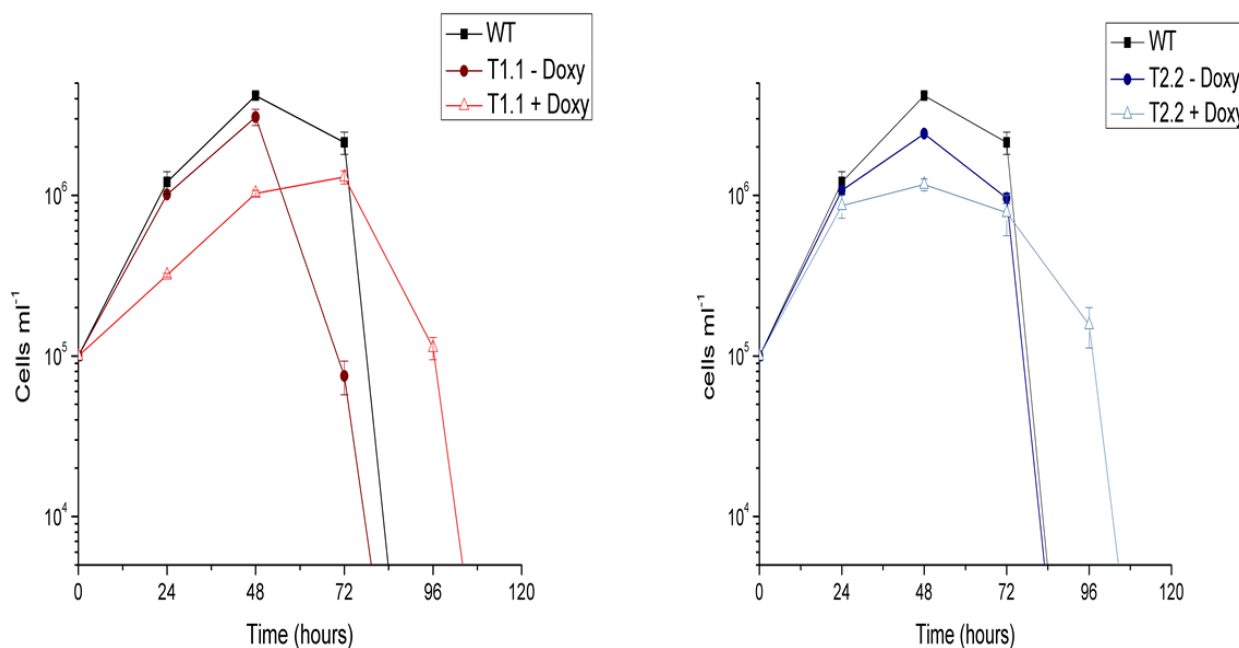
Figure 4.26: Growth curves of RNAi cells lines following the presence (+ Doxy) or absence (- Doxy) of 1 µg/ml doxycycline, in comparison to non-transfected SMB cells lines. The data represent the means ± SD of two biological replicates.

After the *in vitro* proliferation experiments of RNAi cells lines after doxycycline induction, the RNAi-mediated knockdown of the pTbCOX gene caused dramatic changes in the morphology of *T. brucei* bloodstreams forms. We thus moved forward to fully characterize the morphology of the pTbCOX depleted cells using light, fluorescence and electron microscopy. The control SMB trypanosomes cells (without RNAi induction) and the cells depleted of pTbCOX by RNAi were fixed, either DAPI stained or negative stained and examined by light or electron microscopy at different times (0 h, 6 h, 24 h, 48 h, and 72 h) after induction of RNAi by 1 µg/ml doxycycline.

Interestingly, the functional analyses of the pTbCOX gene by RNAi resulted in the appearance of two major phenotypes:

(i) Monster cells with multiple nuclei and multiple flagella, thus suggesting a direct or indirect role in cell division coordination. Those cells progress through multiple rounds of organelle replication but were not able to complete cytokinesis (see Figure 4.27 and Figure 4.28).

(ii) Trypanosomes either multi-nucleated or not, displaying a massive enlargement of the flagellar pocket ("big eye" phenotype) (see Figure 4.28 and Figure 4.29).

Afterward, we produced real time videos of pTbCOX knockdown trypanosomes (data not shown). Our live videomicroscopy showed representatives pTbCOX-KD trypanosomes monster cells and big eye phenotypes.

Trypanosomes showing a knockdown of pTbCOX were fixed and DAPI stained to analyze the kinetoplast-nucleus configuration at various times post doxycycline induction (0 h, 24 h, 48 h, and 72 h). Figure 4.30 shows the result of the pTbCOX silencing. Obviously, the knockdown causes a partial cell cycle arrest and led to accumulation of bloodstream cells with abnormal karyotypes.
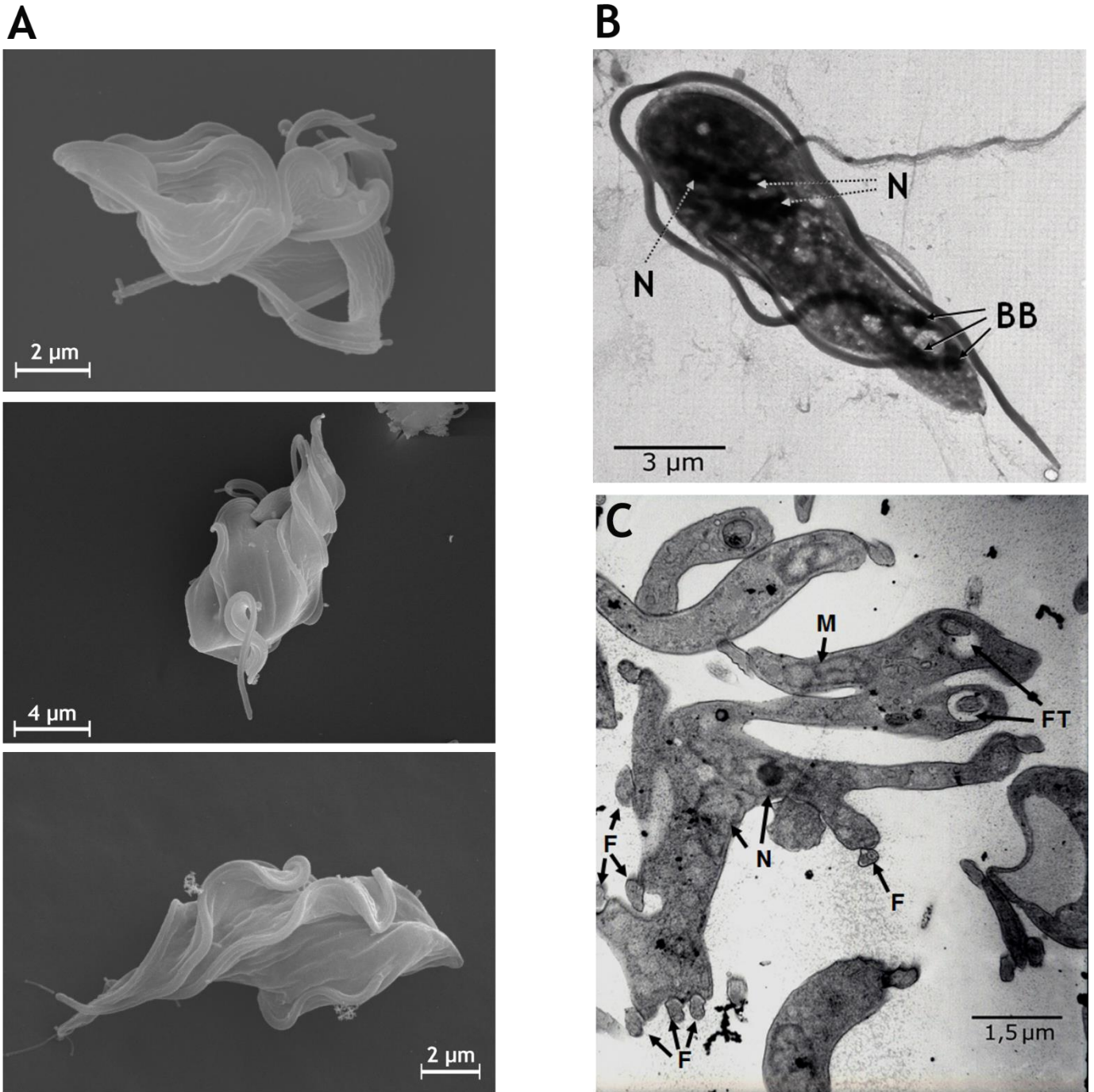
Figure 4.27: **(A)** Scanning electron micrographs of pTbCOX RNAi cells 24 h post-induction of RNAi showing monster cells with multiples nuclei and multiple flagella. **(B)** Electron micrographs of whole-mount negative stained trypanosomes 96 h after doxycycline induction. The cells show 3 nuclei, 3 basal bodies and 3 flagella. **(C)** Transmission electron micrograph taken 42 h after doxycycline induction shows multiple nuclei and flagella as well as protrusion of the cell body associated with peripheral flagella, corresponding to giant cells. Abbreviations: N, nucleus; F, flagellum; FT, flagellar pocket; M, mitochondrion and BB, basal bodies.
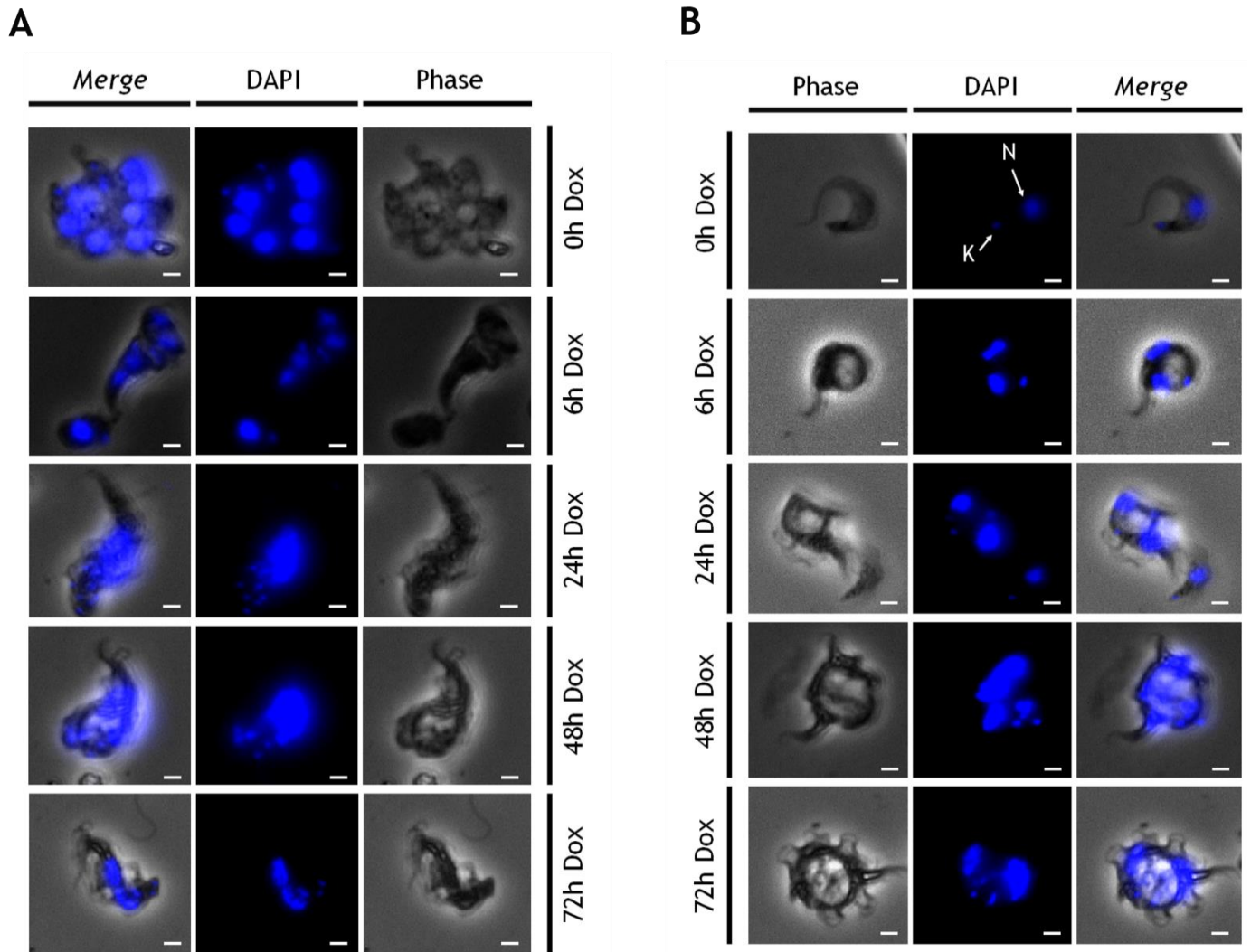
Figure 4.28: **(A)** and **(B)** are representative images of DAPI-stained pTbCOX RNAi clone T1.1 at different time points in the presence of doxycycline (1 µg/ml). **(A)** representative images of multinucleated and multi-flagellated phenotypes observed after 6 h doxycycline induction; **(B)** shows mainly the "Big Eye" phenotype. The images were made using a Zeiss Fluorescence Microscope. Abbreviations: N, nucleus; K, kinetoplast, and Dox, doxycycline.
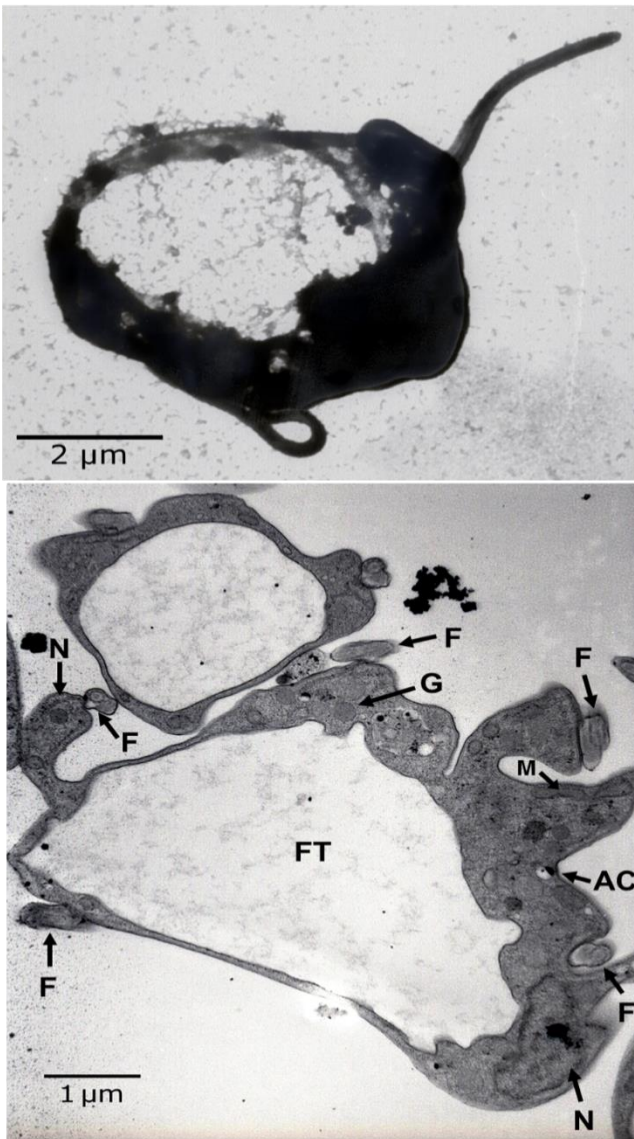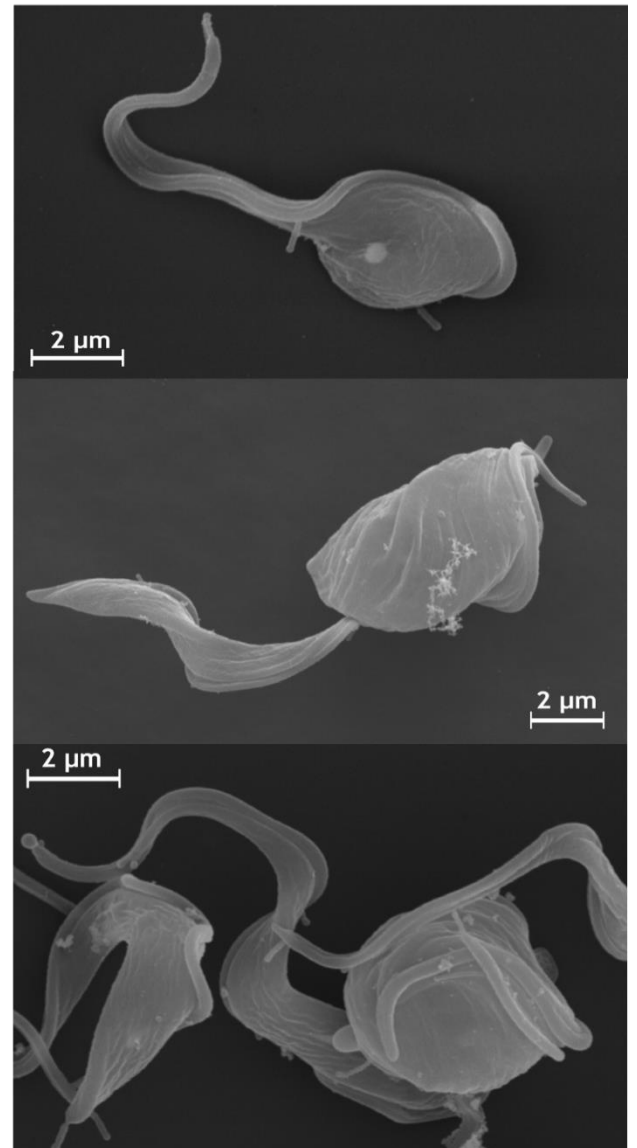
Figure 4.29: Representative images of the morphological changes of the pTbCOX depleted cells after RNAi induction. **(A)** Electron micrographs are showing negative stained pTbCOX RNAi trypanosomes 6 h after doxycycline induction and Transmission electron micrograph showing pTbCOX RNAi trypanosomes 42 h after doxycycline induction. The flagellar pocket is significantly enlarged. **(B)** Scanning electron micrograph of pTbCOX RNAi cells 24 h after doxycycline induction showing the "Big Eye" phenotype: parasites displaying a massive enlargement of the flagellar pocket. Abbreviations: N, nucleus; F, flagellum; FT, flagellar pocket; G, glycosome; M, mitochondrion; AC, acidocalcisome.
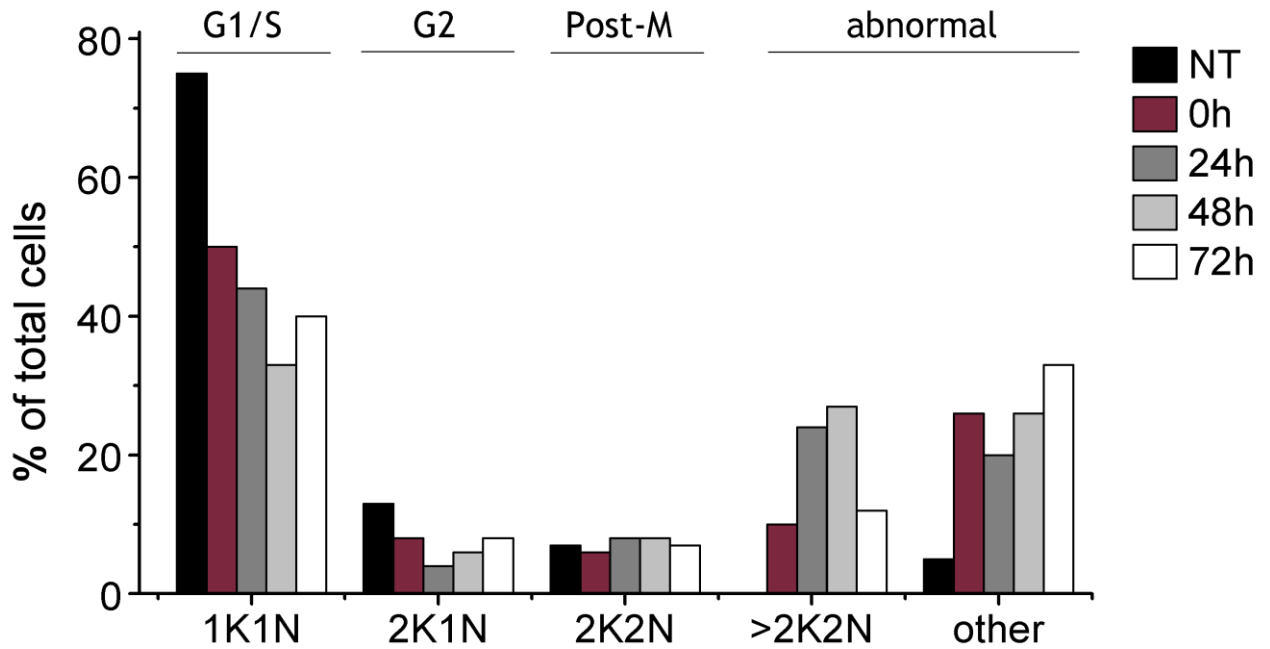
Figure 4.30: Kinetoplast-nucleus configurations of the pTbCOX-KD RNAi cell line at various time points post-induction. Parasites with abnormal karyotypes are subcategorized into multi-nucleated flagellated cells (>2K2N) and other (0K1N, 1K0N, 1K2N, 0K2N). Fluorescence microscopy assessed the number of kinetoplasts (K) and nuclei (N) following DNA-staining with DAPI. At least 100 individual cells were analyzed at each time point. Non-transfected SMB cell line (NT) served as a control.

4.5 Cloning, expression, and localization of an eGFP fused with pTbCOX protein in *Trypanosoma brucei*

For PCR amplification of the pTbCOX, specific forward and reverse primers with HindIII and PvuII restriction sites were designed using Primer 3 software (see section 3.1.6). The pTbCOX gene was amplified by PCR using high fidelity AccuPrime Tag DNA polymerase (Invitrogen) and the trypanosome genomic DNA as a template (see section 3.2.1.1) following the protocol described in section 3.2.1.2. The TbCOX gene was successfully amplified and visualized in 1% agarose gel electrophoresis. The expected size of the TbCOX PCR product is 2079 bp (2 kb). Figure 4.31 shows the results of the pTbCOX gene amplification from trypanosomal genomic DNA as template.
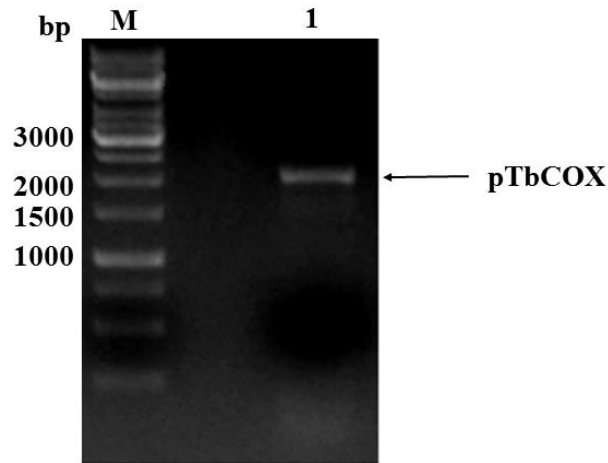
Figure 4.31: PCR amplification of the pTbCOX gene from trypanosome genomic DNA using Accu Prime Tag DNA Polymerase. A 1% (w/v) agarose gel electrophoresis confirming the pTbCOX gene amplification. Lane M: Molecular marker, 1 Kb Gene Ruler (Thermo Fisher Scientific); Lane 1: pTbCOX PCR product sized range of 2079 bp (2 kb).

The pTbCOX PCR product was excised and extracted from the agarose gel. The DNA concentration was determined following the protocol described in section 3.2.1.4. The pTbCOX PCR product was first ligated into pCR 2.1-TOPO TA as a subcloning vector (see section 3.2.1.5) and transformed using chemically competent *E. coli* cells (see section 3.2.1.7). The pTbCOX-pCR 2.1 recombinant clone was validated to be the correct construct by colony PCR and DNA sequencing analysis (see section 3.2.1.12). Figure 4.32 shows the results of the colony PCR analysis using agarose gel electrophoresis.
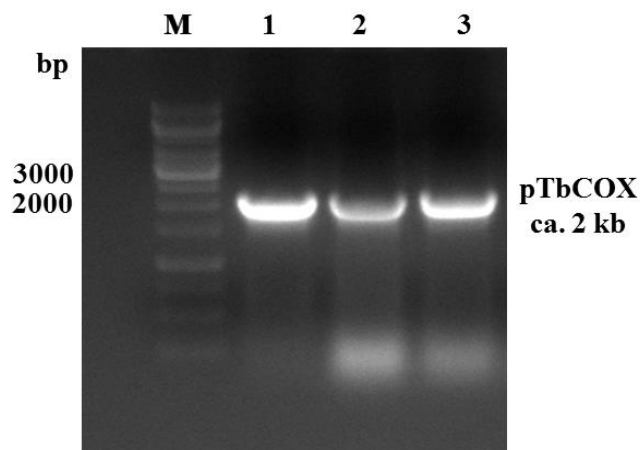
Figure 4.32: Colony PCR of pTbCOX-pCR 2.1 recombinant clones after chemical transformation in *E. coli*. A 1% (w/v) agarose gel electrophoresis suggested the pTbCOX gene amplification. Lane M: Molecular marker, 1 Kb Gene Ruler; lane 1 to 3: colonies from pTbCOX-pCR 2.1 from the plate (pTbCOX insert ca. 2 kb).

The pTbCOX-pCR 2.1 was digested with HindIII and PvuII restriction enzymes (see section 3.2.1.11) and the sample from the restriction digestion analysis was loaded onto a 1% (w/v) agarose gel. Figure 4.33 shows the result of the above restriction digestion analysis by agarose gel electrophoresis.
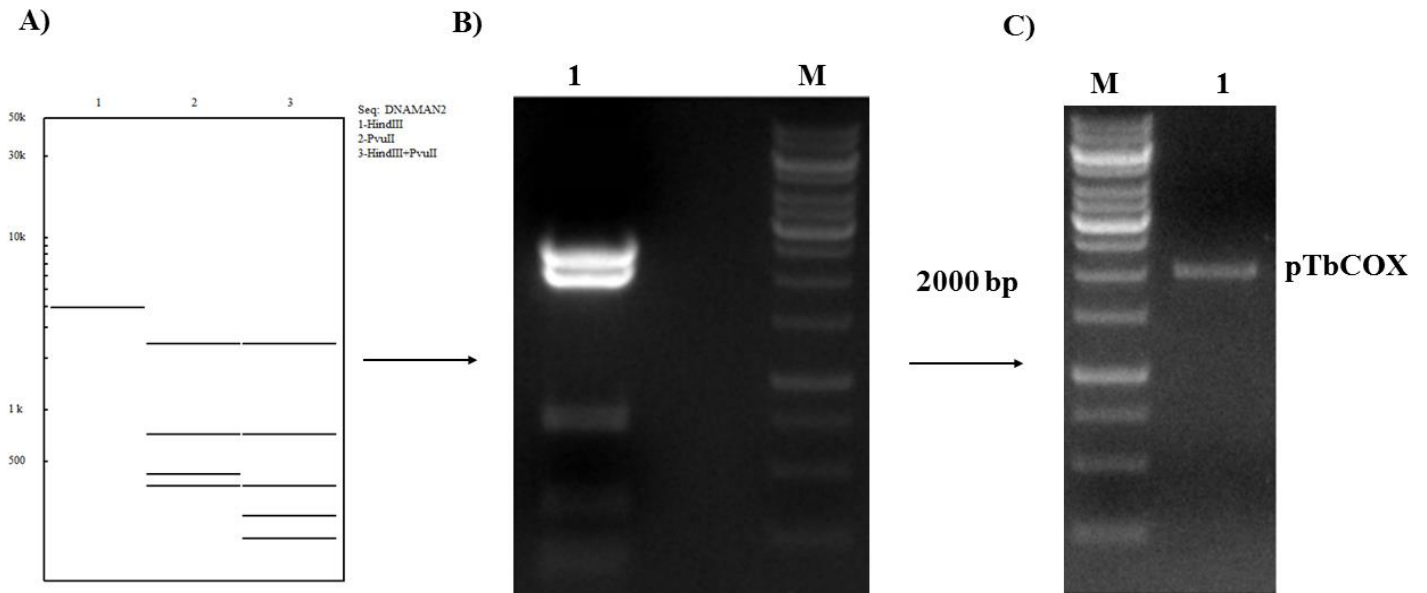
Figure 4.33: A) Illustration of restriction digestion analysis of pTbCOX-pCR 2.1 using DNAMAN software showing in lane 1: pTbCOX-pCR 2.1 single digests with HindIII; lane 2: pTbCOX-pCR 2.1 single digest with PvuII; and lane 3: pTbCOX-pCR 2.1 digests with HindIII and PvuII. **B)** 1% (w/v) agarose gel electrophoresis of the pTbCOX-pCR 2.1 digested with HindIII and PvuII. Lane 1: pTbCOX-pCR 2.1 digests with HindIII and PvuII like predicted in A lane 3. **C)** 1% (w/v) agarose gel electrophoresis of the band ca. 2000 bp lane 1 in B excised and extracted showing a single band of pTbCOX at the right bp size.

The pTbCOX gene was ligated into the pCO57 vector. This vector allows the expression of eGFP fusion to the c-terminus of the desired protein and contains an inducible T7 expression site, which is regulated by a tetracycline operator. Figure 4.34 A shows the results of the ligation and double digestion analysis of the pTbCOX-pCO57 construct with HindIII and PvuII restriction enzymes by agarose gel electrophoresis analysis.

The right and validated pTbCOX-pCO57 construct was linearized with EcoRV (Figure 4.34 B) and then electroporated into SMB cells, which express a T7RNA polymerase and a tetracycline repressor. The electroporated pTbCOX-pCO57 SMB cells line were selected and maintained in *in vitro* culture as described in section 3.2.2.2.6 under Geneticin (2 µg/ml) and Phleomycin (2.5 µg/ml) antibiotics selection pressure for expression of the pTbCOX fused with eGFP in *Trypanosoma brucei*.

I observed that the expression of the green fluorescence pTbCOX protein was leaky and resulted in the death of the electroporated SMB cells 4 days after transfection. Using Zeiss fluorescence microscopy, live imaging of SMB trypanosomes produced single or multi punctuated green fluorescent signals (see Videos).

Next, the electroporated pTbCOX-pCO57 SMB cells line were fixed in 2.5% glutaraldehyde and DAPI stained for fluorescence microscopy analysis. This experiment showed that the pTbCOX green fluorescent protein was not located in the cytosol but appeared as a single dot near the kinetoplast or between kinetoplast and nucleus (Figure 4.35). The pTbCOX fused eGFP overexpression was extremely fast lethal for bloodstream form parasites.
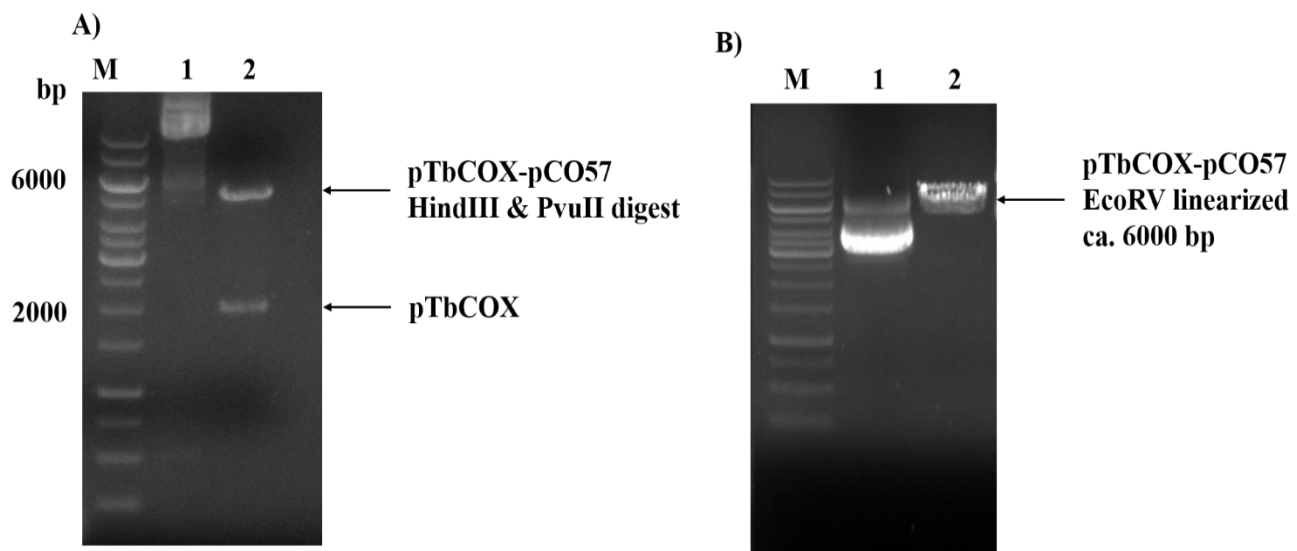
Figure 4.34: A) 1% (w/v) agarose gel electrophoresis after digestion of the pTbCOX-pCO57 recombinant clones with HindIII and PvuII. Lane M: Molecular marker, 1 Kb Gene Ruler; lane 1: Non-digested pTbCOX-pCO57 plasmid; lane 2: digested pTbCOX-pCO57 construct. The upper band corresponds to the pTbCOX-pCO57 HindIII & PvuII digested (ca. 6000 bp), and the lower band corresponds to the size of pTbCOX (ca. 2000 bp). **B)** 1% (w/v) agarose gel electrophoresis of EcoRV linearization the pTbCOX-pCO57 construct prior to electroporation in SMB trypanosomes cells. Lane 1: pTbCOX-pCO57 plasmid and lane 2: pTbCOX-pCO57 EcoRV linearized.
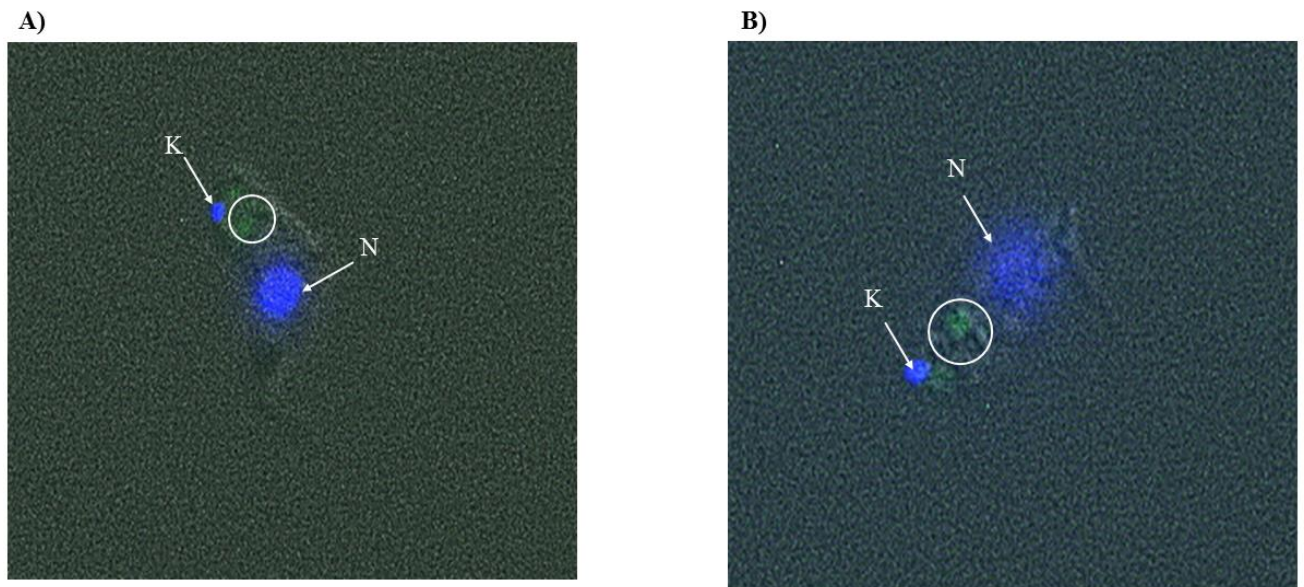
Figure 4.35: Fluorescence micrographs of SMB trypanosomes expressing pTbCOX fused with eGFP protein. **A)** The image is showing green dot signal near the kinetoplast and **B)** Image showing green dot signal between the kinetoplast and nucleus. The images were made from Zeiss Fluorescence Microscope (exposure time: DAPI: 50ms, GFP: 200ms and BF: 100ms) and prepared using image J software. Abbreviations: N, nucleus and K, kinetoplast.

5   Discussion

5.1   Bioinformatics analysis of the hypothetical protein pTbCOX

A hypothetical protein from *T. brucei* was found in our search for a putative COX-like enzyme (pTbCOX) using Western blot analysis, peroxidase activity assay and mass spectrometry analysis.

We were interested to analyze pTbCOX using different bioinformatic tools. No hit was found in terms of specific motif domains, such as signal peptides or membrane anchors. More importantly, however, no homolog proteins have been detected in human or other organisms, except kinetoplastida. pTbCOX is a 74.68 KDa protein encoded by a 2043 bp gene. Blast analysis using NCBI showed 100% identity with other conserved hypothetical proteins of other kinetoplastid species. The facts that, firstly, no homolog proteins seem to exist in other organisms, secondly, pTbCOX seems to be a well conserved protein expressed in the whole kinetoplastids family, and thirdly, it is essential for *T. brucei*, renders this protein into an interesting target for new drugs against kinetoplastid diseases. However, this protein remains to be assessed against other drug target validation criteria such as structure information, assayability, druggability, selectivity/ toxicity and resistance potential (Agüero et al., 2008; Field et al., 2017).

Furthermore, the bioinformatic analysis of pTbCOX revealed the presence of α-helices and ß-strands, considerable coiled-coil structures and a large number of putative phosphorylation sites (Ser/Thr/Tyr) (Figure 4.1 and Figure 4.2). Cellular signaling is driven mainly by protein phosphorylation and de-phosphorylation events, which are controlled by protein kinases and protein phosphatases (Batista et al., 2017). It has been shown that protein phosphorylation is a key regulator of signal transduction pathways that, thus far, has been studied in *T. brucei* principally through the knockdown of putative kinases and the observation of resulting phenotypes (Nett et al., 2009).

Unfortunately, our blast analysis of pTbCOX with well known protein kinases or other kinase-like proteins in *T. brucei* genome did not reveal any similarity in terms of specific or characterized kinase catalytic domains. To the best of our knowledge, pTbCOX is so far not listed in any research study attempted to identify trypanosomal phosphoprotein using phosphoproteomics approaches (Jones et al., 2015; Marchini et al., 2014; McAllaster et al., 2015; Nett et al., 2009; Urbaniak et al., 2013).

The fact that pTbCOX possesses several phosphorylation sites (Ser/Thr/Tyr) may suggest that a cellular activity associated with cell proliferation and differentiation is at work, and this shall be addressed in the future by using mass-spectrometry based phosphoproteomics and RNA-Sequencing.

5.2   Heterologous expression, refolding and purification of pTbCOX

The pTbCOX was amplified and successfully cloned in *E. coli*. Heterologous expression of pTbCOX was clearly achieved, but the protein formed inclusion bodies (IB). Inclusion bodies are insoluble protein aggregates that often occur during high level expression of hydrophobic proteins. Recombinant protein synthesis in *E. coli*, especially when driven by a strong promoter such as the T7 promoter, happens at a faster rate which leads to misfolding and accumulation of insoluble protein within the cells (Lebendiker and Danieli, 2014; Rosano and Ceccarelli, 2014). In this study, cloning of the pTbCOX gene was done in a pProExHTa vector system. The protein was highly expressed, but always found in the pellet fraction despite the use of different IPTG concentrations and induction times. Multiple attempts were made to modify the level of protein expression and to promote the solubility of pTbCOX in *E. coli*. Many studies showed that growing host cells at lower temperatures, co-expressing the protein of interest with chaperones and foldases and using other solubilizing Tag-fusion partners (MBP, NusA and GST) might improve the solubility of the protein expression in bacteria (Deller et al., 2016; Lebendiker and Danieli, 2014; Walls and Loughran, 2011).

A number of host cells are available which have been reported to be efficient in soluble protein expression. In this study, the host strains used were *E. coli* BL21 (DE3). This strain was designed to enhance the expression of eukaryotic proteins that either may be toxic to the host cell or may be cleaved by endogenous proteases. For this purpose, it contains the T7 polymerase that is activated only after IPTG induction, and this strain is deficient of Lon and omp-t proteases and is therefore suitable for protein expression (Deller et al., 2016). Many factors have been reported to lead to protein instability and aggregation. First, once the recombinant protein is expressed in a new *E. coli* microenvironment which may differ from that of the original source in terms of pH, redox potential, osmolarity, cofactors, and folding mechanisms (Deller et al., 2016). Second, the recombinant protein contains a considerable number of hydrophobic amino acids that may co-interact thus leading to protein aggregation and inclusion body formation (Baneyx and Mujacic, 2004). This last scenario fits well with pTbCOX, because the hydrophobicity plot analysis revealed a high content of hydrophobic amino acids within the sequence (Figure 4.3). It has been demonstrated that the high numbers of aromatic and aliphatic residues (ala, cys, val, ile, leu, met, phe, and tryp) are thought to decrease the solubility of proteins during refolding and contribute to the aggregation of protein folding intermediates (Burgess, 1996, 2009).

Since the commonly used methods to express soluble protein were not successful with pTbCOX, a more laborious technique known as inclusion body solubilization and refolding was performed to obtain soluble pTbCOX, properly fold and in its active forms.

This technique is time consuming and often yields a poor recovery (Yamaguchi and Miyazaki, 2014), but many studies have shown that it is possible to successfully refold inclusion body proteins to their biologically

active states. The inclusion body form of pTbCOX was solubilized first using the weak ionic detergent lauroylsarcosine, which was reported to effectively reduce hydrophobic aggregation and allow the recovery of monomeric, active protein molecules from inclusion bodies (Burgess, 1996, 2009). The results of this first approach are presented in chapter 4 (Figure 4.4).

In a second approach, strong denaturants such as guanidine hydrochloride and step-wise dialysis was used as refolding strategy. Many studies have shown that protein refolding from denatured protein is influenced by several factors, including solubility of the respective protein, removal of denaturants, and assistance of refolding by a co-solute or by other additives (Yamaguchi and Miyazaki, 2014).

Unfortunately, all the afore mentioned attempts to purify pTbCOX using affinity chromatography on the ÄKTA FPLC system from the lauroylsarcosine approach were unsuccessful, because the pTbCOX was not binding to the Ni-NTA column and appeared always in the flow through.

The final approach, i.e. treating the pTbCOX inclusion bodies with high grade strong denaturant GuHCl plus the reducing agent ß-mercaptoethanol and a step wise dialysis refolding by adding GSH/GSSH and L-arginine were reasonably effective for refolding pTbCOX. This step wise dialysis technique included denaturation, reduction of the disulphide bonds and then generation of the corrected bond configuration by including GSH/GSSH to prevent protein aggregation of partially folded intermediates by addition of L-arginine. This technique has been used previously for the refolding of two ScFv antibodies constructions (Arakawa and Ejima, 2014).

Arginine hydrochloride or arginine has been applied for refolding of a variety of proteins from inclusion bodies, such as casein kinase (Lin and Traugh, 1993), gamma interferon (Arora and Khanna, 1996), p53 tumor suppressor protein (Bell et al., 2002), and interleukin-21 (Asano et al., 2002). The exact molecular mechanism of arginine is still not well understood. Arginine hydrochloride has a guanidinium group (Gdn) at the distal end of its side chain, similar to GuHCl. The Gdn strongly interacts with hydrophobic amino acids in hen egg-white lysozyme (Mande and Sobhia, 2000) and act as a strong chaotropic agent. The crystal structure of the lysozyme-arginine complex showed that arginine bound at sites different from those of Gdn, and mildly interacted with nearby hydrophobic amino acid of the protein surface (Ito et al., 2011). These interactions included electrostatic, hydrophobic and cation-π interactions. Compared with Gdn, the amino and carboxyl groups of arginine form weaker hydrogen bonds with the denatured protein and water. Thus, arginine might act as an aggregation inhibitor due to its moderate binding to protein (Matsuoka et al., 2009).

In addition, proline has also been reported to enable proteins to refold to their native (active) conformations. It was proposed that proline inhibits protein aggregation by binding to the folding intermediate in the supramolecular assembly with proline (Samuel et al., 2000).

The pTbCOX refolding strategy using the second approach was successful to purify the protein applying a one-step Ni-NTA affinity chromatography on an ÄKTA FPLC. The results are presented in Figure 4.5 and Figure 4.6.

The purified pTbCOX was than dialyzed overnight and checked for stability. DLS measurement, however, demonstrated that the purified pTbCOX was highly aggregated (data not shown) and the COX activity test performed using sensitive TLC radioactive assay on the pTbCOX was negative (data not shown).

5.3 Heterologous expression of pTbCOX in Sf9 insect cells and *in vivo* protein crystallization

In order to produce a proper folded and active pTbCOX with post-translational modifications, a new construct was generated using the baculovirus expression vector pFastBacHTb for production of this protein in Sf9 insect cells and *in vivo* protein crystallization. *In vivo* protein crystallization has been mostly reported by using a heterologous expression system based on the polyhedrin promoter (Koopmann et al., 2012; Redecke et al., 2013a; Schönherr et al., 2015). Using this system, several proteins with unrelated functions, structure and physico-chemical properties have now been reported to crystallize *in vivo*, suggesting that this strategy could be routinely used for structure determination alongside classical crystallographic approaches (Boudes et al., 2016; Duszenko et al., 2015). We have employed this baculovirus system in the past to produce *in vivo* protein crystals of cathepsin B and inosine monophosphate dehydrogenase from *T. brucei* (Duszenko et al., 2015). TbCatB in vivo crystals have been subjected to free-electron laser based serial femtosecond crystallography (SFX), performed in collaboration with Prof. Christian Betzel and Prof. Henry Chapman (DESY, Hamburg) and yielded the TbCatB structure at a resolution of 2.8 Å (Gati et al., 2014b; Redecke et al., 2013b)

The pTbCOX was expressed in the pellet fraction or insoluble fraction (membrane-attached protein like the expression experiment using bacteria BL21(DE3) system) at different days post-infection and led us to observe an *in vivo* crystal-like structure inside cells after 14 days after transfection with the P3 virus stock (Figure 4.11 B).

5.4 Characterization of pTbCOX crystals

The pTbCOX crystals were first confirmed to consist solely of pTbCOX by Western blot analysis. For this purpose, *in vivo* crystals were isolated, concentrated, solubilized and run on SDS gels. For detection a polyclonal anti-his antibody was used after transfer of the protein to a nitrocellulose membrane (Figure 4.12 B). Unfortunately, we were not able to obtain positive mass spectrometry signals of the pTbCOX because of

its low concentration and weak signal in the SDS-PAGE even after multiple concentration efforts using either Coomassie or silver staining.

The pTbCOX was then analyzed by scanning electron microscopy. We observed the micro sized needle shaped crystals progressed from the Sf9 insect cells or on top of Sf9 insect cells. The mechanism by which protein crystallize at a specific location within the cell is still not yet clear understood. So far it has been well demonstrating that high local concentration of the recombinant in baculovirus-infected insect cells is the prior requirement to induce *in vivo* crystallogenesis within an organelle (Duszenko et al., 2015; Koopmann et al., 2012).

SONICC based SHG imaging (Figure 4.14) and X-ray powder diffraction (Figure 4.15) in Prof. Christian Betzel's group at DESY were performed to confirm the crystallinity of the pTbCOX crystals. The SONICC revealed positive signals of the pTbCOX crystals. It has been demonstrated that the SONICC measurement is a selective and sensitive method for detection and characterization of protein crystals. SHG identifies protein crystals by imaging the samples with infrared light and detecting the frequency-doubled response specific of chiral crystals (Boudes et al., 2014). The SHG signals revealed the proteinaceous nature of the pTbCOX crystals because it has been shown that amorphous aggregation or salt crystals do not produce SHG signals. It should be noted that SHG imaging has its limitations: it can give false-negative results in rare instances when the crystal packing is of high symmetry and it can generate false-positive results if, for example, a salt crystal appears (Wampler et al., 2008). Subsequently, the pTbCOX crystals vs lysozyme crystals as positive control analyzed by powder diffraction showed diffraction ring up to 4-5 Å resolution (Figure 4.15), confirming a crystalline state of pTbCOX crystals. Both experiments support preliminary characterization of the pTbCOX *in vivo* crystals prior to XFEL beam or MicroED for data collection. The success of a XFEL or MicroED experiment is highly dependent on crystal quality, size, density and quantity.

The solubilized pTbCOX crystals were used to assess the stability of the pTbCOX protein at the level of secondary structure using DLS and CD spectroscopy methods. Interestingly, DLS measurement of the pTbCOX crystals solubilized with different concentrations of sodium acetate buffer revealed the aggregation tendency behaviors of the pTbCOX protein. This screening step demonstrated the optimal condition or treatment by which the pTbCOX switch from a large oligomer or aggregate (Figure 4.16) to monodisperse molecules with a radius corresponding to the monomeric pTbCOX protein (Figure 4.17). Due to our observation of the pTbCOX expression in bacteria as an insoluble protein and multiple rescue procedures developed during this thesis including: such as refolding of denatured pTbCOX using lauroylsarcosine and guanidine hydrochloride plus L-arginine, alternative expression systems such as yeast, decreasing the culture temperature have proven not effective in producing soluble pTbCOX from *T. brucei* because of its high tendency to aggregate.

This result could be proposed as a new way to rescue pTbCOX so far insolubly expressed in bacteria into inclusion bodies to be easily solubilized by the addition of sodium acetate during bacteria cell lysis. Thus, this protocol should allow us to recover pTbCOX in a soluble and correctly folded form for conventional crystallography and structure determination.

CD spectroscopy of pTbCOX was also done and confirmed the stability of the pTbCOX properly folded at 12.5 mM sodium acetate buffer pH 3.6. Using this buffer, the secondary structure was estimated for the first time and identified the percentage of helix, sheet, turn and random-coiled of the pTbCOX using Yang's reference (Figure 4.18). Therefore, the sodium acetate buffer pH 3.6 stabilizes pTbCOX and can be used for conventional crystallography trials and for biological assays of pTbCOX.

5.5   Knockdown studies of pTbCOX gene and phenotypes analysis

RNAi was employed to investigate the essentiality of pTbCOX in the trypanosome SMB cell line. Therefore, the pTbCOX-KD fragment from the encoding gene was successfully cloned into the p2T7 expression vector which contains two opposing promoters and, hence, allowed transcription of double stranded RNA upon doxycyclin induction (Figure 4.21). The recombinant vector construct was then transfected into bloodstream form *T. brucei* by electroporation. This resulted in the production of two different transgenic clones named pTbCOX RNAi clone T1.1 and pTbCOX RNAi clone T2.2 for further investigations.

RNAi knockdown was efficiently and effectively confirmed by quantitative real time PCR (qRT-PCR). The pTbCOX mRNA levels decreased in both clones to approximately 50% after 18 h and 42 h post-induction by doxycycline and in clone T2.2 to about 25% 66 h post-induction in comparison to the 100% SMB non-transfected cells (Figure 4.25). Quantitative real-time PCR demonstrated that the doxycycline mediated induction of RNAi resulted in a significant reduction of the pTbCOX mRNA level compare to the WT mRNA level. It has been observed in *T. brucei* knockdown experiment that reduction of mRNA level measured by qRT-PCR does not necessarily have to be correlated with the protein level measured by Western blot analysis (Clayton and Shapira, 2007). Since the level protein were not measured because of the lack of specific antibody against pTbCOX, we can assume that the pTbCOX was decreased more significantly in our pTbCOX RNAi cell lines that showed apparition of phenotypes.

However, the use of very accurate tools such as Northern blot analysis or RNA-Sequencing are still necessary to be performed for the validation of the efficiency of the pTbCOX knockdown study at the RNA and pTbCOX expression level in *T. brucei*.

Interestingly, depletion of the pTbCOX mRNA produced a progressively decrease of growth (Figure 4.26), gross morphological defects including multiflagellated and big eye phenotypes which was observed within 6

h post doxycycline induction by fluorescence microscopy (Figure 4.28). Furthermore, analysis of kinetoplast/nucleus progression in the pTbCOX-KD RNAi cell line revealed a partial cell cycle arrest and failure to initiate cytokinesis. Thus, accumulation of cells with abnormal karyotypes have been regularly detected (Figure 4.30).

SEM and TEM microscopy showed that the cell periphery was highly twisted; multiple nuclei and multiple flagella were attached to the outside of the cell, while other cells possessed a highly enlarged flagellar pocket (Figure 4.27 and Figure 4.29). Taken together, these data clearly suggest that pTbCOX is essential for the bloodstream form of the parasite *in vivo*. Knockdown of pTbCOX rapidly produces "monster" cells with multiple nuclei and multiple flagella, thus suggesting a direct or indirect role of pTbCOX in cell cycle coordination. At the same time, we observed also the presence of parasites with an enlarged flagellar pocket, the so called big eye phenotype, after RNAi induction by doxycycline. It has been shown that both phenotypes generally appeared when the function of an essential flagellum protein is perturbed in bloodstream form *T. brucei* (Broadhead et al., 2006; Ralston and Hill, 2008).

The mainly described defects incriminate after the appearance of pTbCOX KD lethal phenotypes were cytokinesis for the multiflagellated phenotype (Brasseur et al., 2013; Broadhead et al., 2006; Hutchings et al., 2002; Olego-Fernandez et al., 2009; Ralston and Hill, 2008) and endocytosis for the big eye phenotype (Adung'a et al., 2013; Allen et al., 2003; Field and Carrington, 2009; Manna et al., 2017; Morriswood and Schmidt, 2015). So far, we have been unable to detect which defect appear as primary event. We found that both phenotypes were consistently observed 6 h post doxycycline induction.

A possible explanation for the lethal phenotype in bloodstream cells is that cytokinesis failure results as a primary event from the absence of correct flagellar motility. This situation will induce a multiple round of cell division without cytokinesis leading to new flagella and pockets formed at inappropriate location. The lack of the precise morphogenetic axes in the resulting "monster cells" leads to pleiotropic effects compromising membrane-cytoskeleton balance during morphogenesis of the pocket structure (Broadhead et al., 2006). It has been suggested that the monster cells phenotype will have a perturbation of endocytosis combined with the secretory pathways, thus will lead to the enlargement of the flagellar pocket result on big eye phenotype as secondary event (Broadhead et al., 2006). Another possible scenario will be that the cytokinesis failure is not the one inducing the endocytosis defect producing the big eye phenotype observed during the pTbCOX knockdown study.

Since pTbCOX is still not fully characterized and remains a hypothetical protein, our detailed results of the morphological changes induced by pTbCOX knockdown give strong light on its essentiality for the parasite. However, further investigations are needed to reveal the precise cellular process by which pTbCOX contribute

to maintain cytokinesis or the endocytic system in *T. brucei* in balance. Thus, we hypothesized that pTbCOX might participate in multiple cellular processes in *T. brucei*.

5.6 Expression of pTbCOX protein fused with eGFP in *Trypanosoma brucei*

In this last experiment, we tried to identify the subcellular localization of pTbCOX inside the bloodstream forms of *T. brucei*. The pTbCOX gene was successfully cloned in the pCO57 vector. This vector allows the expression of eGFP fusion to the C-terminus of the desired protein and contains an inducible T7 expression site, which is regulated by a tetracycline operator. This system is well suited to be inserted into SMB cells, which express T7 RNA polymerase and a tetracycline repressor. The pTbCOX-pCO57 construct was successfully generated and transfected into SMB cells. Surprisingly, the pTbCOX-eGFP was firstly leaky expressed and secondly was readily lethal, because no transfected clones were obtained despite many attempts of repeated transfections with or without tetracycline or doxycycline induction, and all transfected parasite cultures died 4 days post transfection. We initially hypothesized that the autoinduction phenomenon might be linked to the pCO57 vector, the fetal bovine serum with tetracycline, or so far unknown effects of pTbCOX.

The strategy used to decipher the autoinduction mechanism was based firstly on the expression of pTbCOX in SMB trypanosomes using a commercially available tetracycline-free fetal bovine serum. However, since overexpression of pTbCOX in SMB trypanosomes was still lethal for transfected parasites following tetracycline or doxycycline induction, we ruled out the autoinduction phenomenon was due to fetal bovine serum with tetracycline.

However, we consistently observed a fast-lethal process of the transgenic clones expressing the pTbCOX-eGFP fusion protein within the 4 days postinduction. One reason of this lethal phenomenon could be that the pTbCOX protein is tightly regulated in *T. brucei*.

Video fluorescence microscopy showed different morphologies in pTbCOX-eGFP transfected bloodstream form parasites including: stumpy forms, intermediate forms, long slender forms and multiflagellated cells. This fusion protein was not homogenously distributed, but appeared as single or multiple punctate within the transfected bloodstream form parasites. The fluorescence imaging obtained after cell fixation and DAPI staining localized the pTbCOX-eGFP fusion protein as a single dot near the kinetoplast or in between the kinetoplast and nucleus (Figure 4.35). The biological relevance of pTbCOX localization remained unanswered. We could speculate that the fact that knockdown of pTbCOX induce an impairment of cytokinesis and endocytosis requires further investigation to proof the connection of pTbCOX with the flagellar apparatus of *T. brucei*.

6   Future perspectives on pTbCOX as drug target

HAT is one of the deadly neglected tropical diseases affecting people living in sub-Saharan Africa. It is caused by *T. brucei* parasites transmitted to the human host by tsetse flies. HAT therapy still relies upon drugs which use is limited by toxicity and rigorous treatment regimes, while development of vaccines remains up highly unlikely, due to the effectiveness of antigenic variation. There is an eminent need to identify and develop better drugs against HAT.

Currently, efforts have been made to identify better drugs or new lead compounds for the treatment of HAT using phenotypic screening or target-based approaches. Unfortunately, there is no increase of new drug discovery because of the lack of a defined target that is both essential and druggable validated in the trypanosomatids (Field et al., 2017). Therefore, identification of novel targets which are unique and different to the human host must be given priorities for future genetic validation and structure determination.

A major problem with the genome sequence of *T. brucei* is the failure to predict the function of the gene encoding hypothetical proteins, that comprise approximately 50% of the total genome. Analysis of these hypothetical proteins could identify new drug targets, since these genes have no equivalent in the human genome and may, as in the case of pTbCOX, be essential for the parasite's survival. In addition, new protein structures revealing new domains or motifs, and even novel metabolic pathways may appear and contribute to the drug discovery pipeline.

In this thesis, I have analyzed an annotated hypothetical protein of the *T. brucei* genome, called pTbCOX that lacks human homologs, is well conserved among kinetoplastids and was demonstrated to be essential for cell division and morphogenesis in bloodstream form *T. brucei*. Our endeavors were the move forward to comprehensively elucidate the structure-function of pTbCOX by cloning, expressing the pTbCOX gene using different expression systems.

The first challenge of this thesis was that pTbCOX expression in bacteria led consistently to the formation of inclusion bodies. From those, pTbCOX was extracted using strong denaturant guanidine hydrochloride and finally refolded by step-wise dialysis using additives like GSH/GSSH and L-arginine. Afterwards, pTbCOX was purified by affinity chromatography on a Ni-NTA column using the ÄKTA FPLC system.

The second challenge was to get a better understanding of the aggregation of pTbCOX after purification and to obtained a correctly folded and stable pTbCOX. For this purpose, I move forward and produced a new construct of pTbCOX for baculovirus expression and *in vivo* protein crystallization.

Luckily, pTbCOX seems to crystallize inside Sf9 insect cells and I was able to preliminary characterize the pTbCOX crystals before XFEL or MicroED beam data collection.

Interestingly, analysis of the solubilized pTbCOX crystals from Sf9 insect cells by DLS and CD spectroscopy, point into the possible direction how to solve pTbCOX aggregation problem. Firstly, treatment of the pTbCOX expressing bacteria before cell lysis or harvesting the inclusion bodies with sodium acetate as a proposed mechanism to obtain the soluble recombinant protein. Or, secondly, treatment of the purified recombinant pTbCOX in vivo crystals via the one-step purification described in this thesis with sodium acetate by overnight dialysis.

Anyway, further work needs to be done to complete the full characterization of the attractive target pTbCOX in the future:

(a) Identification of the signaling pathway where pTbCOX might play a crucial role in *T. brucei*. As bioinformatic tools revealed the presence of multiple phosphorylation sites within the pTbCOX sequence, mass-spectrometry-based phosphoproteomics and RNA-sequencing using a pTbCOX knockdown cell line will shed light on the phosphorylation patterns and gene expression levels of these cells.

(b) Elucidating the structure of pTbCOX using conventional or *in vivo* protein crystallography approaches is also important to answer the remained question "what is the function of pTbCOX?". The discovery of the pTbCOX structure will shed light on its function and to explore whether or not pTbCOX is a suitable drug target candidate for HAT therapy. It will also make it possible to evaluate new domain motifs or to reveal new biochemical pathways and cascades in the Trypanosoma biochemistry.

In Summary, pTbCOX is well conserved and expressed in Trypanosomatids and lacks human homologs. Genetic knockdown studies demonstrated that it is essential for cell division and morphogenesis in bloodstream form *T. brucei*. Therefore, pTbCOX seems to be a suitable drug target candidate to be added to the drug discovery pipeline for HAT therapy. However, the challenge is still ongoing to obtain native pTbCOX, solving its X-ray crystals structure for druggability and assayability studies.

7 Summary

Trypanosoma brucei comprises a group of extracellular kinetoplastid protozoa including the causative agent of Human African Trypanosomiasis (HAT). Sequencing of their genomes revealed approximately 50% of genes which are so far uncharacterized regarding their biochemical or cellular functions but are identified as hypothetical proteins with no homologs in the human host. This opens possibilities for new target identification and drug discovery. With the initial aim of identifying the gene encoding a putative *T. brucei* cyclooxygenase (pTbCOX), Western blot and mass spectrometry analyses were used to identify a protein that is recognized by a cyclooxygenase ovine polyclonal antibody in trypanosome lysates. This led to a list of hypothetical genes, encoding a cyclooxygenase-like enzyme candidate. Among them, a gene (Tb427.10.13790/Tb927.10.13790) encoding a hypothetical conserved protein was immunologically identified at 74.68 kDa using cyclooxygenase ovine polyclonal antibody during protein expression, and it contained highly hydrophobic amino acids. Therefore, this protein was chosen for further experimental investigations.

In the first part of this work, the bioinformatic analyses of pTbCOX were performed using BLAST/NCBI, Pfam, Prosite, Swiss-Pro, InterPro, TMHMM, Signal P, Hydrophobicity Plot and NetPhos to describe the pTbCOX gene/protein. These analyses revealed no convincing homolog proteins in human or any other organism, except in kinetoplastida. No hit was found regarding specific domains, signal peptides or membrane anchors. However, blast analysis using NCBI showed 100% identity with conserved hypothetical proteins of other kinetoplastid species. The hydrophobicity plot analysis revealed a high content of hydrophobic amino acids within the sequence. Therefore, the pTbCOX is a prime example of a protein annotated as "hypothetical protein" in *T. brucei* genome which fulfilled the above criteria, i.e., no homologs in human or any other organisms to be selected as an attractive target for validation. In the further work, its essentiality in *T. brucei* was analyzed.

In the second part of this work, the full-length coding sequence of the pTbCOX gene was cloned and expressed as a recombinant protein in *E. coli* BL21 (DE3). The pTbCOX was found most entirely in an insoluble form inside inclusion bodies. These inclusion bodies were solubilized using 4 molar guanidine hydrochloride and refolded step-wise by decreasing concentrations of guanidine hydrochloride, and the introduction of redox agents, i.e. reduced and oxidized glutathione as well as L-arginine. Expressed and refolded pTbCOX was purified using a Ni-NTA column on ÄKTA-FPLC system. The attempt to demonstrate the cyclooxygenase activity of the purified pTbCOX by radioisotope thin layer chromatography enzymatic assay using C-14 arachidonic acid as the main substrate to produce prostaglandins was not successful.

This result, however, does not necessarily mean that pTbCOX is not a cyclooxygenase because the lack of enzyme activity might also be due to a refolding failure to produce a correct folded and active protein. In addition, pTbCOX was obtained in low amounts showing a high tendency to aggregate, as revealed by size exclusion chromatography and DLS experiments.

In the third and fourth part of this work, the pTbCOX gene was cloned in the pFastBacHTb baculovirus expression vector to produce properly folded pTbCOX for *in vivo* crystallization experiments. The protein was expressed in Sf9 insect cells and produced *in vivo* crystals which appeared as micro-sized needle-shaped forms 14 days after transfection using the P3 virus stock. The isolated pTbCOX crystals were identified by Western blotting and scanning electron microscopy analysis. Isolated pTbCOX crystals showed diffraction patterns using powder diffraction and a positive signal by second harmonic generation (SONICC) analysis. These experiments present a preliminary characterization of the pTbCOX crystals before XFEL beam or MicroED for data collection. Furthermore, pTbCOX *in vivo* crystals were solubilized using sodium acetate buffer to assess the stability of the pTbCOX at the level of secondary structure using DLS and CD spectroscopy methods. This screening revealed optimal condition for treatment by which pTbCOX switch from large oligomeric aggregates to monodisperse molecules with a radius corresponding to the monomeric pTbCOX protein. CD spectroscopy of solubilized pTbCOX confirmed stability of the (properly) folded protein in 12.5 mM sodium acetate buffer at pH 3.6. Therefore, this result may also lead to a new way to rescue pTbCOX so far insolubly expressed in bacteria, to be easily solubilized by the addition of sodium acetate during bacteria cell lysis. Thus, this protocol should allow recovering pTbCOX in a soluble and correctly folded form for biological assays, conventional crystallography trials and structure determination of pTbCOX.

In the fifth part of this work, RNAi was used to investigate and validate the physiological function of pTbCOX in the trypanosome SMB cell line. Therefore, a fragment of the pTbCOX gene was cloned into an RNAi expression vector which contained two opposing promoters and, hence, allowed transcription of double-stranded RNA upon doxycycline induction. The recombinant vector construct was then transfected into bloodstream form *T. brucei* by electroporation. Two different transgenic clones were produced and quantitative real-time PCR confirmed post-transcriptional silencing of the pTbCOX gene. The level of TbCOX-mRNA decreased to approximately 50% and 25% respectively for each clone in comparison to the untreated SMB trypanosomes at various times post induction. Interestingly, the functional analysis of pTbCOX gene depletion resulted to a progressive decrease of growth, morphological defects including multiflagellated and big eye phenotypes observed by fluorescence, SEM and TEM microscopy. Furthermore, analysis of kinetoplast/nucleus progression in the pTbCOX RNAi cell line revealed a partial cell cycle arrest and failure to initiate cytokinesis.

These results are a genetical validation that pTbCOX is essential for cytokinesis and cell morphogenesis in trypanosome. However, further investigations are needed to reveal the precise cellular processes by which pTbCOX contribute to maintain the cytokinesis/endocytosis system in *T. bru*cei in balance.

Thus, we hypothesize that pTbCOX might participate in multiple cellular processes in *T. brucei* cell division and cell morphogenesis.

In the last part of this work, the pTbCOX gene was cloned in the pCO57 vector. This vector allows the expression of eGFP fusion to the C-terminus of the desired protein and contains an inducible T7 expression site, which is regulated by a tetracycline operator. Surprisingly, pTbCOX-eGFP was expressed leaky and resulted in the death of the transfected cells after four days post transfection. Our data showed, that pTbCOX-eGFP expression is lethal for bloodstream form parasites and appeared as a single dot near the kinetoplast or in between kinetoplast and nucleus.

Altogether, this thesis identified a novel hypothetical protein which is essential for the bloodstream trypanosomes. Thus, pTbCOX could participate in multiple cellular processes in *T. brucei* cell division and cell morphogenesis. The elucidation of structure and detailed mechanism of action of this protein might provide valuable insight, and pTbCOX might become a suitable drug target candidate for future anti-trypanosomatid therapy.

8 Zusammenfassung

Bei den Erregern der afrikanischen Schlafkrankheit handelt es sich um extrazelluläre Protozoen der *Trypanosoma brucei*-Gruppe. Rund 50% der sequenzierten Gene sind bislang bezüglich ihrer biochemischen oder zellulären Eigenschaften nicht charakterisiert und kodieren für hypothetische Proteine ohne bekannte Homologe im Menschen. Dies eröffnet zahlreiche potentielle Möglichkeiten zur Entwicklung neuer Medikamente. Eines dieser Proteine, das von Antikörpern gegen ovine Cyclooxygenase im Western Blot detektiert und mittels Massenspektrometrie identifiziert wurde, sollte hier untersucht werden. Es handelt sich um eine putative *T. brucei* Cyclooxygenase (pTbCOX, Tb427.10.13790/Tb927.10.13790) mit einem hohen Anteil hydrophober Aminosäuren.

Im ersten Teil dieser Arbeit wurde pTbCOX bioinformatisch mittels BLAST/NCBI, Pfam, Proseite, Swiss-Pro, InterPro, TMHMM, SignalP, Hydrophobizitätsplot und NetPhos untersucht. Hierbei konnten keine Homologe im Menschen oder in anderen Organismen (außer Kinetoplastida) gefunden werden. Weiterhin konnten keine spezifischen Domänen, Signalsequenzen oder Membrananker identifiziert werden. Allerdings konnte gezeigt werden, dass pTbCOX zu 100% identisch zu konservierten hypothetischen Proteinen anderer Kinetoplasten ist. Damit ist pTbCOX ein potentiell geeigneter Kandidat für die Entwicklung neuer Medikamente. Im Folgenden sollte untersucht werden, ob das Gen für *Trypanosoma brucei* essentiell ist.

Im zweiten Teil wurde die kodierende Sequenz von pTbCOX kloniert und in *E. coli* BL21(DE3) heterolog exprimiert; das Protein wurde fast ausschließlich in *inclusion bodies* gefunden. Diese wurden mit 4M Guanidinium-HCl solubilisiert und durch schrittweise Reduktion des Guanidinium-HCl und Zuführung von Glutathion und L-Arginine renaturiert. pTbCOX wurde danach mittels ÄKTA-FPLC an Ni-NTA-Säulen aufgereinigt. Es konnte keine Cyclooxygenaseaktivität durch Umsetzung von C-14-markierter Arachidonsäure zu Prostaglandinen über Dünnschichtchromatographie nachgewiesen werden. Dies könnte auf eine unzureichende Rückfaltung, die geringe Ausbeute oder die hohe Tendenz zur Aggregation des Proteins (wie durch Gelpermeationschromatographie und DLS nachgewiesen) zurückzuführen sein.

Im dritten und vierten Teil wird beschrieben, wie pTbCOX in pFastBacHTb kloniert wurde, um nativ gefaltetes Protein für *in vivo* Kristallisationsexperimente mit einem Baculovirussystem zu erhalten. Zur Expression wurden SF9 Insektenzellen genutzt. 14 Tage nach der Infektion mit dem P3 Virusstock wurden nadelförmige Mikrokristalle erhalten. Diese wurden mittels Western Blot, Rasterelektronenmikroskopie und SONICC analysiert. Somit wurde eine vorläufige Charakterisierung als Grundlage für Röntgenkristallstrukturanalysen (XFEL oder MicroED) durchgeführt.

Weiterhin wurden pTbCOX Kristalle mit Natriumacetatpuffer solubilisiert und eine Sekundärstrukturanalyse mit DLS und CD-Spektroskopie durchgeführt. Dabei wurden geeignete Bedingungen gefunden, bei denen oligomere Proteinaggregate zu monodispersen pTbCOX-Molekülen dissoziieren. Mittels CD-Spektroskopie konnte gezeigt werden, dass das solubilisierte und renaturierte Protein in 12,5mM Natriumacetatpuffer bei pH 3,6 stabil war. Diese Methode ließe sich zukünftig nutzen, um Proteine, die in *inclusion bodies* exprimiert werden, bereits während der Zelllyse durch Zugabe von Natriumacetatpuffer zu lösen.

Im fünften Teil dieser Arbeit wurde die physiologische Funktion von pTbCOX durch RNA Interferenz in SMB (*single marker bloodstream form*) Trypanosomen untersucht. Ein Fragment des Gens wurde in einen Vektor mit zwei gegenläufigen Promotorsequenzen kloniert, so dass doppelsträngige RNA nach Doxycyclin-Induktion transkribiert wird. SMB Zellen wurden durch Elektroporation transfiziert und zwei transgene Klone erhalten. Der *knockdown* von pTbCOX wurde durch qPCR bestätigt. Verglichen mit unbehandelten SMB Zellen sank das Expressionslevel auf 25-50% (je nach Klon). Die Zellen zeigten ein verlangsamtes Wachstum, morphologische Defekte mit Multiflagellenbildung, einen *big eye* Phänotyp und einen partiellen Zellzyklusarrest.

Diese Ergebnisse bestätigten auf genetischer Ebene die Bedeutung von pTbCOX für Zytokinese und Morphogenese in Trypanosomen. Weitere Untersuchungen sind nötig, um die zugrundeliegenden molekularen Mechanismen aufzuklären.

Im letzten Teil wurde pTbCOX in den Vektor pCO57 kloniert, um ein C-terminales eGFP-Fusionsprotein in SMB-Zellen induzierbar zu exprimieren. Das Fusionsprotein war als solitärer Punkt in der Nähe des Kinetoplasten (bzw. zwischen Kinetoplast und Zellkern) lokalisierbar. Überraschenderweise war auch die Überexpression innerhalb von vier Tagen letal.

Zusammenfassend wurde in dieser Arbeit ein hypothetisches Protein identifiziert, das essentiell für Blutform-Trypanosomen ist. pTbCOX könnte in multiplen zellulären Prozessen (wie Zellteilung und Morphogenese) eine Rolle spielen. Die Strukturaufklärung und die Aufklärung der molekularen Funktionsweise könnten vielversprechende Ansätze für die Entwicklung neuer Medikamente gegen afrikanische Schlafkrankheit liefern.

9 Bibliography

Adung'a, V.O., Gadelha, C., and Field, M.C. (2013). Proteomic analysis of clathrin interactions in trypanosomes reveals dynamic evolution of endocytosis. Traffic *14*, 440–457.

Agüero, F., Al-Lazikani, B., Aslett, M., Berriman, M., Buckner, F.S., Campbell, R.K., Carmona, S., Carruthers, I.M., Chan, A.E., Chen, F., et al. (2008). Genomic-scale prioritization of drug targets: the TDR Targets database. Nat. Rev. Drug Discov. *7*, 900–907.

Akiyoshi, B., and Gull, K. (2013). Evolutionary cell biology of chromosome segregation: insights from trypanosomes. Open Biol. *3*, 130023.

Allen, C.L., Goulding, D., and Field, M.C. (2003). Clathrin-mediated endocytosis is essential in Trypanosoma brucei. EMBO J. *22*, 4991–5002.

Ancelle, T., Paugam, A., Bourlioux, F., Merad, A., and Vigier, J. P. (1997). Détection des trypanosomes dans le sang par la technique du quantitative buffy coat (QBC): évaluation expérimentale. Médecine Trop. *57*, 245–248.

Arakawa, T., and Ejima, D. (2014). Refolding technologies for antibody fragments. Antibodies *3*, 232–241.

Arora, D., and Khanna, N. (1996). Method for increasing the yield of properly folded recombinant human gamma interferon from inclusion bodies. J. Biotechnol. *52*, 127–133.

Asano, R., Kudo, T., Makabe, K., Tsumoto, K., and Kumagai, I. (2002). Antitumor activity of interleukin-21 prepared by novel refolding procedure from inclusion bodies expressed in Escherichia coli. FEBS Lett. *528*, 70–76.

Axford, D., Ji, X., Stuart, D.I., and Sutton, G. (2014). In cellulo structure determination of a novel cypovirus polyhedrin. Acta Crystallogr. D Biol. Crystallogr. *70*, 1435–1441.

Balaña-Fouce, R., and Reguera, R.M. (2007). RNA interference in Trypanosoma brucei: a high-throughput engine for functional genomics in trypanosomatids? Trends Parasitol. *23*, 348–351.

Baneyx, F., and Mujacic, M. (2004). Recombinant protein folding and misfolding in Escherichia coli. Nat. Biotechnol. *22*, 1399–1408.

Barrett, M.P., Boykin, D.W., Brun, R., and Tidwell, R.R. (2007). Human African trypanosomiasis: pharmacological re-engagement with a neglected disease. Br. J. Pharmacol. *152*, 1155–1171.

Barth, T. (2013). Untersuchungen zum Apoptosemechanismus bei Trypanosoma brucei: Effekte von Staurosporin im Vergleich zu Prostaglandin D2 und die Rolle der Endonuklease G. Universitat Tübingen.

Barty, A., Küpper, J., and Chapman, H.N. (2013). Molecular imaging using X-ray free-electron lasers. Annu. Rev. Phys. Chem. *64*, 415–435.

Batista, M., Kugeratski, F.G., de Paula Lima, C.V., Probst, C.M., Kessler, R.L., de Godoy, L.M., Krieger, M.A., and Marchini, F.K. (2017). The MAP kinase MAPKLK1 is essential to Trypanosoma brucei proliferation and regulates proteins involved in mRNA metabolism. J. Proteomics *154*, 118–127.

Bell, S., Hansen, S., and Buchner, J. (2002). Refolding and structural characterization of the human p53 tumor suppressor protein. Biophys. Chem. *96*, 243–257.

Berriman, M., Ghedin, E., Hertz-Fowler, C., Blandin, G., Renauld, H., Bartholomeu, D.C., Lennard, N.J., Caler, E., Hamlin, N.E., Haas, B., et al. (2005). The genome of the African trypanosome Trypanosoma brucei. Science *309*, 416–422.

Bisser, S., Lumbala, C., Nguertoum, E., Kande, V., Flevaud, L., Vatunga, G., Boelaert, M., Büscher, P., Josenando, T., Bessell, P.R., et al. (2016). Sensitivity and Specificity of a Prototype Rapid Diagnostic Test for the Detection of Trypanosoma brucei gambiense Infection: A Multi-centric Prospective Study. PLoS Negl Trop Dis *10*, e0004608.

Blum, J., Nkunku, S., and Burri, C. (2001). Clinical description of encephalopathic syndromes and risk factors for their occurrence and outcome during melarsoprol treatment of human African trypanosomiasis. Trop. Med. Int. Health *6*, 390–400.

Boudes, M., Garriga, D., and Coulibaly, F. (2014). Reflections on the many facets of protein microcrystallography. Aust. J. Chem. *67*, 1793–1806.

Boudes, M., Garriga, D., Fryga, A., Caradoc-Davies, T., and Coulibaly, F. (2016). A pipeline for structure determination of in vivo-grown crystals using in cellulo diffraction. Acta Crystallogr. Sect. Struct. Biol. *72*, 576–585.

Bradford, M.M. (1976). A rapid and sensitive method for the quantitation of microgram quantities of protein utilizing the principle of protein-dye binding. Anal. Biochem. *72*, 248–254.

Brasseur, A., Rotureau, B., Vermeersch, M., Blisnick, T., Salmon, D., Bastin, P., Pays, E., Vanhamme, L., and Pérez-Morga, D. (2013). Trypanosoma brucei FKBP12 differentially controls motility and cytokinesis in procyclic and bloodstream forms. Eukaryot. Cell *12*, 168–181.

Broadhead, R., Dawe, H.R., Farr, H., Griffiths, S., Hart, S.R., Portman, N., Shaw, M.K., Ginger, M.L., Gaskell, S.J., McKean, P.G., et al. (2006). Flagellar motility is required for the viability of the bloodstream trypanosome. Nature *440*, 224–227.

Brun, R., Blum, J., Chappuis, F., and Burri, C. (2010). Human african trypanosomiasis. The Lancet *375*, 148–159.

Brun, R., Don, R., Jacobs, R.T., Wang, M.Z., and Barrett, M.P. (2011). Development of novel drugs for human African trypanosomiasis. Future Microbiol. *6*, 677–691.

Buchner, J., and Rudolph, R. (1991). Renaturation, purification and characterization of recombinant Fab-fragments produced in Escherichia coli. Nat. Biotechnol. *9*, 157–162.

Buguet, A. (1999). Is Sleeping Sickness a Orcadian Disorder? The Serotonergic Hypothesis. Chronobiol. Int. *16*, 477–489.

Buguet, A., Bourdon, L., Bouteille, B., Cespuglio, R., Vincendeau, P., Radomski, M.W., and Dumas, M. (2001). The duality of sleeping sickness: focusing on sleep. Sleep Med. Rev. *5*, 139–153.

Buguet, A., Bisser, S., Josenando, T., Chapotot, F., and Cespuglio, R. (2005). Sleep structure: a new diagnostic tool for stage determination in sleeping sickness. Acta Trop. *93*, 107–117.

Burgess, R.R. (1996). [12] Purification of overproduced Escherichia coli RNA polymerase σ factors by solubilizing inclusion bodies and refolding from Sarkosyl. Methods Enzymol. *273*, 145–149.

Burgess, R.R. (2009). Refolding solubilized inclusion body proteins. Methods Enzymol. *463*, 259–282.

Caljon, G., Van Reet, N., De Trez, C., Vermeersch, M., Pérez-Morga, D., and Van Den Abbeele, J. (2016). The Dermis as a Delivery Site of Trypanosoma brucei for Tsetse Flies. PLoS Pathog. *12*, e1005744.

Capewell, P., Cren-Travaillé, C., Marchesi, F., Johnston, P., Clucas, C., Benson, R.A., Gorman, T.-A., Calvo-Alvarez, E., Crouzols, A., Jouvion, G., et al. (2016). The skin is a significant but overlooked anatomical reservoir for vector-borne African trypanosomes. eLife *5*, e17716.

Casas-Sánchez, A., and Acosta-Serrano, Á. (2016). Skin deep. eLife *5*, e21506.

Chapman, H.N., Fromme, P., Barty, A., White, T.A., Kirian, R.A., Aquila, A., Hunter, M.S., Schulz, J., DePonte, D.P., Weierstall, U., et al. (2011). Femtosecond X-ray protein nanocrystallography. Nature *470*, 73–77.

Chappuis, F., Loutan, L., Simarro, P., Lejon, V., and Büscher, P. (2005). Options for field diagnosis of human African trypanosomiasis. Clin. Microbiol. Rev. *18*, 133–146.

Checchi, F., Filipe, J.A., Haydon, D.T., Chandramohan, D., and Chappuis, F. (2008). Estimates of the duration of the early and late stage of gambiense sleeping sickness. BMC Infect. Dis. *8*, 1.

Clayton, C., and Shapira, M. (2007). Post-transcriptional regulation of gene expression in trypanosomes and leishmanias. Mol. Biochem. Parasitol. *156*, 93–101.

Clayton, C., Adams, M., Almeida, R., Baltz, T., Barrett, M., Bastien, P., Belli, S., Beverley, S., Biteau, N., Blackwell, J., et al. (1998). Genetic nomenclature for Trypanosoma and Leishmania. Mol. Biochem. Parasitol. *97*, 221–224.

Croft, S.L. (2016). Neglected tropical diseases in the genomics era: re-evaluating the impact of new drugs and mass drug administration. Genome Biol. *17*, 1.

Cross, G.A.M. (1975). Identification, purification and properties of clone-specific glycoprotein antigens constituting the surface coat of Trypanosoma brucei. Parasitology *71*, 393–417.

Deborggraeve, S., and Büscher, P. (2010). Molecular diagnostics for sleeping sickness: what is the benefit for the patient? Lancet Infect. Dis. *10*, 433–439.

Deborggraeve, S., and Büscher, P. (2012). Recent progress in molecular diagnosis of sleeping sickness. Expert Rev. Mol. Diagn. *12*, 719–730.

Deller, M.C., Kong, L., and Rupp, B. (2016). Protein stability: a crystallographer's perspective. Acta Crystallogr. Sect. F Struct. Biol. Commun. *72*, 72–95.

Dey, I., Keller, K., Belley, A., and Chadee, K. (2003). Identification and characterization of a cyclooxygenase-like enzyme from Entamoeba histolytica. Proc. Natl. Acad. Sci. *100*, 13561–13566.

Ding, D., Zhao, Y., Meng, Q., Xie, D., Nare, B., Chen, D., Bacchi, C.J., Yarlett, N., Zhang, Y.-K., Hernandez, V., et al. (2010). Discovery of novel benzoxaborole-based potent antitrypanosomal agents. ACS Med. Chem. Lett. *1*, 165–169.

Djikeng, A., Shi, H., Tschudi, C., and Ullu, E. (2001). RNA interference in Trypanosoma brucei: cloning of small interfering RNAs provides evidence for retroposon-derived 24–26-nucleotide RNAs. Rna *7*, 1522–1530.

Donelson, J.E. (2003). Antigenic variation and the African trypanosome genome. Acta Trop. *85*, 391–404.

Doye, J.P., and Poon, W.C. (2006). Protein crystallization in vivo. Curr. Opin. Colloid Interface Sci. *11*, 40–46.

Duszenko, M., Figarella, K., Macleod, E.T., and Welburn, S.C. (2006). Death of a trypanosome: a selfish altruism. Trends Parasitol. *22*, 536–542.

Duszenko, M., Redecke, L., Mudogo, C.N., Sommer, B.P., Mogk, S., Oberthuer, D., and Betzel, C. (2015). In vivo protein crystallization in combination with highly brilliant radiation sources offers novel opportunities for the structural analysis of post-translationally modified eukaryotic proteins. Acta Crystallogr. Sect. F Struct. Biol. Commun. *71*, 929–937.

Enanga, B., Burchmore, R.J.S., Stewart, M.L., and Barrett, M.P. (2002). Sleeping sickness and the brain. Cell. Mol. Life Sci. CMLS *59*, 845–858.

Engstler, M., Thilo, L., Weise, F., Grünfelder, C.G., Schwarz, H., Boshart, M., and Overath, P. (2004). Kinetics of endocytosis and recycling of the GPI-anchored variant surface glycoprotein in Trypanosoma brucei. J. Cell Sci. *117*, 1105–1115.

Ersfeld, K. (2011). Nuclear architecture, genome and chromatin organisation in Trypanosoma brucei. Res. Microbiol. *162*, 626–636.

Evdokimov, A.G., Moshiri, F., Sturman, E.J., Rydel, T.J., Zheng, M., Seale, J.W., and Franklin, S. (2014). Structure of the full-length insecticidal protein Cry1Ac reveals intriguing details of toxin packaging into in vivo formed crystals. Protein Sci. Publ. Protein Soc. *23*, 1491–1497.

Fairlamb, A.H. (2003). Chemotherapy of human African trypanosomiasis: current and future prospects. Trends Parasitol. *19*, 488–494.

Fairlamb, A.H., Henderson, G.B., and Cerami, A. (1989). Trypanothione is the primary target for arsenical drugs against African trypanosomes. Proc. Natl. Acad. Sci. *86*, 2607–2611.

Fevre, E.M., Wissmann, B. v, Welburn, S.C., and Lutumba, P. (2008). The burden of human African trypanosomiasis. PLoS Negl Trop Dis *2*, e333.

Field, M.C., and Carrington, M. (2009). The trypanosome flagellar pocket. Nat. Rev. Microbiol. *7*, 775–786.

Field, M.C., Allen, C.L., Dhir, V., Goulding, D., Hall, B.S., Morgan, G.W., Veazey, P., and Engstler, M. (2004). New approaches to the microscopic imaging of Trypanosoma brucei. Microsc. Microanal. Off. J. Microsc. Soc. Am. Microbeam Anal. Soc. Microsc. Soc. Can. *10*, 621–636.

Field, M.C., Horn, D., Fairlamb, A.H., Ferguson, M.A., Gray, D.W., Read, K.D., De Rycker, M., Torrie, L.S., Wyatt, P.G., Wyllie, S., et al. (2017). Anti-trypanosomatid drug discovery: an ongoing challenge and a continuing need. Nat. Rev. Microbiol. *15*, 217–231.

Figarella, K., Rawer, M., Uzcategui, N.L., Kubata, B.K., Lauber, K., Madeo, F., Wesselborg, S., and Duszenko, M. (2005). Prostaglandin D2 induces programmed cell death in Trypanosoma brucei bloodstream form. Cell Death Differ. *12*, 335–346.

Figarella, K., Uzcategui, N.L., Beck, A., Schoenfeld, C., Kubata, B.K., Lang, F., and Duszenko, M. (2006). Prostaglandin-induced programmed cell death in Trypanosoma brucei involves oxidative stress. Cell Death Differ. *13*, 1802–1814.

Fire, A., Xu, S., Montgomery, M.K., Kostas, S.A., Driver, S.E., and Mello, C.C. (1998). Potent and specific genetic interference by double-stranded RNA in Caenorhabditis elegans. Nature *391*, 806–811.

Franco, J.R., Simarro, P.P., Diarra, A., and Jannin, J.G. (2014). Epidemiology of human African trypanosomiasis. Clin. Epidemiol. *6*, 257.

Fromme, P. (2015). XFELs open a new era in structural chemical biology. Nat. Chem. Biol. *11*, 895–899.

Gallat, F.-X., Matsugaki, N., Coussens, N.P., Yagi, K.J., Boudes, M., Higashi, T., Tsuji, D., Tatano, Y., Suzuki, M., Mizohata, E., et al. (2014). In vivo crystallography at X-ray free-electron lasers: the next generation of structural biology? Philos. Trans. R. Soc. Lond. B. Biol. Sci. *369*, 20130497.

Gati, C., Bourenkov, G., Klinge, M., Rehders, D., Stellato, F., Oberthür, D., Yefanov, O., Sommer, B.P., Mogk, S., Duszenko, M., et al. (2014a). Serial crystallography on in vivo grown microcrystals using synchrotron radiation. IUCrJ *1*, 87–94.

Gati, C., Bourenkov, G., Klinge, M., Rehders, D., Stellato, F., Oberthür, D., Yefanov, O., Sommer, B.P., Mogk, S., Duszenko, M., et al. (2014b). Serial crystallography on in vivo grown microcrystals using synchrotron radiation. IUCrJ *1*, 87–94.

Grab, D.J., and Kennedy, P.G.E. (2008). Traversal of human and animal trypanosomes across the blood-brain barrier. J. Neurovirol. *14*, 344–351.

Hamm, B., Schindler, A., Mecke, D., and Duszenko, M. (1990). Differentiation of Trypanosoma brucei bloodstream trypomastigotes from long slender to short stumpy-like forms in axenic culture. Mol. Biochem. Parasitol. *40*, 13–22.

Hasegawa, H., Wendling, J., He, F., Trilisky, E., Stevenson, R., Franey, H., Kinderman, F., Li, G., Piedmonte, D.M., Osslund, T., et al. (2011). In vivo crystallization of human IgG in the endoplasmic reticulum of engineered Chinese hamster ovary (CHO) cells. J. Biol. Chem. *286*, 19917–19931.

Hayaishi, O. (2000). Molecular mechanisms of sleep–wake regulation: a role of prostaglandin D2. Philos. Trans. R. Soc. Lond. B Biol. Sci. *355*, 275–280.

Hayaishi, O. (2002). Invited Review: Molecular genetic studies on sleep-wake regulation, with special emphasis on the prostaglandin D2 system. J. Appl. Physiol. *92*, 863–868.

Hayashida, K., Kajino, K., Hachaambwa, L., Namangala, B., and Sugimoto, C. (2015). Direct blood dry LAMP: a rapid, stable, and easy diagnostic tool for Human African Trypanosomiasis. PLoS Negl Trop Dis *9*, e0003578.

Hendry, K.A., and Vickerman, K. (1988). The requirement for epimastigote attachment during division and metacyclogenesis in Trypanosoma congolense. Parasitol. Res. *74*, 403–408.

Holton, J.M., and Frankel, K.A. (2010). The minimum crystal size needed for a complete diffraction data set. Acta Crystallogr. D Biol. Crystallogr. *66*, 393–408.

Hotez, P.J., and Kamath, A. (2009). Neglected tropical diseases in sub-saharan Africa: review of their prevalence, distribution, and disease burden. PLoS Negl Trop Dis *3*, e412.

Hutchings, N.R., Donelson, J.E., and Hill, K.L. (2002). Trypanin is a cytoskeletal linker protein and is required for cell motility in African trypanosomes. J. Cell Biol. *156*, 867–877.

Ito, L., Shiraki, K., Matsuura, T., Okumura, M., Hasegawa, K., Baba, S., Yamaguchi, H., and Kumasaka, T. (2011). High-resolution X-ray analysis reveals binding of arginine to aromatic residues of lysozyme surface: implication of suppression of protein aggregation by arginine. Protein Eng. Des. Sel. *24*, 269–274.

Jacobs, R.T., Nare, B., Wring, S.A., Orr, M.D., Chen, D., Sligar, J.M., Jenks, M.X., Noe, R.A., Bowling, T.S., Mercer, L.T., et al. (2011). SCYX-7158, an orally-active benzoxaborole for the treatment of stage 2 human African trypanosomiasis. PLoS Negl Trop Dis *5*, e1151.

Jakobi, A.J., Passon, D.M., Knoops, K., Stellato, F., Liang, M., White, T.A., Seine, T., Messerschmidt, M., Chapman, H.N., and Wilmanns, M. (2016). In cellulo serial crystallography of alcohol oxidase crystals inside yeast cells. IUCrJ *3*, 88–95.

Jones, A.J., and Avery, V.M. (2015). Future treatment options for human African trypanosomiasis. Expert Rev. Anti Infect. Ther. *13*, 1429–1432.

Jones, D.C., Foth, B.J., Urbaniak, M.D., Patterson, S., Ong, H.B., Berriman, M., and Fairlamb, A.H. (2015). Genomic and Proteomic Studies on the Mode of Action of Oxaboroles against the African Trypanosome. PLoS Negl Trop Dis *9*, e0004299.

Kaiser, M., Bray, M.A., Cal, M., Trunz, B.B., Torreele, E., and Brun, R. (2011). Antitrypanosomal activity of fexinidazole, a new oral nitroimidazole drug candidate for treatment of sleeping sickness. Antimicrob. Agents Chemother. *55*, 5602–5608.

Kang, H.J., Lee, C., and Drew, D. (2013). Breaking the barriers in membrane protein crystallography. Int. J. Biochem. Cell Biol. *45*, 636–644.

Kapuscinski, J. (1995). DAPI: a DNA-specific fluorescent probe. Biotech. Histochem. *70*, 220–233.

Keating, C. (2014). Ken Warren and the Rockefeller Foundation's Great Neglected Diseases Network, 1978–1988: The Transformation of Tropical and Global Medicine. Mol. Med. *20*, S24–S30.

Kennedy, P.G. (2008). The continuing problem of human African trypanosomiasis (sleeping sickness). Ann. Neurol. *64*, 116–126.

Kennedy, P.G. (2013). Clinical features, diagnosis, and treatment of human African trypanosomiasis (sleeping sickness). Lancet Neurol. *12*, 186–194.

Kirian, R.A., Wang, X., Weierstall, U., Schmidt, K.E., Spence, J.C.H., Hunter, M., Fromme, P., White, T., Chapman, H.N., and Holton, J. (2010). Femtosecond protein nanocrystallography-data analysis methods. Opt. Express *18*, 5713–5723.

Kirian, R.A., White, T.A., Holton, J.M., Chapman, H.N., Fromme, P., Barty, A., Lomb, L., Aquila, A., Maia, F.R.N.C., Martin, A.V., et al. (2011). Structure-factor analysis of femtosecond microdiffraction patterns from protein nanocrystals. Acta Crystallogr. A *67*, 131–140.

Kohl, L., Sherwin, T., and Gull, K. (1999). Assembly of the paraflagellar rod and the flagellum attachment zone complex during the Trypanosoma brucei cell cycle. J. Eukaryot. Microbiol. *46*, 105–109.

Kolev, N.G., Tschudi, C., and Ullu, E. (2011). RNA interference in protozoan parasites: achievements and challenges. Eukaryot. Cell *10*, 1156–1163.

Koopmann, R., Cupelli, K., Redecke, L., Nass, K., Deponte, D.P., White, T.A., Stellato, F., Rehders, D., Liang, M., Andreasson, J., et al. (2012). In vivo protein crystallization opens new routes in structural biology. Nat. Methods *9*, 259–262.

Kristensson, K., Nyg\a ard, M., Bertini, G., and Bentivoglio, M. (2010). African trypanosome infections of the nervous system: parasite entry and effects on sleep and synaptic functions. Prog. Neurobiol. *91*, 152–171.

Kubata, B.K., Duszenko, M., Kabututu, Z., Rawer, M., Szallies, A., Fujimori, K., Inui, T., Nozaki, T., Yamashita, K., Horii, T., et al. (2000). Identification of a novel prostaglandin F2α synthase in Trypanosoma brucei. J. Exp. Med. *192*, 1327–1338.

Kubata, B.K., Duszenko, M., Martin, K.S., and Urade, Y. (2007). Molecular basis for prostaglandin production in hosts and parasites. Trends Parasitol. *23*, 325–331.

Lebendiker, M., and Danieli, T. (2014). Production of prone-to-aggregate proteins. FEBS Lett. *588*, 236–246.

Lejon, V., Büscher, P., Sema, N.H., Magnus, E., and Van Meirvenne, N. (1998). Human African trypanosomiasis: a latex agglutination field test for quantifying IgM in cerebrospinal fluid. Bull. World Health Organ. *76*, 553.

Lin, W.-J., and Traugh, J.A. (1993). Renaturation of casein kinase II from recombinant subunits produced in Escherichia coli: purification and characterization of the reconstituted holoenzyme. Protein Expr. Purif. *4*, 256–264.

Liu, S., Hattne, J., Reyes, F.E., Sanchez-Martinez, S., Jason de la Cruz, M., Shi, D., and Gonen, T. (2016). Atomic resolution structure determination by the cryo-EM method MicroED. Protein Sci. Publ. Protein Soc.

Lund, A.H., Duch, M., and Pedersen, F.S. (1996). Increased cloning efficiency by temperature-cycle ligation. Nucleic Acids Res. *24*, 800–801.

Lutumba, P., Robays, J., Miaka, C., Kande, V., Mumba, D., Büscher, P., Dujardin, B., and Boelaert, M. (2006). [Validity, cost and feasibility of the mAECT and CTC confirmation tests after diagnosis of African of sleeping sickness]. Trop. Med. Int. Health TM IH *11*, 470–478.

Lutumba, P., Meheus, F., Robays, J., Miaka, C., Kande, V., Büscher, P., Dujardin, B., and Boelaert, M. (2007). Cost-effectiveness of algorithms for confirmation test of human African trypanosomiasis.

Mande, S.C., and Sobhia, M.E. (2000). Structural characterization of protein–denaturant interactions: crystal structures of hen egg-white lysozyme in complex with DMSO and guanidinium chloride. Protein Eng. *13*, 133–141.

Manna, P.T., Obado, S.O., Boehm, C., Gadelha, C., Sali, A., Chait, B.T., Rout, M.P., and Field, M.C. (2017). Lineage-specific proteins essential for endocytosis in trypanosomes. J Cell Sci *130*, 1379–1392.

Marchini, F.K., de Godoy, L.M.F., Batista, M., Kugeratski, F.G., and Krieger, M.A. (2014). Towards the Phosphoproteome of Trypanosomatids. In Proteins and Proteomics of Leishmania and Trypanosoma, (Springer), pp. 351–378.

Matsuoka, T., Hamada, H., Matsumoto, K., and Shiraki, K. (2009). Indispensable structure of solution additives to prevent inactivation of lysozyme for heating and refolding. Biotechnol. Prog. *25*, 1515–1524.

Matthews, K.R. (2005). The developmental cell biology of Trypanosoma brucei. J. Cell Sci. *118*, 283–290.

McAllaster, M.R., Ikeda, K.N., Lozano-Núñez, A., Anrather, D., Unterwurzacher, V., Gossenreiter, T., Perry, J.A., Crickley, R., Mercadante, C.J., Vaughan, S., et al. (2015). Proteomic identification of novel cytoskeletal proteins associated with TbPLK, an essential regulator of cell morphogenesis in Trypanosoma brucei. Mol. Biol. Cell *26*, 3013–3029.

McPherson, A., and Gavira, J.A. (2014). Introduction to protein crystallization. Acta Crystallogr. Sect. F Struct. Biol. Commun. *70*, 2–20.

Mogk, S., Meiwes, A., Boßelmann, C.M., Wolburg, H., and Duszenko, M. (2014). The lane to the brain: how African trypanosomes invade the CNS. Trends Parasitol. *30*, 470–477.

Mogk, S., Boßelmann, C.M., Mudogo, C.N., Stein, J., Wolburg, H., and Duszenko, M. (2016). African trypanosomes and brain infection - the unsolved question. Biol. Rev. Camb. Philos. Soc.

Morrison, L.J., Majiwa, P., Read, A.F., and Barry, J.D. (2005). Probabilistic order in antigenic variation of Trypanosoma brucei. Int. J. Parasitol. *35*, 961–972.

Morriswood, B., and Schmidt, K. (2015). A MORN Repeat Protein Facilitates Protein Entry into the Flagellar Pocket of Trypanosoma brucei. Eukaryot. Cell *14*, 1081–1093.

Morriswood, B., Havlicek, K., Demmel, L., Yavuz, S., Sealey-Cardona, M., Vidilaseris, K., Anrather, D., Kostan, J., Djinovic-Carugo, K., Roux, K.J., et al. (2013). Novel bilobe components in Trypanosoma brucei identified using proximity-dependent biotinylation. Eukaryot. Cell *12*, 356–367.

Motyka, S.A., and Englund, P.T. (2004). RNA interference for analysis of gene function in trypanosomatids. Curr. Opin. Microbiol. *7*, 362–368.

Mugnier, M.R., Stebbins, C.E., and Papavasiliou, F.N. (2016). Masters of disguise: antigenic variation and the VSG coat in Trypanosoma brucei. PLoS Pathog *12*, e1005784.

Mulenga, C., Mhlanga, J.D., Kristensson, K., and Robertson, B. (2001). Trypanosoma brucei brucei crosses the blood-brain barrier while tight junction proteins are preserved in a rat chronic disease model. Neuropathol. Appl. Neurobiol. *27*, 77–85.

Muniyappan, S., Kim, S.O., and Ihee, H. (2015). Recent Advances and Futur e Prospects of Serial Crystallography using XFEL and Synchrotro n X-Ray Sources. Bio Des. *3*, 98–110.

Nagle, A.S., Khare, S., Kumar, A.B., Supek, F., Buchynskyy, A., Mathison, C.J., Chennamaneni, N.K., Pendem, N., Buckner, F.S., Gelb, M.H., et al. (2014). Recent developments in drug discovery for leishmaniasis and human African trypanosomiasis. Chem. Rev. *114*, 11305–11347.

Nannenga, B.L., Shi, D., Leslie, A.G.W., and Gonen, T. (2014a). High-resolution structure determination by continuous-rotation data collection in MicroED. Nat. Methods *11*, 927–930.

Nannenga, B.L., Shi, D., Hattne, J., Reyes, F.E., and Gonen, T. (2014b). Structure of catalase determined by MicroED. eLife *3*, e03600.

Nass, K., Foucar, L., Barends, T.R.M., Hartmann, E., Botha, S., Shoeman, R.L., Doak, R.B., Alonso-Mori, R., Aquila, A., Bajt, S., et al. (2015). Indications of radiation damage in ferredoxin microcrystals using high-intensity X-FEL beams. J. Synchrotron Radiat. *22*, 225–238.

Nett, I.R., Martin, D.M., Miranda-Saavedra, D., Lamont, D., Barber, J.D., Mehlert, A., and Ferguson, M.A. (2009). The phosphoproteome of bloodstream form Trypanosoma brucei, causative agent of African sleeping sickness. Mol. Cell. Proteomics *8*, 1527–1538.

Neutze, R., and Moffat, K. (2012). Time-resolved structural studies at synchrotrons and X-ray free electron lasers: opportunities and challenges. Curr. Opin. Struct. Biol. *22*, 651–659.

Ngo, H., Tschudi, C., Gull, K., and Ullu, E. (1998). Double-stranded RNA induces mRNA degradation in Trypanosoma brucei. Proc. Natl. Acad. Sci. *95*, 14687–14692.

Odiit, M., Kansiime, F., and Enyaru, J.C. (1997). Duration of symptoms and case fatality of sleeping sickness caused by Trypanosoma brucei rhodesiense in Tororo, Uganda. East Afr. Med. J. *74*, 792–795.

Okano, Y., Inoue, T., Kubata, B.K., Kabututu, Z., Urade, Y., Matsumura, H., and Kai, Y. (2002). Crystallization and Preliminary X-Ray Crystallographic Studies of Trypanosoma brucei Prostaglandin F2α Synthase1. J. Biochem. (Tokyo) *132*.

Olego-Fernandez, S., Vaughan, S., Shaw, M.K., Gull, K., and Ginger, M.L. (2009). Cell morphogenesis of Trypanosoma brucei requires the paralogous, differentially expressed calpain-related proteins CAP5. 5 and CAP5. 5V. Protist *160*, 576–590.

Ooi, C.-P., and Bastin, P. (2013). More than meets the eye: understanding Trypanosoma brucei morphology in the tsetse. Front. Cell. Infect. Microbiol. *3*, 71.

Patrick, K.L., Shi, H., Kolev, N.G., Ersfeld, K., Tschudi, C., and Ullu, E. (2009). Distinct and overlapping roles for two Dicer-like proteins in the RNA interference pathways of the ancient eukaryote Trypanosoma brucei. Proc. Natl. Acad. Sci. U. S. A. *106*, 17933–17938.

Pentreath, V.W., Rees, K., Owolabi, O.A., Philip, K.A., and Doua, F. (1990). The somnogenic T lymphocyte suppressor prostaglandin D2 is selectively elevated in cerebrospinal fluid of advanced sleeping sickness patients. Trans. R. Soc. Trop. Med. Hyg. *84*, 795–799.

Pfaffl, M.W. (2001). A new mathematical model for relative quantification in real-time RT–PCR. Nucleic Acids Res. *29*, e45–e45.

Pfaffl, M.W. (2004). Real-time RT-PCR: neue Ansätze zur exakten mRNA Quantifizierung. BIOspektrum *1*, 92–5.

Priotto, G., Kasparian, S., Mutombo, W., Ngouama, D., Ghorashian, S., Arnold, U., Ghabri, S., Baudin, E., Buard, V., Kazadi-Kyanza, S., et al. (2009). Nifurtimox-eflornithine combination therapy for second-stage African Trypanosoma brucei gambiense trypanosomiasis: a multicentre, randomised, phase III, non-inferiority trial. The Lancet *374*, 56–64.

Ralston, K.S., and Hill, K.L. (2008). The flagellum of Trypanosoma brucei: new tricks from an old dog. Int. J. Parasitol. *38*, 869–884.

Rawer, M. (2004). Prostaglandinstoffwechsel in Trypanosoma brucei: Klonierung und Charakterizierung der Prostaglandin $F_{2α}$ Synthase und der PGD_2 induzierte Zelltod. Universität Tübingen.

Redecke, L., Nass, K., DePonte, D.P., White, T.A., Rehders, D., Barty, A., Stellato, F., Liang, M., Barends, T.R.M., Boutet, S., et al. (2013a). Natively inhibited Trypanosoma brucei cathepsin B structure determined by using an X-ray laser. Science *339*, 227–230.

Redecke, L., Nass, K., DePonte, D.P., White, T.A., Rehders, D., Barty, A., Stellato, F., Liang, M., Barends, T.R., Boutet, S., et al. (2013b). Natively inhibited Trypanosoma brucei cathepsin B structure determined by using an X-ray laser. Science *339*, 227–230.

Robinson, D.R., Sherwin, T., Ploubidou, A., Byard, E.H., and Gull, K. (1995). Microtubule polarity and dynamics in the control of organelle positioning, segregation, and cytokinesis in the trypanosome cell cycle. J. Cell Biol. *128*, 1163–1172.

Roditi, I., Schwarz, H., Pearson, T.W., Beecroft, R.P., Liu, M.K., Richardson, J.P., Bühring, H.J., Pleiss, J., Bülow, R., and Williams, R.O. (1989). Procyclin gene expression and loss of the variant surface glycoprotein during differentiation of Trypanosoma brucei. J. Cell Biol. *108*, 737–746.

Rodriguez, J.A., Ivanova, M.I., Sawaya, M.R., Cascio, D., Reyes, F.E., Shi, D., Sangwan, S., Guenther, E.L., Johnson, L.M., Zhang, M., et al. (2015). Structure of the toxic core of α-synuclein from invisible crystals. Nature *525*, 486–490.

Rosano, G.L., and Ceccarelli, E.A. (2014). Recombinant protein expression in Escherichia coli: advances and challenges. Recomb. Protein Expr. Microb. Syst. *7*.

Samuel, D., Ganesh, G., Yang, P.-W., Chang, M.-M., Wang, S.-L., Hwang, K.-C., Yu, C., Jayaraman, G., Kumar, T.K.S., Trivedi, V.D., et al. (2000). Proline inhibits aggregation during protein refolding. Protein Sci. *9*, 344–352.

Sanishvili, R., Yoder, D.W., Pothineni, S.B., Rosenbaum, G., Xu, S., Vogt, S., Stepanov, S., Makarov, O.A., Corcoran, S., Benn, R., et al. (2011). Radiation damage in protein crystals is reduced with a micron-sized X-ray beam. Proc. Natl. Acad. Sci. U. S. A. *108*, 6127–6132.

Sawaya, M.R., Cascio, D., Gingery, M., Rodriguez, J., Goldschmidt, L., Colletier, J.-P., Messerschmidt, M.M., Boutet, S., Koglin, J.E., Williams, G.J., et al. (2014). Protein crystal structure obtained at 2.9 Å resolution from injecting bacterial cells into an X-ray free-electron laser beam. Proc. Natl. Acad. Sci. U. S. A. *111*, 12769–12774.

Sawaya, M.R., Rodriguez, J., Cascio, D., Collazo, M.J., Shi, D., Reyes, F.E., Hattne, J., Gonen, T., and Eisenberg, D.S. (2016). Ab initio structure determination from prion nanocrystals at atomic resolution by MicroED. Proc. Natl. Acad. Sci. U. S. A. *113*, 11232–11236.

Schlichting, I., and Miao, J. (2012). Emerging opportunities in structural biology with X-ray free-electron lasers. Curr. Opin. Struct. Biol. *22*, 613–626.

Schönherr, R., Klinge, M., Rudolph, J.M., Fita, K., Rehders, D., Lübber, F., Schneegans, S., Majoul, I.V., Duszenko, M., Betzel, C., et al. (2015). Real-time investigation of dynamic protein crystallization in living cells. Struct. Dyn. Melville N *2*, 041712.

Sherwin, T., and Gull, K. (1989). Visualization of detyrosination along single microtubules reveals novel mechanisms of assembly during cytoskeletal duplication in trypanosomes. Cell *57*, 211–221.

Shi, D., Nannenga, B.L., Iadanza, M.G., and Gonen, T. (2013). Three-dimensional electron crystallography of protein microcrystals. eLife *2*, e01345.

Shi, D., Nannenga, B.L., de la Cruz, M.J., Liu, J., Sawtelle, S., Calero, G., Reyes, F.E., Hattne, J., and Gonen, T. (2016). The collection of MicroED data for macromolecular crystallography. Nat. Protoc. *11*, 895–904.

Shi, H., Tschudi, C., and Ullu, E. (2006). Functional replacement of Trypanosoma brucei Argonaute by the human slicer Argonaute2. RNA N. Y. N *12*, 943–947.

Sliz, P., Harrison, S.C., and Rosenbaum, G. (2003). How does radiation damage in protein crystals depend on X-ray dose? Struct. Lond. Engl. 1993 *11*, 13–19.

Stein, J., Mogk, S., Mudogo, C.N., Sommer, B.P., Scholze, M., Meiwes, A., Huber, M., Gray, A., and Duszenko, M. (2014). Drug development against sleeping sickness: old wine in new bottles? Curr. Med. Chem. *21*, 1713–1727.

Sternberg, J.M., Gierliński, M., Biéler, S., Ferguson, M.A., and Ndung'u, J.M. (2014). Evaluation of the diagnostic accuracy of prototype rapid tests for human African trypanosomiasis. PLoS Negl Trop Dis *8*, e3373.

Steverding, D. (2008). The history of African trypanosomiasis. Parasit. Vectors *1*, 1.

Sudarshi, D., Lawrence, S., Pickrell, W.O., Eligar, V., Walters, R., Quaderi, S., Walker, A., Capewell, P., Clucas, C., Vincent, A., et al. (2014). Human African trypanosomiasis presenting at least 29 years after infection—what can this teach us about the pathogenesis and control of this neglected tropical disease? PLoS Negl Trop Dis *8*, e3349.

Tarral, A., Blesson, S., Mordt, O.V., Torreele, E., Sassella, D., Bray, M.A., Hovsepian, L., Evene, E., Gualano, V., Felices, M., et al. (2014). Determination of an optimal dosing regimen for fexinidazole, a novel oral drug for the treatment of human African trypanosomiasis: first-in-human studies. Clin. Pharmacokinet. *53*, 565–580.

Torreele, E., Trunz, B.B., Tweats, D., Kaiser, M., Brun, R., Mazue, G., Bray, M.A., and Pecoul, B. (2010). Fexinidazole–a new oral nitroimidazole drug candidate entering clinical development for the treatment of sleeping sickness. PLoS Negl Trop Dis *4*, e923.

Trindade, S., Rijo-Ferreira, F., Carvalho, T., Pinto-Neves, D., Guegan, F., Aresta-Branco, F., Bento, F., Young, S.A., Pinto, A., Van Den Abbeele, J., et al. (2016). Trypanosoma brucei Parasites Occupy and Functionally Adapt to the Adipose Tissue in Mice. Cell Host Microbe *19*, 837–848.

Truc, P., Jamonneau, V., N'Guessan, P., Diallo, P.B., and Garcia, A. (1998). Parasitological diagnosis of human African trypanosomiasis: a comparison of the QBC® and miniature anion-exchange centrifugation techniques. Trans. R. Soc. Trop. Med. Hyg. *92*, 288–289.

Tschudi, C., Djikeng, A., Shi, H., and Ullu, E. (2003). In vivo analysis of the RNA interference mechanism in Trypanosoma brucei. Methods San Diego Calif *30*, 304–312.

Tsumoto, K., Shinoki, K., Kondo, H., Uchikawa, M., Juji, T., and Kumagai, I. (1998). Highly efficient recovery of functional single-chain Fv fragments from inclusion bodies overexpressed in Escherichia coli by controlled introduction of oxidizing reagent—application to a human single-chain Fv fragment. J. Immunol. Methods *219*, 119–129.

Turner, C.M. (1999). Antigenic variation in Trypanosoma brucei infections: an holistic view. J Cell Sci *112*, 3187–3192.

Ullu, E., Djikeng, A., Shi, H., and Tschudi, C. (2002). RNA interference: advances and questions. Philos. Trans. R. Soc. Lond. B. Biol. Sci. *357*, 65–70.

Urade, Y., and Hayaishi, O. (2011). Prostaglandin D 2 and sleep/wake regulation. Sleep Med. Rev. *15*, 411–418.

Urbaniak, M.D., Martin, D.M., and Ferguson, M.A. (2013). Global quantitative SILAC phosphoproteomics reveals differential phosphorylation is widespread between the procyclic and bloodstream form lifecycle stages of Trypanosoma brucei. J. Proteome Res. *12*, 2233.

Vassella, E., Reuner, B., Yutzy, B., and Boshart, M. (1997). Differentiation of African trypanosomes is controlled by a density sensing mechanism which signals cell cycle arrest via the cAMP pathway. J. Cell Sci. *110 (Pt 21)*, 2661–2671.

Vaughan, S., and Gull, K. (2003). The trypanosome flagellum. J. Cell Sci. *116*, 757–759.

Vaughan, S., Kohl, L., Ngai, I., Wheeler, R.J., and Gull, K. (2008). A repetitive protein essential for the flagellum attachment zone filament structure and function in Trypanosoma brucei. Protist *159*, 127–136.

Vickerman, K., Tetley, L., Hendry, K.A., and Turner, C.M. (1988). Biology of African trypanosomes in the tsetse fly. Biol. Cell *64*, 109–119.

Walls, D., and Loughran, S.T. (2011). Tagging recombinant proteins to enhance solubility and aid purification. Protein Chromatogr. Methods Protoc. 151–175.

Wampler, R.D., Kissick, D.J., Dehen, C.J., Gualtieri, E.J., Grey, J.L., Wang, H.-F., Thompson, D.H., Cheng, J.-X., and Simpson, G.J. (2008). Selective detection of protein crystals by second harmonic microscopy. J. Am. Chem. Soc. *130*, 14076–14077.

Wolburg, H., Mogk, S., Acker, S., Frey, C., Meinert, M., Schönfeld, C., Lazarus, M., Urade, Y., Kubata, B.K., and Duszenko, M. (2012). Late stage infection in sleeping sickness. PloS One *7*, e34304.

Woo, P.T.K., and others (1970). The haematocrit centrifuge technique for the diagnosis of African trypanosomiasis. Acta Trop. *27*, 384–6.

Yamaguchi, H., and Miyazaki, M. (2014). Refolding techniques for recovering biologically active recombinant proteins from inclusion bodies. Biomolecules *4*, 235–251.

Yang, J.T., Wu, C.-S.C., and Martinez, H.M. (1986). [11] Calculation of protein conformation from circular dichroism. Methods Enzymol. *130*, 208–269.

Yonekura, K., Kato, K., Ogasawara, M., Tomita, M., and Toyoshima, C. (2015). Electron crystallography of ultrathin 3D protein crystals: atomic model with charges. Proc. Natl. Acad. Sci. U. S. A. *112*, 3368–3373.

Zhou, Q., Liu, B., Sun, Y., and He, C.Y. (2011). A coiled-coil- and C2-domain-containing protein is required for FAZ assembly and cell morphology in Trypanosoma brucei. J. Cell Sci. *124*, 3848–3858.

10 CURRICULUM VITAE

I. PERSONAL DATA

Name : MUDOGO NZANZU Célestin

Address : Philosophenweg 79, 72076 Tübingen, Germany

Date of Birth : 26th May 1980 in Kinshasa, DR Congo

Nationality : Congolese

Sex : Male

Téléphone : **+49 (0) 157 38561189**

E-Mail : cmudogo@gmail.com/cmudogo@yahoo.fr

Marital Status: Single

II. EDUCATION BACKGROUND

❖ 1986 – 1992: Primary School at the Institute of Mont – Amba

❖ 1993 – 1998: High School at the Institute of Mont – Amba

❖ 1999 – 2006: M.D Degree obtained at the Université de Kinshasa, Medical Doctor Degree in Medical General Surgery and Childbirth

❖ 2007 – 2008: Junior Assistant at Cliniques Universitaires de Kinshasa; Department of Clinical Biochemistry, Democratic Republic of the Congo

❖ 2008 – 2011: M.Sc. in Biochemistry and Molecular Biology at Faculty of Sciences/Department of Biochemistry and Molecular Biology, Egerton University, Kenya

❖ June 2012 – September 2012: German Language Courses at Mannheim-Heidelberg Goethe Institute (Intensive 4 months)

- ❖ October 2012 – July 2017: PhD research work in Biochemistry and Molecular Parasitology at the Interfaculty Institute of Biochemistry, Eberhard-Karls Tübingen University, Germany. Thesis Title: Analysis of a putative cyclooxygenase from *Trypanosoma brucei* and its eligibility as a possible drug target. Supervisor: Prof. Dr. Michael Duszenko

III. HONORS AND AWARDS

- ❖ 2008, The New Partnership for Africa's Development (NEPAD) & Biosciences eastern and central Africa Network (BecaNeT) scholarship for Master study at Egerton University, Kenya

- ❖ 2009, DFG Fund Project "Late Stage African Sleeping Sickness: Elucidation of Brain Infection by African Trypanosomes", Master scholar, October 2009

- ❖ 2012, Bourse d'Excellence Bringmann aux Universités Congolaises (BEBUC) scholarship for PhD study from the Université de Kinshasa (UNIKIN)

- ❖ 2012, DAAD scholarship for PhD study at Eberhard-Karls Tübingen University, Germany. PhD Project Title: Expression, Refolding and Purification of a putative cyclooxygenase like-enzyme from *trypanosoma brucei* for structural studies

IV. PROFESSIONAL EXPERIENCE

- ❖ MD General practitioner

- ❖ NEPAD & BecaNET Sponsored Student from East and Central African region.

  MSc. Thesis Title: Purification and Characterization of a Cyclooxygenase – like enzyme from *Trypanosoma brucei.* Supervisors: Prof. Dr. Michael Duszenko (Tübingen University) Prof. Bruno Kilunga Kubata (coordinator of Health/NEPAD), Prof. Raphael Ngure (Egerton University)

- ❖ Sandwich program between Africa and Germany that allowed me to undertake their research work at the Interfaculty Institute of Biochemistry (IFIB), Eberhard-Karls Tübingen University under the DFG Fund Project "Late Stage of African Sleeping Sickness: Elucidation of Brain Infection by African Trypanosomes."

- ❖ PhD research work at the Interfaculty Institute of Biochemistry, Eberhard-Karls Tübingen University, Germany. Thesis Title: Analysis of a putative cyclooxygenase from *Trypanosoma brucei* and its eligibility as a possible drug target. Supervisor: Prof. Dr. Michael Duszenko

V. PUBLICATIONS AND PRESENTATIONS

- ❖ Oral presentation PhD project at the 2nd Interfaculty Institute of Biochemistry (IFIB) - Tübingen University PhD symposium in Blaubeuren, September 20th-September 22nd, 2013

- ❖ Stein J, Mogk S, **Mudogo CN**, Sommer BP, Scholze M, Meiwes A, Huber M, Gray A, Duszenko M. (2014) Drug Development Against Sleeping Sickness: Old Wine in New Bottles? **Curr Med Chem., 2014, 21, 1713-1727**

- ❖ Barth T, Bruges GA, Meiwes A, Mogk S, **Mudogo CN** and Duszenko M. (2014) Staurosporine-induced cell death in Trypanosoma brucei and the role of Endonuclease G during apoptosis. **Open J. of Apoptosis, 2014, 3, 16-31**

- ❖ Duszenko M, Redecke L, **Mudogo CN**, Sommer BP, Mogk S, Oberthür D, Betzel C. (2015) In *vivo* protein crystallization in combination with novel highly brilliant radiation source opportunities for structural analysis of post-translationally modified eukaryotic proteins. **Acta Crystallographica F Struc. Biol. Commun., 2015, 71: 927-937**

- ❖ Abstract and Poster presentation at the forthcoming Sao Paulo School of Advanced Science on Neglected Disease Drug Discovery focus on Kinetoplastids at the Brazilian Center for Research in Energy and Materials (CNPEM), Campinas, Brazil, June 14th – June 24th, 2015

- ❖ Oral presentation PhD project & Method talk at the Interfaculty Institute of Biochemistry (IFIB) - Tübingen University PhD symposium in Freudenstadt, April 21th-23rd, 2016

- ❖ Mogk S, Boßelmann CM, **Mudogo CN**, Stein J, Wolburg H, Duszenko M. (2016) African trypanosomiasis and brain infection – the unsolved question. **Biol Rev Camb Philos Soc. 2016 Oct 14 [Epub ahead of print]**

VI. REFEREES

- ❖ **Prof. Michael Duszenko**

  Interfaculty Institute of Biochemistry (IFIB) - Tübingen University

  Tübingen University-Hoppe-Seyler-Str. 4

  72076 Tübingen

  Tel: +49 (0) 7071 2973343

  E-Mail: **michael.duszenko@uni-tuebingen.de**